Flashback Prevention in Lean-Premixed Hydrogen Combustion

vorgelegt von
Diplom-Ingenieur
Thoralf G. Reichel
geb. in Berlin

von der Fakultät V – Verkehrs- und Maschinensysteme
der Technischen Universität Berlin
zur Erlangung des akademischen Grades

Doktor der Ingenieurwissenschaften
– Dr.-Ing –

genehmigte Dissertation

Promotionsausschuss:

Vorsitzender	Prof. Dr.-Ing. Neda Djordjevic
Gutachter	Prof. Dr.-Ing. Christian Oliver Paschereit
Gutachter	Prof. Dr. Yeshayahou Levy
Gutachter	Associate Prof. Dr. Arvind Rao

Tag der wissenschaftlichen Aussprache: 20. Juli 2017

Berlin 2017

Für meine Frau Lucie

Contents

List of Figures

Abstract

The focus of this study is the combustion of hydrogen in air as it relates to typical gas turbine engines. Hydrogen–air combustion occurs in the absence of any carbon-based emissions and the only combustion products are water vapor and oxides of nitrogen (NO_x). However, due to the very low flammability limit of hydrogen, it can be burned at much lower equivalence ratios than typical hydrocarbon fuels, resulting in excellent low NO_x potential.

Lean premixed combustion of low reactivity fuels, such as natural gas, is nowadays state of the art in stationary gas turbines. In the long term, it is also a promising approach for aero engines. For lean premixed combustion, with increasing fuel reactivity lean blow out limits are extended but the disposition for flashback, an undesired event of upstream flame propagation, is increased. Therefore, combustor design strategies that are applied for conventional fuels have to be revisited in case of hydrogen, which represents the upper end of the scale of high reactivity fuels.

The current thesis aims at developing a combustor design that is capable of safely operating on hydrogen–air mixtures up to stoichiometric conditions while meeting strict emission regulations. To this end, several measures affecting the flashback resistance of a hydrogen–air combustor are investigated. In addition to their effect on flashback resistance, all measures are evaluated with respect to their impact on fuel–air mixing which directly affects NO_x emissions. Unlike most previous investigations on hydrogen–air combustion, the current investigations are conducted at partially premixed instead of perfectly premixed conditions. This poses a challenging task with respect to achieving flashback resistance as well as low NO_x emissions with limited premixing space and time.

Experimental investigation of non-reacting and reacting combustor flow fields of a partially premixed model combustor were conducted using particle image velocimetry in an atmospheric combustor tests rig. Results reveal a strong influence of geometric modifications and fuel momentum on the combustor flow field. Stability maps were recorded that allow for comparison of the operational range of different combustor geometries with respect to flashback and lean blow out. It was shown that already moderate flow rates of a central non-swirling air jet significantly extend the flashback limits, while the lean blow out limits

remained unaffected.
Moreover, recordings of planar laser-induced fluorescence of the hydroxyl radical (OH-PLIF) within the flame revealed that, the axial location of the upstream flame front, x_f, constitutes a telling estimator for flashback resistance. At the investigated conditions, x_f is shifted downstream with increasing equivalence ratio due to the added momentum of the fuel flow. Thereby, the local gain in axial velocity due to fuel momentum supersedes any parallel augmentation in the turbulent flame speed. This has been identified as a driving mechanism affecting the combustor stability limit.
Performance and emissions data facilitate the conclusion that the desired flashback-safe operation at very low NO_x emissions at ambient pressure and relevant combustor inlet temperatures is feasible.

Zusammenfassung

Der Fokus dieser Arbeit liegt auf der experimentellen Untersuchung von Maßnahmen zur Gewährleistung der sicheren und schadstoffarmen Verbrennung von Wasserstoff mit Luft in einer Gasturbine. Die Verbrennung von Wasserstoff mit Luft geschieht ohne den Ausstoß jeglicher Kohlenwasserstoffe, sodass sich das Abgas ausschließlich aus Wasserdampf und Stickoxiden zusammensetzt. Der Stickoxidanteil kann dabei auf ein Minimum begrenzt werden da Wasserstoff aufgrund seiner weiten Zündgrenzen extrem mager verbrannt werden kann.

Mager vorgemischte Verbrennung, wie sie heutzutage bereits in stationären Gasturbinen zum Standard gehört, stellt mittelfristig auch einen vielversprechenden Ansatz für Fluggasturbinen dar. Der Einsatz hochreaktiver Brennstoffe, zum Beispiel wasserstoffreiche Synthesegase oder reiner Wasserstoff, erweitert zwar einerseits deutlich den mageren Betriebsbereich. Andererseits erhöht sich auch enorm das Risiko des Auftretens von Flammenrückschlag, welcher zu massiver Beschädigung von Bauteilen führen kann. Die konventionellen Konzepte der Brennerentwicklung müssen daher für hochreaktive System neu gedacht werden, insbesondere für die Verbrennung von reinem Wasserstoff, der das obere Ende der Skala hochreaktiver Gasturbinentreibstoffe darstellt.

Im Rahmen dieser Doktorarbeit wird der Einfluss verschiedener Maßnahmen zur Vermeidung von Flammenrückschlag auf das nicht-reagierende und reagierende Strömungsfeld experimentell untersucht. Darüber hinaus werden die Auswirkungen dieser Änderungen des Strömungsfeldes auf die Flammenstabilisierung mit Hilfe moderner optischer Messtechnik gezeigt. Die daraus gewonnenen Erkenntnisse vermögen die Beobachtungen der gemessenen Stabilitätskarten zu erklären. Durch die Identifikation von Indikatoren für Flammenrückschlag lassen sich außerdem Voraussagen für die Stabilität jenseits des experimentell bestimmten Betriebsbereichs treffen. Im Rahmen der Untersuchungen stellte sich insbesondere das Störungsfreie Einbringen des hohen Brennstoffimpulses als kritische Maßnahme zur Wahrung von Flammenrückschlagsicherheit heraus. Weiterhin wurde gezeigt das verschiedene Maßnahmen zur Vermeidung von Flammenrückschlag interagieren und teilweise interferieren.

Es konnte jedoch gezeigt werden dass die vorgeschlagene Kombination der Maßnahmen in

der Brennergeometrie in der Lage ist Flammenrückschlag auf dem gesamten Betriebsbereich der Versuchsanlage zu verhindern und gleichzeitig ambitionierte Emissionsziele zu erfüllen.

CHAPTER 1

Introduction

This cumulative PhD thesis contains the following publications:

- [1] – Reichel, T. G., Terhaar, S., and Paschereit, C. O. (2017[1]). Flashback Resistance and Fuel-Air Mixing in Lean Premixed Hydrogen Combustion, *Journal of Propulsion and Power, (2017),* accessed October 12, 2017
  doi:10.2514/1.B36646

- [2] – Reichel, T. G., Terhaar, S., and Paschereit, C. O. Increasing Flashback Resistance in Lean Premixed Swirl-Stabilized Hydrogen Combustion by Axial Air Injection. *Journal of Engineering for Gas Turbines and Power*, Bd. 137 (2015b) (7): 071503.
  doi:10.1115/1.4029119

- [3] – Reichel, T. G., Göckeler, K., and Paschereit, C. O. Investigation of Lean Premixed Swirl-Stabilized Hydrogen Burner With Axial Air Injection Using OH-PLIF Imaging. *Journal of Engineering for Gas Turbines and Power*, Bd. 137 (2015a) (11): 111513.
  doi:10.1115/1.4031181

- [4] – Reichel, T. G. & Paschereit, C. O., Interaction Mechanisms of Fuel Momentum with Flashback Limits in Lean-Premixed Combustion of Hydrogen: *International Journal of Hydrogen Energy*, Bd. 42 (2017) (7): 4518–4529
  doi:10.1016/j.ijhydene.2016.11.018

.

1 The *Journal of Propulsion and Power* publication is based on a conference paper [5] from the *43rd AIAA Fluid Dynamics Conference and Exhibit* in 2013 and is therefore placed first in this chronological listing of publications

1.1 Hydrogen - a Potential Future Energy Carrier

The increased demand and limited supply of fossil fuels drive the interest in the search for alternative fuels for all modes of transportation and electrical power generation. Clean Sky, the European private public partnership, states that air transport's contribution to climate change represents 2% of human-induced CO_2 emission. Taking into account further aspects that contribute to radiative forcing like contrail-cirrus, atmospheric ozone, methane, water vapor, and particle concentrations, a 2% contribution to carbon dioxide emissions turns into a roughly 5% contribution to climate change [6]. This aspect is of particular importance as aviation is predicted to globally grow at a rate of 5% per year in the coming decades [6]. Despite this 5% annual growth of aviation, the International Air Transport Association (IATA) has set a target for CO_2 reduction for 2050 at 50% of the CO_2 emissions in 2005.

One promising candidate fuel for replacing conventional fossil fuels in aviation and power generation is hydrogen. If produced from a regenerative source of primary energy (see Sec. 1.4.1), hydrogen is a carbon-free fuel and eliminates CO_2 from its life cycle. Anyhow, the direct emissions are free of carbon monoxide (CO), carbon dioxide (CO_2), sulfur oxides (SO_x), unburnt hydrocarbons (UHC), and smoke which is a big environmental benefit over current systems. The only emissions from the combustion process with air are water vapor and oxides of nitrogen (NO_x).

Water vapor also contributes to global warming and its radiative force[1] is even greater than that of CO_2. However, residence time of water vapor is at all times much lower than that of CO_2 and can be significantly reduced by cruise altitude optimization. Moreover, the high water vapor content exhaust gases of hydrogen-air combustion are more likely to form contrails, which itself increase the radiative forcing. A thorough study of these combined effects was conducted by Grewe et al. [7] which stated the utilization of hydrogen in aviation still promised a net decrease in climate impact.

The NO_x emissions in comparison to conventional fuels can potentially be reduced significantly due to the wide flammability range of hydrogen which allows for ultra lean combustor operation (see Sec. 1.2).

Other fuel alternatives that are currently being investigated are bio fuels mainly derived from crops. However, bio fuels are not substantially cleaner than kerosene and their production capacity is rather limited and competing with food production for the crop area.

1 Radiative forcing by a climate variable is a change in earth's energy balance between incoming solar radiation energy and outgoing thermal infrared emission energy when the variable is changed while all other factors are held constant.

1.1.1 Hydrogen in Civil Aviation

The earliest flight of a hydrogen based aircraft was in 1956, when one engine of a B–57 was flown with hydrogen by the NACA Lewis Flight Propulsion Laboratory. It was not before 1988, until another hydrogen powered flight was reported with a 164-passenger Tupolev TU-154 commercial jet, that was converted for use of liquid hydrogen. The airplane was equipped with a hydrogen fuel system, independent of the regular fuel system, and one engine was modified to operate with hydrogen. Take-off and climb where done on its regular fuel. After reaching the desired flight level the fuel on one engine was switched from kerosene to hydrogen. The maiden flight lasted 21 min. This event sparked the interest in hydrogen fuel for aviation and many authors promoted and investigated the idea of hydrogen replacing traditional jet fuel [8, 9, 10].

Since 1991, a design project for a subsonic aircraft operating on cryogenic fuels on the basis of an existing Airbus A310 was developed by NASA. They adopted spherical tanks for liquid hydrogen, increasing the thermal insulation due to the reduced surface to volume ratio. In 2000 the European Commission funded the Cryoplane project for assessing the feasibility of liquid hydrogen as fuel in aviation with respect to technology, safety, environmental compatibility and economic viability [10]. This project was the first to publish details regarding the work on the combustion system. Ziemann et al. [11] conducted a screening on various combustor designs for NO_x reduction potential and wide operational range. For demonstration purposes, the chosen hydrogen combustor concept replaced the conventional kerosene combustion system of a GTCP 36-600 auxiliary power unit and reportedly achieved reduced NO_x emissions [12].

Since 2012 experimental tests on a low NO_x hydrogen combustor for aero engines have been conducted within the European Union-supported FP7 project Advanced Hybrid Engines for Aircraft Development (AHEAD). The concept proposed in the AHEAD project is a contra-rotating turbofan engine with sequential dual hybrid combustors using two different fuels [13]. The engine is operated on pure hydrogen in the first stage and bio fuel under flameless conditions [14] in the second stage, aiming to reduce CO_2 and NO_x emissions, respectively. The combustion mode of the first stage is lean-premixed, swirl-stabilized hydrogen combustion. The investigations presented in this thesis were conducted within the frame work of the AHEAD project.

1.1.2 Hydrogen in Power Generation

Lean premixed, swirl-stabilized combustion of natural gas, a fuel that is mainly composed of methane, is nowadays state of the art in stationary gas turbines. High reactivity fuels are commonly fired at steam-diluted conditions [15, 16] or use water injection to comply with emission regulations. Schimek et al. [17] even demonstrated steam-diluted combustion of a stoichiometric hydrogen-oxygen mixtures, that they suggest could be obtained from

high pressure electrolysis, However, the required additional hardware for steam generation adds to the system complexity in case of stationary gas turbines and makes this approach unsuitable for aviation purposes.

Recently, the interest is curbed in safe and efficient combustion of high hydrogen-content fuels while complying with strict emission regulations. This interest originates, on the one hand, from an effort to reduce CO_2 emissions by the means of new cycles, such as the integrated gasification combined cycle (IGCC [18]). On the other hand, concerns about energy supply security also lead to growing interest in alternate energy resources, The syn gases derived from gasification of coal are mainly composed of CO, CH_4, and H_2, with an H_2 content of up to 50% by volume. Waste gas, from the platforming process, used to increase the H/C ratio in the refining of liquid fuels can even exhibit a hydrogen content of up to 90% by volume [19]. Neat hydrogen is, thus, a meaningful test case for flashback resistance of a burner geometry. In the long term, when efficient means of hydrogen production from renewable sources are realized on an industry scale, neat hydrogen could become a viable fuel option for power generation [20].

1.2 Lean Premixed Combustion

Flames are typically classified in two main classes: premixed flames and diffusion flames – depending on whether the fuel and air are mixed prior to combustion, or mixed by diffusion in the flame zone.

Diffusion flames supply both fuel and oxidizer to a reaction zone in an unmixed state. The reaction zone is established where stoichiometric conditions occur. As a result the flame is stabilized, since at these conditions the flame speed is insensitive to mixture perturbations. Simultaneously, the resulting flame temperatures are maximum since the combustion is conducted in the absence of any excess air. Such high flame temperatures lead to high NO_x emissions which compromise the strict emission goals of modern combustion systems. Therefore, the application of diffusion combustion is limited to systems where flame stability is more important than emission restrictions.

Premixed flames have fuel and oxidizer mixed prior to arriving at the flame and are characterized by the equivalence ratio. The equivalence ratio ϕ represents the actual fuel–air ratio normalized by the fuel–air ratio at stoichiometric conditions, i.e., when the fuel is oxidized in the absence of excess air. For lean conditions, i.e., combustion with excess air and a equivalence ratio $\phi < 1$, premixed combustion allows for lower flame temperatures and, thus, reduced NO emissions. The rate of combustion is determined by the flame speed. The flame speed determines how fast a flame will propagate through a combustible mixture. In practical combustion systems, the flame is usually fixed at one location by the means of a solid flame holder or aerodynamic flame stabilization. It

is then fed with a constant rate of a combustible mixture. If the flow rate is too high relative to the flame speed, the flame will blow off. At the other extreme, if the flame speed is large compared to the local gas velocity, the flame will propagate upstream into the combustible mixture and stabilize in regions not designed for flame holding. This upstream propagation is referred to as flashback (FB) and constitutes an operability limit for gas turbine combustors [21].

Hydrogen or high hydrogen-content syn gases exhibit flame speeds that are one order of magnitude above that of conventional hydrocarbons like natural gas (see Sec. 1.4.5). For such high reactivity fuels, FB disposition is substantially increased. However, with increasing fuel reactivity lean blow out (LBO) limits are extended, which allows to operate at lower flame temperatures offering excellent low-NO_x potential [11, 22, 23, 24].

Another important consideration in premixed combustion is autoignition. Given a sufficiently high mixture temperature or pressure, reaction can occur spontaneously without requiring an ignition source. The required time for initiating spontaneous combustion is termed the autoignition delay time. In premixed gas turbine combustors, the autoignition delay time may not exceed the residence time in the premixing section to prevent flame holding. Autoignition delay times of hydrogen–air mixtures are multiple times lower compared to natural gas–air mixtures (Sec. 1.4.4) and, thus, need to be taken into account during combustor design.

1.3 Swirling Combustor Flows

As discussed in the previous section, in premixed combustion measures need to be applied to anchor the flame at a fixed location and prevent it from traveling upstream into the combustible mixture. To realize flame stabilization, modern premixed combustors of all major gas turbine manufacturers rely on swirl-stabilized combustion [25, 26, 27]. The main advantage of swirl-stabilized combustors, in comparison to jet flames or bluff body-

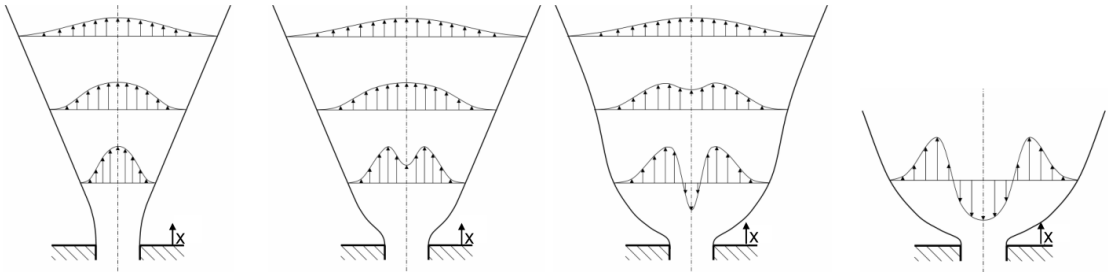

a) no swirl b) weak swirl c) medium swirl d) high swirl

Figure 1.1: Axial velocity profiles for increasing swirl number

stabilized combustors, is the aerodynamic flame stabilization. No combustor parts are located in the direct vicinity of the flame which reduces the thermal load and increases combustor life time.

Swirl-stabilized combustion relies on a phenomenon referred to as vortex breakdown (VB) which yields the formation of a central recirculation zone (CRZ). This CRZ exhibits reverse flow and by these means constantly supplies heat and active species to the flame root. Moreover, the region of relative low velocity allows for flame anchoring at the location where flow velocity and burning velocity of the mixture match. The requirement for the occurrence of VB is a sufficiently high ratio of angular to axial velocity, also termed swirl.

A graphical representation of the onset of VB is illustrated in Fig. 1.1. Increasing the swirl of an otherwise non-swirling jet (Fig. 1.1a) generates a radial pressure gradient. Downstream of the sudden expansion, the continued widening of the jet causes an axial decay of tangential velocity and hence a decay of the radial pressure gradient. The stronger radial pressure gradient at an upstream location leads to a negative axial pressure gradient near the axis, which in turn reduces the axial velocity on the central axis. With increasing level of initial swirl, this axial velocity deficit increases until it leads to reverse flow and the formation of a CRZ (Fig. 1.1b – Fig. 1.1d). Comprehensive reviews about the mechanisms that are involved into vortex breakdown are available by Escudier and Keller [28], and Lucca-Negro and O'Doherty [29].

The combustor used in this thesis also employs swirl-stabilized combustion. Its isothermal flow field obtained from PIV measurements in a water tunnel is depicted in Fig. 1.2. The flow field exhibits the typical features that constitute in a CRZ enveloped by an annular jet, and an outer recirculation zone (ORZ) which is caused by the confinement of the flow.

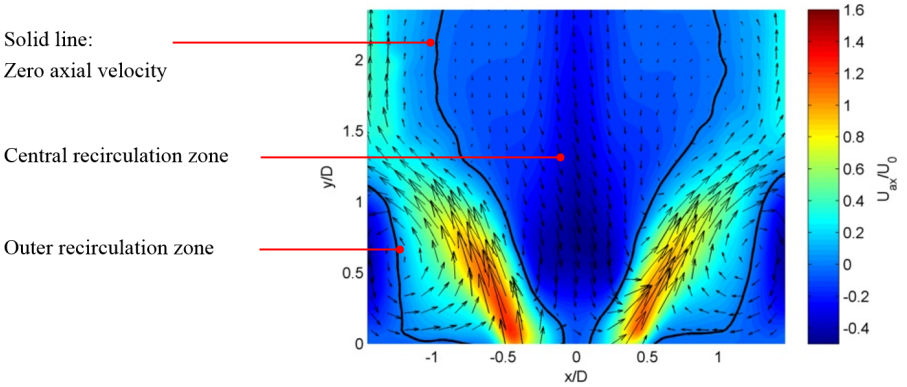

Figure 1.2: Isothermal combustor flow field; velocity vectors imposed on normalized axial velocity

1.3.1 Quantification of Swirl

Beer and Chigier [30] proposed the swirl number S' as a non-dimensional criterion to characterize the amount of rotation imparted on the flow

$$S' = \frac{G_\phi}{G_x \cdot R}$$

where R is the radius, G_ϕ is the axial flux of angular momentum and G_x is the axial thrust. These are defined as

$$G_\phi = \int_0^R U_t \rho U 2\pi r \, \mathrm{d}r \tag{1.1}$$

$$G_x = \int_0^R U \rho U 2\pi r \, \mathrm{d}r + \int_0^R p 2\pi r \, \mathrm{d}r \tag{1.2}$$

In an effort to define a geometric swirl number S, that depends entirely on the burner geometry Beer [30] suggested neglecting the static pressure term and radial dependence of U in Eq. 1.2 and introducing the parameter $\sigma = \sigma\,(z,s,\alpha)$, which is only a function of geometrical dimensions of the radial swirler, in Eq. 1.1. This yields

$$G'_x = \frac{\dot{m}^2}{2\pi\rho R}$$

$$G'_\phi = \sigma \frac{\dot{m}^2}{\rho 2\pi l_s}$$

Consequently, one can define the geometric swirl number S, depending only on the geometrical dimensions slot length l_s and radius R of the radial swirler:

$$S = \frac{G'_\phi}{G'_x \cdot R} \tag{1.3}$$

1.4 Hydrogen Characteristics

1.4.1 Hydrogen Production

If discussing the CO_2 savings resulting from the use of hydrogen fuel, one needs to take into account the life cycle CO_2 emissions, i.e. the CO_2 emissions related to hydrogen production. Several ways of hydrogen production exist. Today, nearly the 50% of the global hydrogen demand is generated via steam reforming of natural gas, 30% by oil/naphtha reforming, 18% by coal gasification, 3.9% by water electrolysis and 0.1% from other sources [31]. It

was estimated that the global warming potential (GWP) of hydrogen production via the steam reforming process of natural gas is 13.7 kg CO_2 (equiv.) per kg of net hydrogen produced [32]. If instead, hydrogen was generated by coal gasification for example, the amount of CO_2 associated to hydrogen production would even double (compared to steam reforming of natural gas) [20].

These numbers blur the illusion of a carbon-free fuel under today's production conditions. This flaw could only be overcome, if hydrogen was produced from renewable energy-based processes. However, Muradov and Veziroglu [20] state that the "renewable energy-based processes of hydrogen production like solar photo chemical and photo biological water decomposition, electrolysis of water coupled with photo voltaic cells or wind turbines" [are] "unlikely to yield significant reduction in hydrogen costs in the next one-to-two decades". This leaves us with the conclusion that, in the medium term hydrogen production technology needs to mature its technology level to allow for CO_2 neutral hydrogen production, a prerequisite to fulfill the promise of a carbon-free fuel.

1.4.2 General Properties of Hydrogen

Hydrogen's high specific energy per unit mass gave it a reputation as the perfect fuel for aviation. However, this advantage is compromised by the very low energy density per unit volume (Fig. 1.3). Due to its low energy density and intended cryogenic storage in pressurized tanks, the resulting cylindrical fuel tanks assume large volumes. For aviation applications that use a conventional air frame, storing such tanks contributes significantly to losses due to increased drag. To overcome this limitation, the AHEAD project suggested the use of a blended wing body configuration [13].

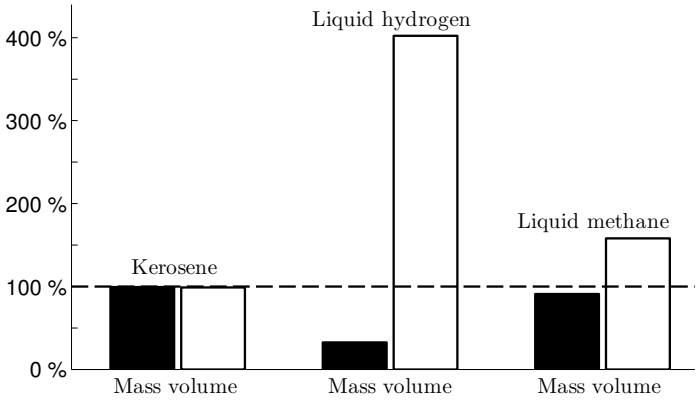

Figure 1.3: Comparison of mass and volume of aviation fuels for equivalent energy content.

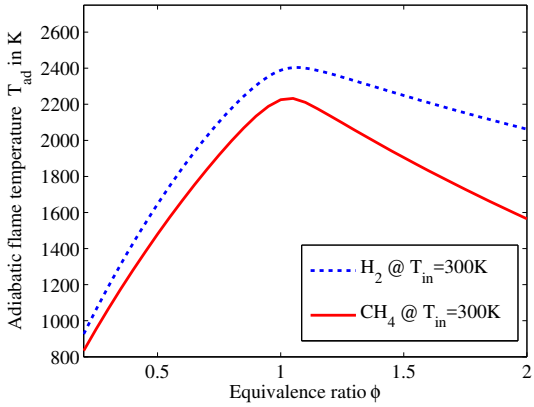

Figure 1.4: Calculated adiabatic flame temperature for methane and hydrogen

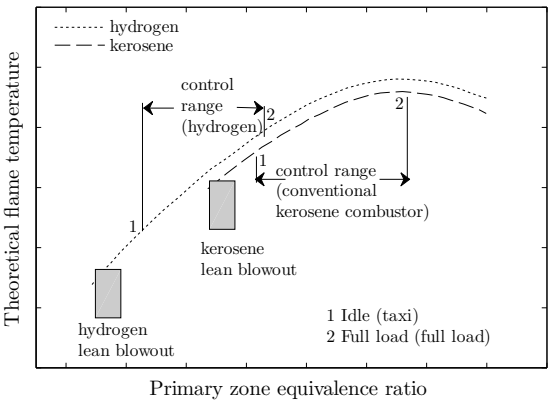

Figure 1.5: Temperature characteristics of the combustion primary zone

From a combustion characteristics point of view, the wide flammability range of hydrogen (4–75 vol.-% in air) yields the possibility of operating at ultra-lean conditions. Such conditions, lead to significantly reduced flame temperatures and, thus, NO_x reduction potential. Schefer et al. [33] report significantly reduced LBO limits of natural gas with increasing hydrogen content from atmospheric combustor tests. The combustor used for this thesis safely operated with neat hydrogen at equivalence ratios as low as $\phi = 0.15$ at ambient pressure and inlet temperatures of $T_{\text{in}} = 620\,\text{K}$. Lieuwen et al. [34] reported LBO limits below $\phi = 0.2$ for hydrogen at an elevated pressure of 4.4 atm and a temperature of 458 K. Thus, hydrogen flames can be operated at much lower equivalence ratios than natural gas or kerosene, however, in order to make a statement regarding the NO_x reduction potential one also needs to take into account the resulting flame temperature.

To this end, the adiabatic flame temperature variation with equivalence ratio for both fuels, methane and hydrogen, at a mixture temperature of 300 K has been calculated in the chemical kinetics software Cantera (Fig. 1.4). Adiabatic flame temperature T_{ad} is the temperature that the flame attained, if the net energy liberated by the chemical reaction, was fully utilized in heating the combustion products. In practice, heat is lost from the flame by radiation and convection, so the adiabatic flame temperature is rarely achieved. However, it can be used as an indicator for the actual flame temperatures of the respective fuel types. For both fuels, the maximum temperature is slightly shifted to the rich side of the equivalence ratio. Note, that for equivalence ratios in the range of ϕ =0.4–1, the adiabatic flame temperature of hydrogen exceeds that of methane by 150–170 K.

So for a given equivalence ratio, the flame temperature of hydrogen is higher, which would lead to increased NO_x emissions. However, the wider flammability range of hydrogen

in comparison to conventional fuels allows to shift the primary zone equivalence ratio into the lean region. Such a shift outweighs the effect of the higher flame temperature. This can be seen in Fig. 1.5, which depicts the flame temperature of kerosene and hydrogen versus primary zone equivalence ratio. The resulting reduced primary zone temperature leads to excellent NO_x reduction potential. Note, that the turbine inlet temperature of the kerosene and hydrogen case remain the same. In the hydrogen case, due to the lower primary zone equivalence ratio less air needs to be added via the liner.

1.4.3 Emission of Pollutants

As a carbon-free fuel, hydrogen does not emit any carbon monoxide (CO) and carbon dioxide (CO_2). Also, the direct emissions are free of sulfur oxides, unburned hydrocarbons (UHC) or soot. The only combustion products of hydrogen–air combustion are water vapor and NO_x. While the environmental impact of water vapor was discussed previously, the following section focusses on NO_x emissions.

NO_x pollutants in hydrogen combustion are generated by oxidation of nitrogen from the combustion air. At high temperatures (T>1700K), diatomic nitrogen and oxygen dissociate into their atomic states, participating in a series of reactions that result in formation of NO as given below. This can further oxidize to NO_2. Both pollutants are collectively described as NO_x. They play a role in the production of acid rain and tropospheric ozone, which harms the respiratory systems and affects crop production. Therefore, stringent regulations of NO_x emissions have been established for power generation and aviation.

The chemical mechanisms that produce NO_x are listed here. These reactions represent

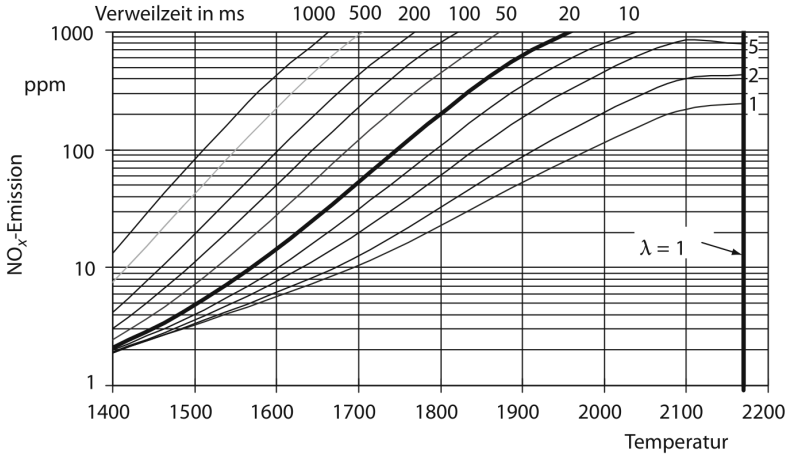

Figure 1.6: Dependence of NO_x emissions on adiabatic flame temperature T_{ad} in °C for varied residence times t_{res} in ms; emissions are normalized to 15 vol.-% oxygen (dry)

the major pathways for NO_x formation.

Extended Zeldovich or Thermal NO:

$$\begin{aligned} O + N_2 &\leftrightarrow NO + N \\ N + O_2 &\leftrightarrow NO + O \\ N + OH &\leftrightarrow NO + H \end{aligned}$$

NNH route:

$$\begin{aligned} N_2 + H &\leftrightarrow NO + NNH \\ NNH + O &\leftrightarrow NO + NH \end{aligned}$$

Nitrous Oxide route:

$$\begin{aligned} N_2 + O + M &\leftrightarrow N_2O + M \\ N_2O + O &\leftrightarrow NO + NO \\ N_2O + H &\leftrightarrow NO + NH \end{aligned}$$

Prompt mechanism:

$$\begin{aligned} N_2 + CH &\leftrightarrow HCN + N \\ HCN + OH &\leftrightarrow CN + H_2O \\ CN + O_2 &\leftrightarrow NO + CO \end{aligned}$$

The thermal route is a primary mechanism for NO_x, when flame temperatures are above approximately 1800 K. Below this temperature, the thermal reactions are relatively slow. This motivates the common approach to control NO_x by reducing the combustion temperature. In the absence of thermal NO_x, the other mechanisms become significant.

The NNH path is most important for rich mixtures at high temperatures (2200 K) in connection with low residence times, and moderate temperatures (1900 K) at all residence times [35].

The nitrous oxide path depends on the intermediate species N_2O, which itself is generated by O-atom attack of nitrogen. The nitrous oxide path is considered a particularly important chemical path in lean burning gas turbines [19].

The prompt mechanism, also referred to as Fenimore, results from N_2 being in contact with radicals like C, CH and CH_2, causing them to react to species containing N and getting further oxidized to NO. One such example is given above. While the prompt mechanism is relevant in case of, e.g., syn gases, it is of no relevance in combustion of neat hydrogen due to the lack of carbon containing reactants.

Besides flame temperature, the residence time also affects NO_x emissions. Both dependencies are depicted in Fig. 1.6. At a given adiabatic flame temperature, increased residence times increase NO_x emissions. However, this statement is contradicted by Leonard and Stegmayer [36], who claim that in extremely well premixed flames operating at less than 1900 K the amount of NO_x did not increase with increasing residence time. This statement renders the residence time less important and underlines the necessity of achieving excellent fuel–air mixing.

1.4.4 Autoignition Delay Time

Typical inlet temperatures (600–900 K) and pressures (5–35 bar) of gas turbines are sufficiently high for autoignition of many fuels. Autoignition terms a spontaneous ignition of a combustible mixture without an ignition source, e.g. a spark plug, which occurs in case of sufficiently high pressure and temperatures.

Beerer and McDonnell [37] compare the autoignition delay times of hydrogen and methane at the combustor inlet pressures and temperatures of several existing aeronautical

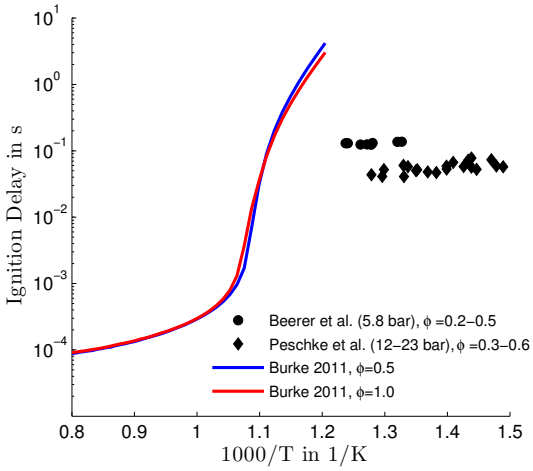

Figure 1.7: Ignition delay time calculated at ambient pressure using Cantera compared to measurements [37, 38]

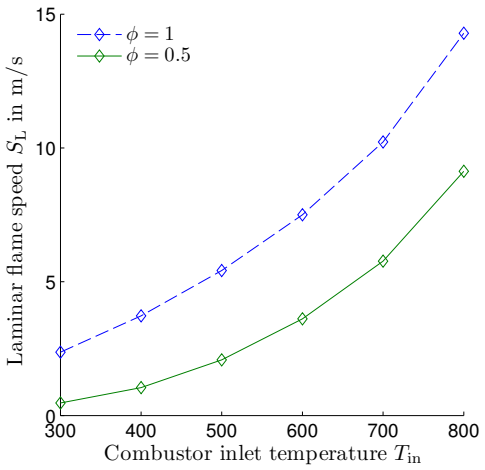

Figure 1.8: Laminar flame speed for increasing mixture temperature calculated at ambient pressure using Cantera

and power generation gas turbine engines. They observe that the autoignition delay times of hydrogen at these conditions are multiple times shorter compared to methane. Investigating the autoignition of coal-derived syn gases, Peschke et al. [38] concluded that the ignition delay time is nearly independent of the CO or CO_2 concentration, indicating that the ignition properties of syn gas are dominated by hydrogen kinetics.

An autoignition of already small portions of the main flow is sufficient to ignite the rest of the mixture and cause flame holding in the premixing section. This was previously reported by Schönborn et al. [39] for hydrogen-air mixtures in a pressurized turbulent flow reactor at 8–12 bar and by Sayad et al. [40] for a generic gas turbine combustor firing H_2/CH_4 mixtures already at a relatively low hydrogen fractions of only 12 vol.-%. Therefore, as a design rule, the residence time in the premixing section may not exceed the autoignition delay time at the combustor inlet conditions. The time scale associated with fuel–air mixing in current lean premixed combustors is estimated to be of the order of 1–5 ms, based on bulk velocities and premixer volumes [34]. Certain parts of the mixture are likely to exceed the residence time based on bulk flow velocity due to the complex character of the flow in a premixing section. Thus, the premixer design is a trade-off between finding a residence time long enough to achieve sufficient fuel–air mixing and short enough to prevent autoignition.

Estimates of the autoignition delay time for the premixer design process can be obtained from chemical kinetics modeling or experimental investigations. Ströhle and Myhrvold [41] evaluated six chemical kinetics mechanisms for hydrogen-air combustion by comparing the simulation results for autoignition delay time and laminar burning velocity to experimental findings derived from shock tube measurements and burner experiments. Below a pressure of 5 bar and relevant compressor discharge temperatures from 600–900 K, they observed a strong discrepancy between simulated and measured autoignition delay times. However, for higher pressures the chemical kinetics simulations and experiments showed excellent agreement with respect to both, auto ignition delay time and laminar flame speed. They conclude that the mechanisms of Li [42] or Ó'Conaire [43] best represent H_2 /O_2 kinetics under gas turbine conditions.

Autoignition delay times can be obtained experimentally from either shock tube, rapid compression machine or continuous flow reactor measurements. A comparison of the experimental procedures and an overview of relevant experimental studies is given in Schönborn et al. [39]. Shock-tubes utilize shock wave compression to bring premixed reactants to their autoignition condition and, thus, are most suited for measuring at high temperatures ($T > 1250$ K) and ignition delays shorter than a few milliseconds. Rapid compression machines compress reactants to their autoignition pressures and temperature by means of a piston in a short time span (10–30 ms). They are most suited to measure ignition delays of about 10–100 ms. Flow reactors generally operate under constant pressure and utilize turbulent premixing of the reactants. This type of experimental apparatus is

not suitable for ignition delay times in the order of the mixing time scales. They are, thus, applied for measurements of long ignition delay times (100–500 ms) at low temperatures (600–1150 K) and intermediate pressures (1–20 bar)[39].

At high temperatures (> 900 K) there is general agreement between experimental and chemical kinetic modeling results. However, a considerable difference exists for the relatively low temperature (600-900 K) and high pressure conditions of the so called mild ignition regime, that is most relevant for gas turbine premixer conditions [37, 39, 41]. At these conditions the chemical kinetic modeling overpredicts the autoignition delay time by orders of magnitude (Fig. 1.7). Ströhle and Myhrvold [41] suggest that the experimental conditions in the mild ignition tests deviate so far from the assumed ideal homogeneous and zero dimension behavior that a simple homogeneous reactor alone is no longer sufficient to predict accurately the delay time.

Thus, experimental results from continuous flow reactors, that pose a more realistic representation of the flow conditions in a premixing section, and the resulting empirically derived correlations remain the only reliable way of predicting the ignition delay for conditions seen inside a gas turbine premixer. Such correlations can be found in Beerer and McDonnell [37], who also report that measured ignition delay times are considerably shorter than any model (Fig. 1.7). However, they are still at least one order of magnitude greater than most premixer residence times. Due to large uncertainties in the measurements, they recommend “a fairly large safety factor (between 5 and 10)”. In spite of a certain ambiguity in the results, even for conservative estimations of the ignition delay it will not be a significant problem for most engines, only those with considerably long premixing times or ones with very high combustor inlet temperatures or pressures.

For the current burner design, the bulk flow estimated residence time is in the order of $\tau_{\mathrm{res}} = 5\,\mathrm{ms}$. For the combustor inlet conditions of the suggested AHEAD airplane at take-off ($p = 40\,\mathrm{bar}$, $T = 900\,\mathrm{K}$), representing the worst case conditions with respect to autoignition of the premixed fuel, chemical kinetic modeling in Cantera using the Burke mechanism yields an ignition delay time of $\tau_{\mathrm{mod}} = 200\,\mathrm{ms}$. As discussed above, for this temperature region the chemical kinetic modeling overpredicts the ignition delay. A correlation for hydrogen-air combustion derived from flow reactor experiments from Beerer and McDonnell [37] yields $\tau_{\mathrm{corr}} = 35\,\mathrm{ms}$. While the resulting safety margin, $\tau_{\mathrm{corr}}/\tau_{\mathrm{res}} = 7$, is significantly smaller than predicted from the chemical modeling, it is still well within the range of 5–10 suggested by Beerer and McDonnell.

1.4.5 Laminar Burning Velocity

The laminar burning velocity S_{L} of hydrogen–air mixtures is very important in designing and predicting the progress of combustion and performance of combustion systems where hydrogen is used as fuel. The challenges related to hydrogen combustion are revealed when

Table 1.1: Fuel properties I, all quantities are given at $\phi = 1$, ambient temperature and pressure from [44]

fuel	laminar flame speed S_L in cm/s	quenching distance δ_q in mm
hydrogen	210	0.64
methane	40	2.5

comparing the burning velocity of hydrogen, methane, and hydrogen–methane mixtures. Figure 1.9a shows that the burning velocity of neat hydrogen is an order of magnitude higher in comparison to methane. For a binary mixture of hydrogen-methane, the burning velocity is shown to increase exponentially with increasing hydrogen content (Fig. 1.9b). Note, that for methane the maximum burning velocity is found slightly on the rich side of stoichiometric conditions. However, for blends of methane and hydrogen the maximum burning velocity is shifted towards richer conditions, up to $\phi = 2$ for neat hydrogen. (Fig. 1.9a). This underlines the importance of sufficient fuel–air mixing to prevent rich pockets. These rich pockets do not only lead to hot spots that increase NO_x emissions. They also locally increase the burning velocity and, thus, have a detrimental effect on FB resistance.

Although the laminar flame speed is an important combustion parameter, most engine applications rely on turbulent flame propagation into mixtures, which are preheated by compression. The actual flame propagation speed rises significantly with premixed gas temperature and turbulence level. While the effect of increasing mixture temperature on the laminar burning velocity is described in Fig. 1.8, the effect of increased turbulence levels can be accounted for by introducing a turbulent flame speed S_T. Manifold correlations have been suggested to estimate the turbulent flame speed. Many of them are summarized in Lefebvre [45]. The simplest correlation was suggested by Damköhler.

$$S_T = S_L + u'_{rms} \tag{1.4}$$

However, even if the turbulent burning velocity of the combustible mixture was known, due to the complex flow conditions residing in a swirl-stabilized combustor, it is not sufficient to prevent the local flow velocity from exceeding the turbulent burning velocity to prevent FB. Various types of FB, that lead to an upstream propagation of the flame into the premixed region, are differentiated. These types will be discussed in Sec. 22.

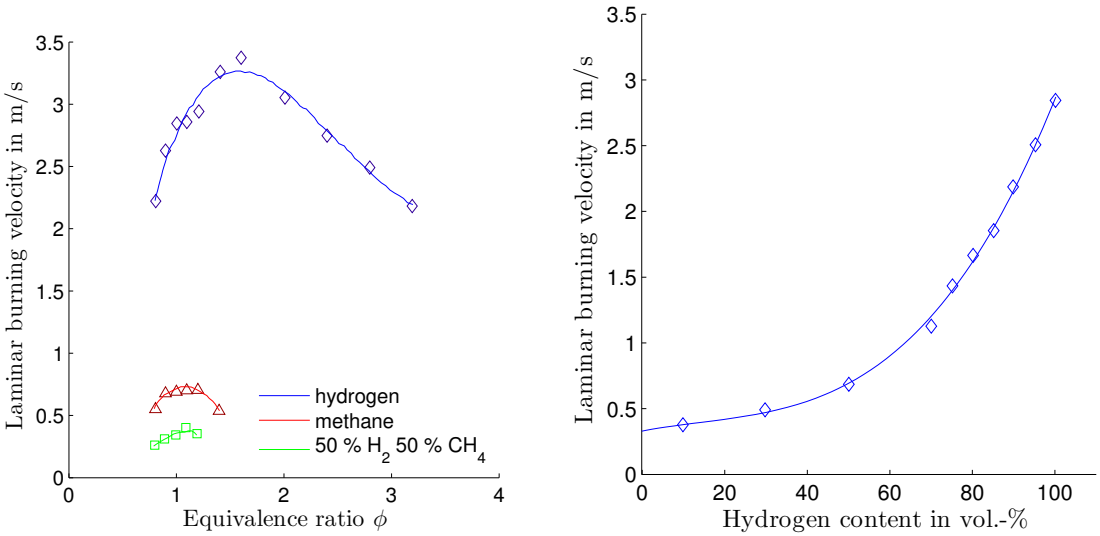

(a) Measured burning velocities for different fuel compositions and equivalence ratios at ambient pressure and temperature; data from [46]

(b) Measured burning velocities for increasing hydrogen content in hydrogen-methane-air mixtures ($\phi = 1$) at ambient pressure and temperature; data from [46]

Figure 1.9: Laminar burning velocity of syn gas mixtures with increasing hydrogen content

1.4.6 Fuel Momentum

High reactivity fuels, such as high-hydrogen syn gases or neat hydrogen, exhibit a much higher volumetric heating value and lower density compared to, e.g., natural gas. This leads to substantially increased volumetric flow rates when a conventional fuel, such as natural gas, is replaced with the aforementioned high reactivity fuels. This increase in volumetric fuel flow rates alters the penetration depth of the fuel jets into the air flow and, thus, the fuel–air mixing characteristics. Moreover, the increased fuel momentum can potentially alter the flow field in both, the premixing section and combustion chamber. By these means, the fuel momentum affects fuel–air mixing and the combustor stability limits which, however, strongly depends on geometry and alignment of the fuel injectors.

Table 1.2: Fuel properties II from [44]

fuel	chem. formula	lower heating value H_i in MJ/m^3	Wobbe index W_i in MJ/m^3
hydrogen	H_2	10.8	40.9
methane	CH_4	35.8	48.1

To quantify the interchangeability of fuels with varying volumetric heating values and densities, commonly the Wobbe index W_i is used for comparing gaseous fuels during the preliminary assessment of the design requirements for the fuel system [45]. Gas turbine manufacturer typically determine a W_i range within which the combustor operation can be guaranteed [26]. The Wobbe index W_i is defined as the ratio between energy density, represented by the volumetric lower heating value H_i, and relative density of the fuel with respect to air at identical conditions (Eq. 1.5). The relative density is then expressed by the molar mass.

$$W_i = \frac{H_i}{\sqrt{\frac{\rho}{\rho_{\text{air}}}}} = H_i \sqrt{\frac{M_{\text{air}}}{M}} \tag{1.5}$$

Essentially, the Wobbe index provides a measure of the energy throughput for a given fuel injection geometry. If the fuel of a given combustion system is changed, it should not be allowed to vary by more than about 5% from the nominal value for which the system was designed. Evaluating Eq. 1.5 for hydrogen and methane yields that, the Wobbe index is increased by 17 %, if one changes the fuel of a combustion system designed for methane to hydrogen.

$$\frac{W_{\text{H}_2}}{W_{\text{CH}_4}} = \frac{H_{\text{H}_2}}{H_{C\text{H}_4}} \sqrt{\frac{M_{\text{CH}_4}}{M_{\text{H}_2}}} = 1.17$$

This exceeds the allowed Wobbe index variation of 5% by far and underlines the importance of fuel momentum in case of hydrogen combustion. However, while the Wobbe index gives a good general idea of the contribution of fuel momentum when interchanging fuels for a given combustion system, it is insensitive to changes in operational conditions like air preheating or equivalence ratio which also strongly affect fuel momentum. Instead, the fuel–air momentum ratio is used to quantify the impact of fuel momentum for varied operational conditions.

$$J = \frac{\rho_{\text{fuel}} u_{\text{fuel}}^2}{\rho_{\text{air}} u_{\text{air}}^2} \tag{1.6}$$

To compare the momentum ratio (Eq. 1.6) of hydrogen and methane at the same combustor power, P, the differences in volumetric heating value and in molecular mass need to be taken into account (Table 1.2). This yields an increase in momentum ratio J for hydrogen by almost 40% in comparison with methane.

$$\left.\frac{J_{\mathrm{H2}}}{J_{\mathrm{CH4}}}\right|_{P=\mathrm{const.}} = 1.37$$

A detailed comparison for hydrogen and methane of the impact of varying operating conditions like air preheating and equivalence ratio on both, the momentum ratio J and bulk outlet velocity u_0 are given in Fig. 2 in publication 2.3.

To achieve a desired power output for hydrogen fuel, about 3.5 times higher volumetric fuel flow rates in comparison to natural gas are required due to its smaller volumetric heating value. Therefore, a considerable amount of additional volume flow and, thus, momentum compared with natural gas is introduced into the system. For technical premixing, where the fuel is injected directly into the premixing section, with increasing hydrogen content of the fuel, the additional fuel momentum increasingly alters the flow field. Thus, the additional fuel momentum needs to be utilized in a manner beneficial for FB resistance, since desired flow field features contributing to FB resistance are potentially eliminated otherwise.

1.5 Flashback in Premixed, Swirling Combustor Flow

For lean-premixed combustion with increasing fuel reactivity, lean blow out (LBO) limits are extended, offering excellent low-NO_x potential. Simultaneously, FB disposition is increased. FB denotes the upstream propagation of a flame in a combustible mixture into regions not designed for flame holding and constitutes an operability limit for gas turbine combustors [21]. Aspects limiting the operational range of swirl-stabilized combustors are intensively detailed in the work by Huang and Yang [47] and Lieuwen [48]. The increased FB tendency of various mixtures with increasing hydrogen content has been investigated in numerous studies [33, 49, 50, 51]. Detailed investigations regarding the effect of inlet or outlet conditions by Syred et al.[52], swirl number by Sayad et al. [53], or a hydrodynamic instability by Schönborn et al. [54] on the stability limits of high-hydrogen content fuels have also been reported.

For hydrogen–air combustion basically two inherently different combustion systems have experienced relevant development progress in the past decades. On the one hand, micro-mix combustors, where multiple compact flames are generated at multiple fuel injection locations aiming to distribute the heat release to prevent hot spots and minimize residence time. In these concepts, minimal premixing times in conjunction with high main flow velocities are utilized to suppress FB, which is why these systems are also referred to as lean direct injection (LDI) systems.

On the other hand, swirl-stabilized premix combustors which are state-of-the-art in modern gas turbines firing natural gas, have experienced a push to extend their operational range to high reactivity fuels. These systems employ a strongly swirling flow to achieve a high degree of premixing which makes their premixing section particularly susceptible to FB when firing high reactivity fuels.

1.5.1 Minimal Premixing: LDI / Micro-Mix Combustors

Already in the 1970s, NASA examined new fuel injector designs for potential hydrogen gas turbine engines. Anderson [22] investigated a LDI concept, which basically consisted of a perforated plate flame holder, where 80 smaller flames were stabilized downstream of small passages through a plate. Fuel was injected via a jet in cross flow configuration inside the small passages. In the early 2000s, the experimental work on LDI injectors by Anderson was utilized to validate a CFD code which was then used for preliminary combustor design purposes by Shih et al. [55]. Schefer et al. [56] conducted OH-PLIF investigations with a conceptual fuel nozzle, that was similar to the LDI injector used by Anderson, and provided insight into the flame stabilization and flame structure of hydrogen–air flames. These efforts by NASA were concluded by an investigation of Marek et al. [57] who compared several perforated plate designs for their ability to minimize the FB risk in hydrogen–air combustion. The authors report FB limits and NO_x emissions at elevated air preheat temperatures and pressures up to 7 bar. They conclude, that the best investigated configuration yields satisfying FB characteristics and NO_x emissions comparable to state of the art LDI combustor concepts firing kerosene. However, they also report difficulties to achieve uniform fuel distribution to the numerous injection ports and massive cooling problems due the the hydrogen flame anchoring close to the injectors, leading to failure during test execution.

Relevant research on a low NO_x combustion system was contributed by Ziemann et al. [11] in the context of the Cryoplane project [58]. They conducted a screening on various combustor designs with respect to NO_x reduction potential and wide operational range. They investigated, amongst others, concepts of micro-mix and premixed swirl-stabilized combustors. For these two concepts, they report the lowest NO_x emissions of all investigated concepts. However, they abandoned the premixed swirl concept and continued further tests only with the micro-mix concept. Dahl and Suttrop [12] proved the technical feasibility of the micro-mix hydrogen combustor when they replaced the conventional kerosene combustion system of a GTCP 36-600 auxiliary power unit with such a micro-mix combustor and achieved significantly reduced NO_x emissions.

The next development step, beyond the basic micro-mix concept of a perforated plate with a fuel jets in cross flow, was suggested by Hernandez et al. [59] and Lee et al. [60]. The new concept applies internal fuel and air staging within the 6–12 mm micro-mix injectors

which are designed to achieve compact flames aiming to minimize residence times at the high flame temperatures. It is suggested, that when applied to a gas turbine, a full-scale combustor will contain 30-60 closely-packed micro-mix injectors for every megawatt of thermal power. The authors report single injector tests at ambient [59] and elevated temperature and pressure conditions up to 5 bar [60]. Two categories of injectors were distinguished, radial inflow and axial flow injection geometries. While the radial inflow injectors achieved lower emissions, they proved robust to FB for pressures up to 3 bar. Above 3 bar the radial injector was reportedly prone to FB. The axial injection concept, that achieves higher axial velocities at the injector outlet, exhibits a higher FB resistance, while it does not achieve the mixing quality and low emissions of the radial concept.

1.5.2 High Degree of Premixing: Swirl-Stabilized Combustors

Similar to other modern premixer concepts [25], in the current thesis, a cylindrical mixing tube without centerbody is used to ensure sufficient mixing. The FB mechanisms prevailing in this type of combustor have been discussed by Lieuwen et al. [34]. They distinguish between four generally different types of FB which may lead to fast upstream flame propagation. Type 1–3 rely on mechanisms that are driven by the competition between the flame speed and local flow velocities. These types of FB can generally occur in both, swirling and non-swirling flows. Type 4 is the result of the interaction between a swirling flow and heat release from the flame and this type's occurrence is, thus, limited to swirling flows. Additionally, reports in the literature exist for FB events caused by autoignition, representing type 5. Thus, the FB types are categorized as follows:

1. Flashback in the core flow
2. Flashback due to combustion instabilities
3. Wall boundary layer flashback
4. Combustion-induced vortex breakdown
5. Flashback due to autoignition

The first type, FB due to flame propagation in the core flow occurs when the turbulent burning velocity in the premixing section exceeds the flow velocity as discussed in the previous section. A conservative estimate of turbulence intensities in a gas turbine combustor of 20% of the main flow $u'_{\mathrm{rms}} = 0.2u_0$ yields for the critical condition at FB, when the bulk flow velocity u_0 matches the turbulent flame speed S_{T}

$$S_{\mathrm{T}}/u'_{\mathrm{rms}}\Big|_{\mathrm{fb}} = 5. \tag{1.7}$$

Utilizing the simple relationship for the turbulent flame speed from Eq. 1.4, the laminar flame speed at the combustor inlet condition of an intensely recuperated combustor and conservative estimates of the turbulence intensity Lieuwen et al. [34] derive a worst-case ratio of

$$S_{\mathrm{T}}/u'_{\mathrm{rms}}\Big|_{\text{worst case}} < 1.3.$$

Since this value is substantially lower than required for flame propagation against the main flow velocity (Eq. 1.7), there is no indication that this type of FB is the most critical. However, in case of poorly conditioned combustor flow fields, e.g., vortex breakdown in the mixing tube, this FB type may still occur. For experimental studies on swirling flames with a low reactivity fuel, here natural gas, Blesinger et al. [61] describe a flow configuration where already at isothermal conditions the axial location of vortex breakdown was located inside the mixing tube. Due to the comparably low reactivity of the fuel, for low equivalence ratios the flame was still anchored downstream of the mixing tube, inside the combustion chamber. Increasing the equivalence ratio above a critical value, allowed the turbulent burning velocity of the mixture to exceed the local flow velocity and lead to FB in the core flow, along the vortex axis.

The second type is FB due to combustion instabilities. Such instabilities manifest in high pressure fluctuations which are associated with velocity fluctuations. The fluctuating velocity can cause the local, instantaneous flow velocity to fall below the burning velocity of the combustible mixture. Given a sufficiently low frequency of the velocity fluctuations this mechanism will lead to FB. FB occurrence due to this mechanism was previously reported for both, a generic backward-facing step by Keller et al. [62] and more recently in a model combustor setup by Laperey et al. [63]. However, this FB type will not be considered throughout this thesis, since combustion instabilities have to be avoided for other reasons and FB due to this mechanism did not occur during regular, stable combustor operations assured during test execution.

The third type is FB in the wall boundary layer investigated by Lewis and von Elbe [64]. The wall-parallel flow velocity continuously decreases towards the wall due to the no-slip condition. Only flame quenching prevents upstream flame propagation along the wall to occur in any case. The chemical reactions cannot sustain within a certain distance from the wall due to heat loss and third body recombination reactions. This distance is referred to as quenching distance δ_{q}. However, FB occurs when the burning velocity exceeds the flow velocities outside of the quenching distance, i.e., when a critical velocity gradient suggested by Lewis and von Elbe [64] is undercut. In laminar flows, FB limits correlate with the velocity gradient at the wall [64]. This lead to the concept of a critical velocity gradient g_f, below which FB occurs. The critical velocity gradient g_f correlates

with the laminar burning velocity S_L and the quenching distance δ_q.

$$g_f \sim S_\mathrm{L}/\delta_\mathrm{q} \tag{1.8}$$

Taking into account the laminar burning velocities S_L and quenching distances δ_q of hydrogen and methane (Table 1.1) yields

$$\frac{g_{f\,\mathrm{H2}}}{g_{f\,C\mathrm{H4}}} = 20.5.$$

The required velocity gradient of hydrogen is approximately one order of magnitude higher than that for natural gas which underlines the elevated risk of boundary layer FB for hydrogen combustion.

The fourth type is FB due to combustion-induced vortex breakdown (CIVB). This mechanism describes that, even if at isothermal conditions the vortex breakdown is located downstream of the sudden expansion of the mixing tube, the chemical reaction can nevertheless lead to a further upstream breakdown of the flow, resulting in an upstream flame propagation. This effect was first identified by Fritz et al. [65]. Konle and Sattelmayer [66] reported time-resolved data of the flow field in the mixing tube and the upstream flame front during CIVB. They reveal that typically during the transient process of upstream flame propagation, the vortex breakdown, i.e. the low velocity region in the flow, travels upstream first and the flame follows. However, the initiation of upstream flame propagation is caused by an interaction between vortex breakdown and heat release. This interaction leads to a negative azimuthal vorticity gradient in axial direction which causes streamline divergence and, thus a declining axial velocity on the axis of rotation (Fig. 1.10). This declined axial velocity results in an upstream shift of VB. Once the VB is located inside the mixing tube, this effect is reinforced due to the high volume specific heat release resulting in the upstream propagation of the flame. Thus, the further downstream the initial location of VB, the higher is the resistance of the flow field against this type of FB. The interaction of heat release and the flow field was modeled by Duwig and Fuchs [67]. They also reported flame stability to benefit from a vortex breakdown location well downstream of the mixing tube, since under these conditions they observe a decoupling of the flame and hydrodynamic flow instabilities.

The fifth type of FB is observed, if the residence time in the premixing section exceeds the autoignition delay time associated with the combustible mixture at the current combustor inlet conditions. In this case, premature ignition of the mixture leads to flame holding in the premixing section as was previously reported by Sayad et al. [40].

1.6 Controlling Parameters for Flashback Prevention

1.6.1 Flow Velocity Variation

In fact, a higher bulk flow velocity u_0 of the combustible mixture in premixed combustion results in higher FB resistance, since the flow velocity increases while the burning velocity remains constant. This was reported in previous studies [66, 68] and is also observed for the burner utilized in the current thesis (Sec. 2.2). However, an increased flow velocity also results in an increased fundamental pressure loss Δp_{hot} that occurs whenever heat is added to a flowing gas. It is given by the following expression from [45]

$$\Delta p_{\mathrm{hot}} = 0.5 \rho u_0^2 \left(T_{\mathrm{out}}/T_{\mathrm{in}} - 1\right) \tag{1.9}$$

According to Eq. 1.9 a square dependence of the fundamental pressure loss on bulk flow velocity exists. This pressure loss directly translates into a decrease in efficiency, since pressure generated by the compressor is lost.

However, the wide flammability range of hydrogen in comparison to conventional fuels like natural gas yields the possibility to operate premixed hydrogen combustors at very low equivalence ratios. At these very lean conditions a much smaller ratio of the main air needs to be fed through the burner and premixing section and a higher air split is allowed in the combustion chamber via the liner. This small portion of the overall air mass flow that passes the premixing section could flow at a higher bulk velocity, since its detrimental effect on overall engine efficiency is small. Consequently, a certain margin exists for increasing the bulk flow velocity in the premixing section in hydrogen combustion.

1.6.2 Burner Geometry

The geometry of a premixed burner for high reactivity fuels needs to comply with constraints regarding the cold flow pressure loss of typically less than 5%, assure sufficiently high fuel–air mixing to comply with the emission targets, and tailor the combustor flow to achieve maximum FB resistance. With respect to the latter aspect, different measures are applied to suppress different types of FB.

Boundary layer conditioning

General measures against wall boundary layer FB, suggested by Lieuwen et al. [34], are to keep boundary layers thin and avoid local separation. Another measure is to apply dilution holes to achieve a leaner near-wall region of the mixing tube. This approach locally reduces the equivalence ratio which results in reduced burning velocities S_{L} and

increased quenching distances δ_q. Both measures reduce the critical velocity gradient (Eq. 1.8) and, thus, increase the resistance against wall boundary layer FB. Baumgartner and Sattelmayer [69] conducted an experimental investigation regarding the effect of varied dilution air mass flows and injection angles and reported significantly extended FB limits for premixed hydrogen–air mixtures. Accordingly, air dilution in the premixing section is also applied in the burner setup of the current thesis.

Swirl number reduction

As discussed in the previous section, swirl is imposed on the flow in order to achieve fuel–air mixing and create a central recirculation zone that provides low flow velocities for flame anchoring. Between a swirl number too low for the occurrence of VB and a swirl number so high, that it requires an unaffordable pressure loss, a certain margin for swirl number variation exists. In case of incomplete mixing, the high flame temperatures associated to rich pockets of hydrogen would lead to increased NO_x emissions. This poses an argument in favor of a high swirl number for hydrogen combustion. An argument in favor of a lower swirl number is the reported increased FB resistance. Sayad et al. [53] reported a significantly extended operational range when decreasing the swirl number from $S = 0.66$ to $S = 0.53$ for a generic swirl burner operating on syn gases containing up to 80 vol.-% hydrogen. With decreasing swirl number, the swirling jet opening angle downstream of the mixing tube outlet was also reduced. This reduction in jet opening angle was previously reported by Terhaar et al. [70] and Reichel et al. [2] to also occur when the swirl number was reduced due to increasing injection rates of a non-swirling central air jet. Similar to the swirl number reduction of Sayad et al., the non-swirling air jet also increased FB resistance. This is reasonable, since a decreasing jet discharge angle reduces the area consumed by the mixture downstream of the mixing tube and leads to higher axial velocities.

The same tendency of increased FB resistance with reduced swirl number was also reported by Konle and Sattelmayer [66], when they conducted experimental investigations on a swirl-stabilized premix burner at atmospheric conditions firing natural gas. Moreover, they report velocity measurements in the premixing section at isothermal and reacting conditions. At isothermal conditions, the axial velocity profile 0.5D upstream of the mixing tube outlet exhibits the typical axial velocity deficit found in strongly swirling flows. At reacting conditions, although the flame is stabilized downstream of the mixing tube outlet, the axial velocity on the central axis is further reduced. Simultaneously, on a higher radius, $r/D = 0.2$, a velocity increase is observed. This observed difference in isothermal and reacting velocity field in the mixing tube is an important mechanism that needs to be taken into account, when judging FB resistance of combustor geometries based on isothermal flow fields.

An opposite trend in the correlation of swirl number with respect to FB is observed by Syred et al. [52]. They report increased FB resistance with increasing swirl number in the range of $S = 0.8$–1.47 from their investigation of blow off and FB limits of a generic swirl burner firing high-hydrogen content coke oven gas (65% H_2 , 25% CH_4, 6% CO, 4% N_2). In this case the complex interaction of partially premixed fuel injection with the flow field seems to contribute to this somewhat unexpected correlation.

Obviously, the definition of a swirl number becomes to some extent ambiguous, when the high volumetric fuel flow rates associated to hydrogen-rich fuels alter flow field characteristics like the swirl number. Since this important effect is under investigated and not fully understood for partially premixed, swirling combustor flows further light will be shed on the correlation of swirl number and FB with respect to varying AI rates and fuel flow rates throughout this thesis.

Non-swirling central air jet (axial air injection)

In order to avoid FB of the types three and four, turbulent flame propagation in the core flow and combustion induced vortex breakdown, "a major design criterion for nozzle aerodynamics is that the axial velocity must be as high and as uniform as possible and free of strong wakes" [34]. The applications of non-swirling central air jets in swirling combustor flows had been reported previously, e.g., by McVey et al. [71]. However, Burmberger and Sattelmayer [72] first suggested its application to influence the position of vortex breakdown aiming to increase FB resistance of high reactivity fuels. They suggest that, the mechanism by which a non-swirling central air jet delays VB and, thus increases FB resistance, is is linked to the axial gradient of the azimuthal vorticity $\partial\omega_\phi/\partial z$, here expressed in cylindrical

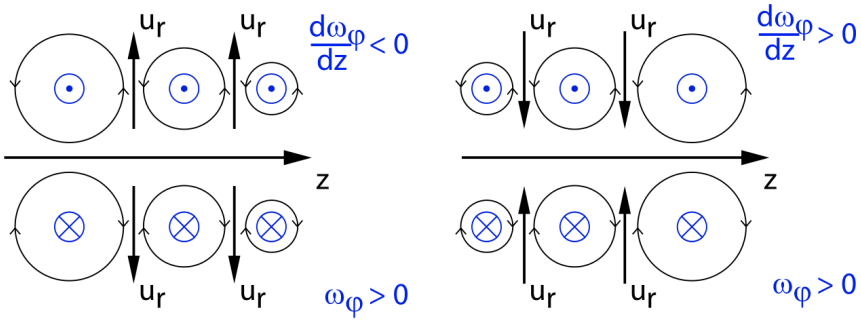

a) b)

Figure 1.10: Effect of azimuthal vorticity on streamline divergence: a) decreasing azimuthal vorticity causes streamline divergence ($u_r > 0$); b) increasing azimuthal vorticity prevents streamline divergence ($u_r < 0$)

coordinates. In a swirling flow without AI, the absolute value of the azimuthal vorticity ω_ϕ decreases in flow direction, i.e. $\partial\omega_\phi/\partial z < 0$. This causes a declining axial velocity on the axis of rotation which results in streamline divergence ($u_r > 0$), as is illustrated in Fig. 1.10a. The streamline divergence may trigger the isothermal vortex breakdown to occur upstream of the combustion chamber leading to flame FB. A non-swirling axial air jet delays the streamline divergence and shifts the location of VB downstream (Fig. 1.10b).

Burmberger et al. [73] proved that a burner, applying this concept, allows for FB-free operation of stoichiometric methane-diluted hydrogen mixtures under unconfined conditions. Besides the use of diluted hydrogen and unconfined flames, the study is also limited to perfectly premixed combustion and omits the challenges related to achieving FB safety as well as low NO_x emissions for pure hydrogen in a technically premixed case.

Previous investigations revealed that, in the presence of a high momentum [74, 75, 76] or low momentum [70] non-swirling jet the flow field is less prone to exhibit self-excited flow oscillations. Such self-excited flow instabilities were previously observed by Paschereit et al. [77] in swirling combustor flows for both, isothermal and reacting conditions. Galley et al. [78] report a hydrodynamic instability to trap the fuel in a precessing vortex core and lead to strong temporal fuel concentration fluctuations. Consequently, the suppression of a hydrodynamic instability, could increase the temporal mixing quality. This is identified as one possible interaction mechanism between axial injection of air and fuel–air mixing quality.

Terhaar et al. [70] recorded isothermal and reacting flow field data for methane in the presence of varied amounts of axial air injection, which were controlled by a mass flow meter. They present a correlation where, depending on the combination of primary swirl number and amount of axial air injection, the hydrodynamic instability is suppressed. This suppression is observed to coincide with a change in VB type from bubble type to cone type (compare Billant et al. [79]). Whereas the bubble type VB exhibits a local minimum in axial velocity in the plane upstream of VB, the cone type VB does not and is therefore preferred for FB safety.

Depending on the initial swirl number, i.e., swirl in the absence of axial injection, above a certain AI rate, VB is suppressed as reported by Terhaar et al. [70]. Therefore, the use of a central air jet is limited as such, that for the sake of flame stability, a sufficiently large inner recirculation zone has to be preserved at all times. Another potential limiting factor of AI is the fuel–air mixing quality. Application of a central non-swirling jet alters the flow field, reduces the resulting swirl number and, thus, potentially reduces fuel–air mixing quality. However, other mechanisms like the suppression of a hydrodynamic instability could positively affect fuel–air mixing. The net impact of varied AI rates on fuel–air mixing is currently not understood and therefore subject of the current thesis.

1.6.3 Equivalence Ratio / Fuel Momentum

With increasing equivalence ratio, the laminar burning velocity of lean hydrogen–air mixtures increases (Sec. 1.4.5). Therefore, for a given flow field configuration the likelihood of upstream flame propagation in a turbulent flow is increased with equivalence ratio. For conventional fuels like natural gas, even at stoichiometric conditions the fuel volume flow, representative for the fuel momentum, is very low compared to the total volume flow. However, for hydrogen fuel, operation at the same combustor power and fuel injection geometry results in about 3.5 times higher volumetric fuel flow rates in comparison to natural gas. As discussed in Sec. 1.4.6, this translates into a 37% increase in momentum ratio J between fuel and air. The amount of additional momentum introduced into the premixer by the fuel, has the potential to significantly alter the flow field characteristics. Depending on the initial state of the flow field and the fuel injection geometry, the effect of fuel momentum can thus negatively affect FB resistance. However, when accounted for during the design phase, one can take advantage of the additional fuel momentum and utilize it to increase the FB resistance of the burner by properly conditioning the flow field.

To be able to observe the influence of the additional fuel momentum on the flow field, the investigations need to be carried out at partially premixed conditions using a realistic fuel injection geometry. Only in this case, the specific impact of the fuel jets on the combustor flow field can be determined. However, all of the above cited publications utilizing hydrogen or high hydrogen syn gases were conducted at perfectly premixed conditions. In this case, the additional fuel momentum contributes only to an increased bulk flow velocity, which typically preserves the general features of the swirling combustor flow due to its Reynolds number independence [80, 81]. To this end, perfectly premixed conditions are inherently different from partially premixed conditions and not representative of engine conditions with respect to the impact of fuel momentum.

The interaction between the combustor flow field and fuel momentum and its effect on combustor stability has been scarcely investigated in the past. Mayer et al. [82] and Sangl et al. [83] investigated a partially premixed case, where instead of an air jet they applied a non-swirling, axial fuel jet. By shifting the fuel injection mode from trailing edge injection in the radial swirler vanes towards the axial fuel jet they reported a downstream shift of VB under isothermal conditions. Application of their fuel jet at reacting conditions yielded an extension of the FB limits, but also highly increased NO_x emissions.

1.7 Approach

The overall aim of this thesis is to develop a combustor design that is capable of safely operating on hydrogen–air mixtures up to stoichiometric conditions while meeting single

digit NO_x emission below adiabatic flame temperatures of 2000 K. Along this way, several measures affecting the FB resistance of a combustor operating on high reactivity fuels are investigated. Simultaneously to their effect on FB resistance, all measures are evaluated with respect to their impact on fuel–air mixing which directly affects NO_x emissions. To this end, unlike most previous investigations on hydrogen–air combustion, the current investigations are conducted at partially premixed conditions, which poses a challenging task with respect to achieving FB resistance as well as low NO_x emissions with limited premixing space and time. However, these conditions allow for the detailed investigation of fuel momentum and are much more relevant with respect to engine conditions.

First, an investigation of various geometric aspects and their impact on the isothermal combustor flow field was conducted. To this end, the velocity field in the mixing tube and combustion chamber was obtained from particle image velocimetry (PIV) measurements in a water tunnel. Based on the isothermal flow field, the expected FB resistance was evaluated according to the criteria discussed in Sec. 1.6. The investigated parameters included varied AI rates, different initial swirl numbers, and various mixing tube lengths. The most promising configurations were additionally investigated for spatial and temporal fuel–air mixing quality by the means of laser-induced fluorescence (LIF) in a water tunnel. Subsequently, the postulated FB resistance of the identified candidate geometries was tested at reacting conditions in an atmospheric combustion test rig, that also allowed recording of NO_x emissions. Stability maps were recorded which express the operational range of a combustor geometry with respect to FB and lean blow out.

During these first tests, documented in publication 2.1, a somewhat surprising and previously undocumented behavior was observed. While all tested configurations could operate at stoichiometric conditions, FB occurred when decreasing the equivalence ratio at a constant mass flow. At first, it may appear counter-intuitive that FB resistance could be achieved at a higher equivalence ratio, although turbulent burning velocities of lean hydrogen–air mixtures are known to increase with equivalence ratio. It was postulated, that the high volumetric fuel flow rates of hydrogen with increasing equivalence ratio, i.e., the high fuel momentum, cause significant changes in the combustor flow field, which lead to the observed increased FB resistance with increasing equivalence ratio.

To shed further light on the effect of the geometric variations and varied fuel momentum, the interaction of the reacting velocity field and flame stabilization was investigated by the means of simultaneous time-resolved PIV and OH* chemiluminescence measurements (publication 2.2). The downstream shift of VB with increasing AI rates, that was observed at isothermal conditions, was shown to prevail at reacting conditions. Moreover, the OH* chemiluminescence measurements indicated a downstream shift of the upstream flame front with increasing equivalence ratio. This observation supported the hypothesis of the strong impact of fuel momentum on the FB limits and was, thus, investigated in more detail and with a measurement technique capable of unambiguously resolving the upstream flame

front: planar LIF of the hydroxyl radical (OH-PLIF) as documented in publication 2.3.

Previously reported OH-PLIF investigations of high reactivity fuels in gas turbine model combustors were limited either to low hydrogen contents of the fired syn gases [33, 84, 85, 86, 87] or to low equivalence ratios of the neat hydrogen [88], presumably due to scope or stability issues. Therefore, the current OH-PLIF investigation covers a previously unprecedented range of operating conditions, especially, with respect to high equivalence ratios up to stoichiometric conditions. Within the institute, this was the first time that the OH-PLIF technique was applied in the atmospheric combustion test rig for such a high combustor power up to $P = 200$ kW and a large combustion chamber diameter of 105 mm.

The main aim of the investigations was not only to quantify the impact of fuel momentum, but also to identify a governing parameter that correlates fuel momentum with FB resistance. The fuel–air momentum ratio J was identified to correlate with the upstream flame front location x_f over a wide range of operating conditions and geometrical variations. The OH-PLIF measurements in the atmospheric combustion test rig were accompanied by another exhaustive water tunnel campaign aiming to identify the combined effect of axial injection and fuel momentum on the isothermal combustor flow field.

Next, an effort was made to determine a quantity that reliably judges a combustors FB resistance and is experimentally accessible with moderate efforts. Candidates were the axial location of VB, x_VB, which is reportedly sensitive to both AI and fuel momentum [83] and the axial location of the leading edge flame front, which is reported to travel upstream when approaching conditions where FB occurs [2, 33, 86]. Both flow features are evaluated regarding their suitability as an indicator of the FB safety margin for the respective condition, as is reported in publication 2.4.

The experimental results of this thesis, presented hereafter, should put us in the position to answer the following questions:

1. Which measures are most effective in extending the flashback limits in premixed hydrogen combustion?
2. Do different measures against flashback interact or interfere?
3. What is the trade-off for flashback resistance?
4. What are suitable estimators for flashback resistance?

CHAPTER 2

Publications

The following pages include the publications, which are discussed in the subsequent chapter.

2.1 [1] Reichel, T. G., Terhaar, S., and Paschereit, C. O. (2017[1]). Flashback Resistance and Fuel–Air Mixing in Lean Premixed Hydrogen Combustion, *Journal of Propulsion and Power, (2017),* accessed October 12, 2017
doi:10.2514/1.B36646

2.2 [2] Reichel, T. G., Terhaar, S., and Paschereit, C. O. Increasing Flashback Resistance in Lean Premixed Swirl-Stabilized Hydrogen Combustion by Axial Air Injection. *Journal of Engineering for Gas Turbines and Power*, Bd. 137 (2015) (7): 071503.
doi:10.1115/1.4029119

2.3 [3] Reichel, T. G., Göckeler, K., and Paschereit, C. O. Investigation of Lean Premixed Swirl-Stabilized Hydrogen Burner With Axial Air Injection Using OH-PLIF Imaging. *Journal of Engineering for Gas Turbines and Power*, Bd. 137 (2015) (11): 111513.
doi:10.1115/1.4031181

2.4 [4] Reichel, T. G. & Paschereit, C. O., Interaction Mechanisms of Fuel Momentum with Flashback Limits in Lean-Premixed Combustion of Hydrogen: *International Journal of Hydrogen Energy*, Bd. 42 (2017) (7): 4518–4529
doi:10.1016/j.ijhydene.2016.11.018

1 The *Journal of Propulsion and Power* publication is based on a conference paper [5] from the *43rd AIAA Fluid Dynamics Conference and Exhibit* in 2013 and is therefore placed first in this chronological listing of publications.

2.1 First Publication

Flashback Resistance and Fuel–Air Mixing in Lean Premixed Hydrogen Combustion

Thoralf G. Reichel,* Steffen Terhaar,* and Christian Oliver Paschereit†
Technische Universität Berlin, 10623 Berlin, Germany

DOI: 10.2514/1.B36646

To prevent flame flashback in swirl-stabilized, lean premixed combustion, a nonswirling air jet is introduced on the central axis of the radial swirl generator. This axial injection of air alters the flowfield as required for flashback-resistant combustion of premixed hydrogen. This study evaluates the impact of axial injection on the isothermal flowfield in a water tunnel by particle image velocimetry. Atmospheric reacting tests with hydrogen for inlet temperatures up to 620 K and up to stoichiometric conditions show a substantial increase in flashback resistance for the burner setup with axial injection. To verify the increase in flashback resistance to not be achieved at the expense of increased NO_x emissions, fuel–air mixing is evaluated in a water tunnel by planar laser-induced fluorescence of a fuel tracer. Even for high axial injection rates, the recorded unmixedness and NO_x emissions are uncorrelated. This results in single-digit NO_x emissions below adiabatic flame temperatures of 2000 K. Consequently, axial injection significantly extends the operational range of the combustor without increasing the NO_x emissions.

Nomenclature

$C(\boldsymbol{x}, t)$	=	local mixture concentration
C_{hom}	=	homogeneous mixture concentration
C_{∞}^{*}	=	maximum mixture concentration
D	=	burner outlet diameter
D_{or}	=	orifice diameter for axial air injection
G_x	=	axial thrust
G_{ϕ}	=	axial flux of angular momentum
J	=	fuel–air momentum flux ratio
l_b	=	Batchelor scale
l_k	=	Kolmogorov microscale
l_{mt}	=	length of mixing tube
S	=	geometric swirl number
T_{ad}	=	theoretic adiabatic flame temperature
T_{in}	=	air inlet temperature
U_s	=	spatial unmixedness
U_t	=	temporal unmixedness
u_{t0}	=	bulk velocity at the nozzle outlet
$\dot{V}$	=	volume flow
ϵ	=	dissipation rate
Λ^x	=	integral macroscale
ν	=	kinematic viscosity
χ	=	axial air injection ratio
$\overline{(\cdot)}$	=	temporal averaging operator
$\langle\cdot\rangle$	=	spatial averaging operator

I. Introduction

FUTURE demands on air transport systems dictate that aircraft should be less polluting, less noisy, and more fuel-efficient. In the long term, alternative fuels, such as biofuels and hydrogen, are likely to replace traditional jet fuel [1–3]. Hydrogen is an excellent candidate fuel for aviation, due to its very high specific energy content per unit mass (Fig. 1) and the absence of any CO_2 in the direct emissions. Experimental tests on a low NO_x hydrogen combustor for aeroengines have been conducted within the European Union-supported Seventh Framework Programme (FP7) project Advanced Hybrid Engines for Aircraft Development (AHEAD). The concept proposed in the AHEAD project is a contra-rotating turbofan engine with sequential dual hybrid combustors using two different fuels [4]. The engine is operated on pure hydrogen in the first stage and biofuel under flameless conditions [5] in the second stage, aiming to reduce CO_2 and NO_x emissions, respectively. The concept addresses the challenge of increased drag from storing cylindrical hydrogen tanks by the dual-fuel approach as well as using a blended wing–body airplane. Such an airplane configuration has inherent extra volume, which can be used to accommodate the cylindrical fuel tanks. The current study focuses on the lean premixed, swirl-stabilized hydrogen combustion of the first stage. It is, therefore, also relevant to syngas combustion in integrated gasification combined cycles, where the burned syngases are mainly composed of CO, CH_4, and H_2, with an H_2 content of up to 50% by volume. Pure hydrogen is, thus, a meaningful test case for flashback (FB) resistance of a burner geometry.

For lean premixed combustion with increasing fuel reactivity, lean blowout (LBO) limits are extended, offering excellent potential for low NO_x emissions [6–8]. Simultaneously, FB disposition is increased. FB denotes the upstream propagation of a flame in a combustible mixture into regions not designed for flame holding and poses an operability limit for gas turbine combustors [9]. The increased FB propensity of various mixtures with increasing hydrogen content has been investigated in numerous studies [10–16]. Detailed investigations regarding the effect of inlet or outlet conditions by Syred et al. [15], swirl number by Sayad et al. [16], or hydrodynamic instability by Schönborn et al. [17] on the stability limits of high-hydrogen-content fuels have been reported.

To minimize the FB risk in hydrogen–air combustion, Marek et al. [18] pursued the approach of lean direct injection (LDI). The LDI technology maintains high flow velocities and very short premixer residence times to minimize FB. Additionally, the multiple injection points lead to distributed heat release, which prevents hot spots detrimental for NO_x emissions. Marek et al. report FB limits and NO_x emissions at elevated air preheat temperatures and pressures up to 7 bar. They conclude that the best investigated configuration yields satisfying FB characteristics and NO_x emissions comparable to state of the art Jet-A LDI combustor concepts. However, they also report difficulties to achieve uniform fuel distribution to the numerous injections ports and cooling problems due to the hydrogen flame anchoring close to the injectors, which lead to failure during test execution.

Similar to other modern premixer concepts [19], in the current study, a cylindrical mixing tube without center body is used to ensure

Presented as Paper 2013-2603 at the 43rd AIAA Fluid Dynamics Conference, San Diego, CA, 24–27 June 2013; received 17 February 2017; revision received 1 September 2017; accepted for publication 2 September 2017; published online 5 October 2017.

*Ph.D. Student, Chair of Fluid Dynamics, Hermann-Föttinger-Institut, Mueller-Breslau-Str. 8.

†Professor, Chair of Fluid Dynamics, Hermann-Föttinger-Institut, Mueller-Breslau-Str. 8.

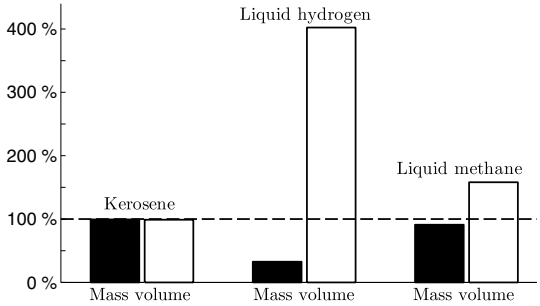

Fig. 1 Comparison of mass and volume of aviation fuels for equivalent energy content.

sufficient mixing. The swirling flow downstream of such a mixing tube or nozzle without center body exhibits a flowfield with a recirculation zone, whose vortex breakdown under most conditions is situated just at or even upstream of the nozzle exit. Mayer et al. [20] showed that, without further effort, such a flowfield is prone to combustion-induced FB for high reactivity fuels. For the prevention of flame FB into the premixing section, the combustor flowfield is of utmost importance. To avoid FB due to turbulent flame propagation in the core flow and combustion-induced vortex breakdown [21], "a major design criterion for nozzle aerodynamics is that the axial velocity must be as high and as uniform as possible and free of strong wakes" [12]. To meet these criteria, Burmberger and Sattelmayer [22] suggested that the combustor should employ a nonswirling air jet on the central axis of the radial swirl generator, which ultimately leads to an increasing axial velocity on the axis of rotation, moving the vortex breakdown away from the mixing tube exit. This idea is adapted and exploited in the current burner setup.

The ratio of axially injected, nonswirling airflow to total airflow is defined as $\chi = \dot{V}_{ax}/(\dot{V}_{ax} + \dot{V}_{swirl})$. A burner employing axial injection (AI) of air in the range $\chi = 7.5$–12.5% was shown to significantly extend the FB limits of a model combustor in a previous study by the authors [23,24]. In this context, the high volumetric fuel flow rates associated to hydrogen fuel were reported to strongly affect stability limits, which was further investigated in Reichel et al. [25]. Generally, when increasing the equivalence ratio at a fixed air mass flow, on the one hand, additional fuel momentum is introduced into the system, which can promote a downstream shift of the flame front because it alters the flowfield and increases the local axial velocities. Simultaneously, the burning velocity of lean premixed hydrogen–air mixtures increases with increasing equivalence ratio, which would promote an upstream shift of the flame front. However, Reichel et al. [25] reported a net downstream shift of the upstream flame front with increasing equivalence ratio, which revealed that the impact of the fuel momentum supersedes the impact of the simultaneous augmentation in flame speed.

To the knowledge of the authors, the impact of a central jet on fuel–air mixing has not been investigated, although fuel–air mixing is of paramount importance for NO_x emissions. For lean fuel–air mixtures, NO_x emissions increase exponentially with temperature. It is thus desirable to achieve the overall equivalence ratio over the entire flame front, at all times. Fuel–air mixtures that burn closer to stoichiometric result in higher emitted levels of NO_x. Mixtures that burn leaner than the overall equivalence ratio show reduced NO_x emissions. However, because of the nonlinearity of this effect, the net effect is an increase in NO_x emissions [26]. Previous work successfully related mixing quality to NO_x emissions via the spatial and temporal unmixedness parameters U_s and U_t suggested by Danckwerts [27]. These previous correlations of unmixedness and NO_x emissions were obtained either numerically [28,29] or experimentally by correlating NO_x emissions from reacting tests with unmixedness parameters from cold flow experiments in air [26] or water [30–33]. The latter approach is also pursued in the current study to quantitatively compare the fuel distribution of different swirling combustor flow configurations.

Galley et al. [34] investigated fuel–air mixing in a configuration similar to the one used in the current investigation, also employing a radial swirler and a mixing tube without center body, in absence, however, of AI. They identified a fuel-rich mixing pattern in the shape of a comma, originating from the fuel-rich core flow in the mixing tube, which describes a precessing motion as it enters the combustion chamber. Moreover, they suggested a link between the mixing pattern and the precessing vortex core (PVC), that is, a helical self-excited coherent structure occurring in swirling flows after the onset of vortex breakdown [35]. Paschereit et al. [36] showed that, for the same burner, the helical mode of the isothermal flow from a water tunnel corresponded to the helical mode in the reacting experiments when they investigated the reacting and nonreacting flows in a model premixed burner. The impact of a nonswirling jet on the PVC, in the absence [37–39] and presence [40] of a mixing tube, was investigated earlier. All authors reported the PVC to be suppressed in the presence of a nonswirling, central jet. However, none of the authors investigated the impact of AI on fuel–air mixing.

The aim of the work presented in this paper is to investigate the effect of varied levels of AI on the combustor flowfield with respect to varied burner geometries such as swirl number and mixing tube length (Table 1). The combustor flowfield is obtained from particle image velocimetry (PIV) in a water tunnel and evaluated with respect to achieving the required shape for FB-resistant operation. Subsequently, the postulated FB resistance is confirmed in reacting tests. The flame is verified by OH* imaging to remain anchored in the combustion chamber. Furthermore, to quantify the impact of AI on the mixing quality, and hence NO_x emissions, the spatial and temporal unmixedness are evaluated by quantitative planar laser-induced fluorescence (PLIF) measurements in a water tunnel. The unmixedness data are compared to NO_x emissions, recorded in reacting tests. The results of this study show the feasibility of FB prevention in a lean premixed, swirl-stabilized hydrogen combustor while maintaining very low NO_x emissions.

II. Experimental Setup and Diagnostics

A. Burner Design

A detailed drawing of the investigated swirl burner is given in Fig. 2. The burner incorporates the concept of a nonswirling central air jet, suggested by Burmberger and Sattelmayer [22], into an existing geometry previously used for natural gas combustion at dry and steam-diluted conditions [41,42]. The nonswirling central air jet, termed AI of air, successfully extends the application range of the burner to hydrogen–air combustion, as was demonstrated in previous work by the authors [23,24].

The main airflow can enter the cylindrical mixing tube via two paths: first, through the radial swirl generator, whereby a certain amount of swirl is imposed on the flow depending on the number of blocking rings used, and second, through a variable-size orifice on the central axis, constituting the AI.

According to Beér and Chigier [43] the swirl number S' is defined as a nondimensional criterion to characterize the amount of rotation imparted on the flow:

$$S' = \frac{G_\phi}{G_x \cdot R} \tag{1}$$

where R is the radius, G_ϕ is the axial flux of angular momentum, and G_x is the axial thrust. These are defined as

Table 1 Investigated configurations of the burner concept

Configuration	Swirl number	Mixing tube length l_{mt}, mm	AI rate, % (of total mass flow)
1	0.7	40	[0, 7.5, 12.5]
2	0.7	60	[0, 7.5, 12.5]
3	0.9	40	[0, 7.5, 12.5]
4	0.9	60	[0, 7.5, 12.5]

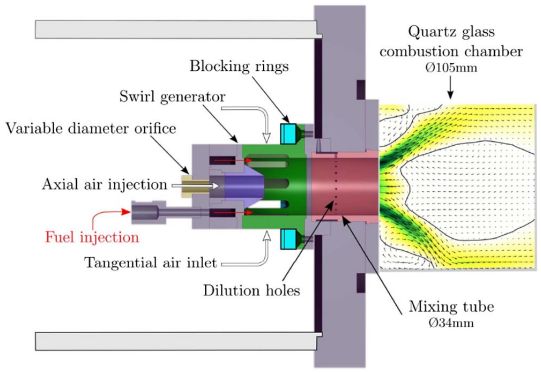

Fig. 2 Schematic of burner model, indicating different volume flow pathways through swirl generator or axial injection.

$$G_\phi = \int_0^R U_t \rho U 2\pi r \, \mathrm{d}r \tag{2}$$

$$G_x = \int_0^R U \rho U 2\pi r \, \mathrm{d}r + \int_0^R p 2\pi r \, \mathrm{d}r \tag{3}$$

In an effort to define a geometric swirl number S, which depends entirely on the burner geometry, Beér and Chigier [43] suggested neglecting the static pressure term and radial dependence of U in Eq. (3) and introducing the parameter $\sigma = \sigma(z, s, \alpha)$, which is only a function of geometrical dimensions of the radial swirler, in Eq. (2). This yields

$$G'_\phi = \sigma \frac{\dot{m}^2}{\rho 2\pi l_s}$$
$$G'_x = \frac{\dot{m}^2}{2\pi\rho R}$$

Consequently, one can define the geometric swirl number S, depending only on the geometrical dimensions slot length l_s and radius R of the radial swirler:

$$S = \frac{G'_\phi}{G'_x \cdot R} \tag{4}$$

For the current study, either a 4 or 7 mm blocking ring was used, which yielded a geometric swirl number of $S = 0.7$ and $S = 0.9$, respectively. The fuel was injected into the premixing section through 16 injection ports located on an annular ring around the truncated center body. The mixing tube was located downstream of the swirl generator and had an inner diameter of $D = 34$ mm. A short ($l_{\mathrm{mt}} = 40$ mm, displayed in Fig. 2) and a long ($l_{\mathrm{mt}} = 60$ mm) mixing tube were tested. Dilution holes, distributed around the circumference of the mixing tube at $x/D = -0.7$, are clearly visible; their purpose was to reduce the near-wall equivalence ratio to prevent boundary-layer FB.

Varying the orifice diameter D_{or} allowed to adjust the ratio of axially injected, nonswirling volume flow to total volume flow $\chi = \dot{V}_{\mathrm{ax}}/(\dot{V}_{\mathrm{ax}} + \dot{V}_{\mathrm{swirl}})$. For a given orifice diameter D_{or}, the amount of axially injected air was not metered but would adjust based on the ratio of pressure loss between the swirl generator and axial injection orifice. The values of $\chi = 7.5\%$ and $\chi = 12.5\%$ correspond to an orifice diameter of $D_{\mathrm{or}} = 8.0$ mm and $D_{\mathrm{or}} = 8.8$ mm, respectively. They were validated by a numerical investigation using RANS and LES by Tanneberger et al. [44].

Because of the high absolute value of the primary zone flame temperature, which exceeds the measurement range of thermocouples, it was not determined experimentally. Instead, the calculated adiabatic flame temperature T_{ad} was used to differentiate between operating conditions with respect to equivalence ratio and air preheating. Note that, because of neglecting heat loss, T_{ad} represents a slight overestimation of the actual primary zone flame temperature.

B. Water-Tunnel Setup

Water-tunnel testing is a cost effective, flexible, and rapid way to investigate turbulent flow and mixing phenomena of the flow inside the mixing tube as well as in the combustion chamber for a variety of combustor geometries. For the mixing experiments, a water flow mixed with dye represented the fuel and was injected through the fuel injection holes. For the velocity measurements, seeding was added to both the main and fuel flow. The 400×400 mm vertical test section allowed optical access to the streamwise plane from four sides (PIV setup, Fig. 3b) as well as to the crosswise plane from the downstream end of the combustion chamber (LIF setup, Fig. 3a). An acrylic glass model of the burner that maintained exact geometric similarity was designed and placed in the test section. Other than the stainless steel burner, the new burner model provided full optical access to the premixing section. The Reynolds number was set to 40,000 with respect to the diameter D of the mixing tube to comply with the Reynolds number from the reacting tests. The density ratio of the two water flows representing air and fuel in the water test rig deviates from the density ratio of fuel and air in the atmospheric test rig. Therefore, the momentum ratio J was kept constant to achieve similarity between the experiments on both platforms:

$$J = \frac{\rho_{\mathrm{fuel}} u^2_{\mathrm{fuel}}}{\rho_{\mathrm{air}} u^2_{\mathrm{air}}} \tag{5}$$

To justify the comparison of the current water and air test rig, Lacarelle [45] compared the mean and fluctuating velocities obtained from PIV and achieved excellent agreement between both platforms. Also, the mean concentration distributions obtained from either PLIF (water) or Mie scattering (air) showed very good agreement. Moreover, according to Lacarelle [45], maintaining both Reynolds number similarity ($Re_a = Re_w$) and geometric similarity ($\Lambda^x_a = \Lambda^x_w$) between the two fluids water (index w) and air (index a) yields similarity in turbulent Reynolds number $Re_t = u'_{\Lambda^x}\Lambda^x/\nu$, which then yields identical Kolmogorov length scales in air and water $l_{k,a} = l_{k,w}$. Hence, if Reynolds similarity is conserved between two fluids used to investigate one setup, both the turbulent macro- and microscales are identical. This property is, however, not true for passive scalars like concentration or temperature. In this case, the fluid properties, in particular the coefficient of diffusivity of a specie A in the medium B, Γ_{AB}, play an important role and vary greatly between the fluids considered. The scale at which the molecular diffusion takes place is called the Batchelor scale and, according to [45], is defined as

$$l_b = \left(\frac{\nu \Gamma^2_{AB}}{\epsilon}\right)^{1/4} \tag{6}$$

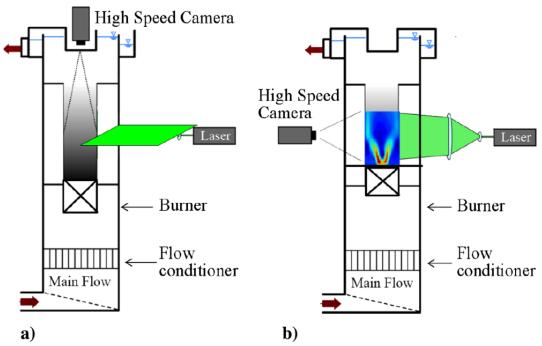

Fig. 3 Schematic of water test rig and the experimental setups for a) PLIF, and b) PIV measurements.

The dimensionless Schmidt number can be written as

$$Sc = \frac{\nu}{\Gamma_{AB}} \tag{7}$$

Combining Eqs. (6) and (7) yields

$$l_b = l_k / Sc^{0.5} \tag{8}$$

For airflows, the Schmidt number verifies $Sc \approx 1$, whereas in aqueous solutions, typical Schmidt numbers are of the order $Sc \approx 10^3$. This means that the Batchelor scale l_b is approximately equal to the Kolmogorov dissipation scale l_k in air, whereas in water it is approximately 30 times smaller. It is concluded that water-tunnel results will always give a conservative estimation of the fuel–air mixing quality because molecular diffusion is underestimated.

1. Particle Image Velocimetry Setup in the Water Test Rig

High-speed particle image velocimetry using a double-pulsed Nd:YLF laser (0.75 kHz) with a wavelength of 527 nm and a pulse energy of 30 mJ per pulse was applied. The laser light sheet illuminated the streamwise plane downstream of the burner exit. The flow was seeded by adding silver-coated hollow glass spheres with a nominal diameter of 15 μm to the water. The scattered light is detected by a high-speed complementary metal–oxide–semiconductor (CMOS) camera recording at 1500 Hz with a resolution of 7.2 pixel/mm. The pulse separation was set to 0.1 to 0.2 ms, depending on the volume flow. For the cross-correlation, an interrogation area of 16×16 pixels and 50% overlapping was selected. This resulted in a vector spacing of 1.6 mm. The data were filtered for outliers (typically less than 2%) and interpolated from adjacent interrogation areas. Based on the uncertainty of the correlation peak-finding algorithm of 0.1 pixel, the random uncertainty of the instantaneous velocities is estimated as 0.07–0.1 m/s, depending on the pulse separation and the camera magnification. This error, which is approximately 4.5–6% of the bulk velocity, contributes mostly to the rms error. The velocity fields were averaged over 1000 image pairs and normalized with the bulk velocity u_0 at the burner exit.

2. Planar Laser-Induced Fluorescence Setup in the Water Test Rig

For the mixing experiments in the water tunnel, the PLIF method was applied. The measurements provided insight into spatial as well as temporal mixing quality in a plane parallel to the nozzle exit plane, 2 mm downstream of the sudden expansion of the combustion chamber. The same high-speed laser as for the PIV measurements, operating in single pulse mode, excited Rhodamine G6 dye, which was added to the water representing the fuel and emitted fluorescence radiation at a wavelength of 550 nm. A band-pass-filtered high-speed CMOS camera, which was mounted perpendicular to the measurement plane, recorded 3000 images with a frame rate of 1000 frames per second and a spatial resolution of 4 pixel/mm. Lacarelle [45] reports the accuracy of the LIF system, calculated from reference concentrations taken during different measurement campaigns. The measured concentration with respect to the set concentration exhibits a bias of 2.5% at the investigated volume flow, which is due to small variations in the main flow.

3. Evaluation of Mixing Quality

The local concentration of the mixture $C(\boldsymbol{x}, t)$ was obtained from the measured light intensity of the fluorescence $I(\boldsymbol{x}, t)$. The background intensity $I_{\text{back}}(\boldsymbol{x}, t)$ was subtracted, and the measured intensity was related to the intensity $I_{\text{hom}}(\boldsymbol{x}, t)$ of a known homogeneous concentration C_{hom}:

$$C(\boldsymbol{x}, t) = C_{\text{hom}} \cdot \frac{I(\boldsymbol{x}, t) - I_{\text{back}}(\boldsymbol{x}, t)}{I_{\text{hom}}(\boldsymbol{x}, t) - I_{\text{back}}(\boldsymbol{x}, t)}$$

To evaluate the mixing quality of a configuration, the Danckwerts [27] unmixedness parameter U was used, defined as

$$U = \frac{\sigma^2}{\sigma_0^2} = \frac{\sigma^2}{C_\infty^*(1 - C_\infty^*)} \tag{9}$$

Here, σ_0 is the maximum variance determined from the highest possible concentration, the initial concentration of the injected fuel C_∞^*. The elegance of using U to quantify unmixedness is that its value ranges from 0 for a perfectly mixed case to 1 for a case of maximum variance. Depending on how the variance σ of the mixture is calculated, Eq. (9) yields either the spatial unmixedness $U_s = \sigma_x^2/\sigma_0^2$ or temporal unmixedness $U_t = \sigma_t^2/\sigma_0^2$ with

$$\sigma_x^2 = \langle (\overline{C(\boldsymbol{x})} - \langle \overline{C} \rangle)^2 \rangle \text{ and } \sigma_t^2 = \overline{\langle (C(\boldsymbol{x}, t) - \langle \overline{C} \rangle)^2 \rangle}$$

The spatial unmixedness U_s is independent of the amplitude of any temporal fluctuations in the mixing field because only the time-averaged concentration $\overline{C(x)}$ is considered. It is, hence, a measure of the time-averaged spatial distribution of fuel. Other than the spatial, the temporal unmixedness U_t does consider temporal fluctuations in the calculation of the variance σ_t and is thus a measure of the temporal fluctuations in the mixing field. The spatial and temporal unmixedness yield a scalar value. Hence, the normalized time mean concentration

$$\overline{C(\boldsymbol{x})} / \langle \overline{C} \rangle$$

and the normalized time mean spatial variance

$$\sigma_t'^2/\sigma_0^2 = \overline{(C(\boldsymbol{x}, t) - \langle \overline{C} \rangle)^2}/\sigma_0^2$$

are plotted in the results section, respectively. Because of their lack of spatial averaging they still contain the information of the spatial distribution.

C. Combustion Test Rig for OH* Imaging and Emission Measurements

A schematic drawing of the atmospheric combustor test rig used for the present investigations is given in Fig. 4. At a mass flow of 180 kg/h, the air entering the swirl generator was preheated up to $T_{\text{in}} = 620$ K. The 105-mm-diam quartz glass combustion chamber was located downstream of the burner model, separated by a sudden expansion. The location of the flame was captured using a band-pass-filtered intensified charge-coupled device camera for the chemiluminescence of the OH* radical, which correlates with the location of heat release. The Reynolds number during the experiments was varied between 40,000 and 60,000. Exhaust gas was extracted 850 mm downstream of the burner outlet and transported through a heated tube to a cold steam trap to remove humidity. It was then analyzed for CO (±1%), NO (±0.8%), NO_2 (±1.5%), O_2 (±1%), and CO_2 (±1%) on a dry basis. The given measurement uncertainties denote relative quantities from the measured value and are based on the calibration of the gas analyzer.

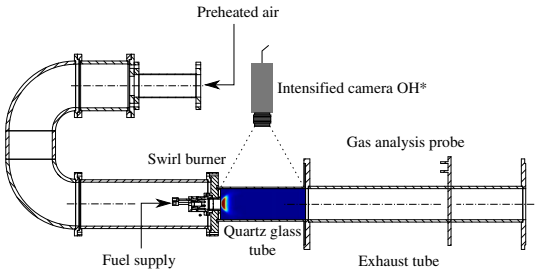

Fig. 4 Experimental setup of atmospheric combustion test rig.

III. Results and Discussion

A. Flowfield Obtained from Water-Tunnel Testing

To assess the general impact of varied AI rates on the velocity field inside the mixing tube and combustion chamber, the combustor flowfield is obtained from PIV measurements in the water test rig. Configuration 4 in the absence and presence of a medium ($\chi = 7.5\%$) and high amount ($\chi = 12.5\%$) of AI is given in Figs. 5a–5c, respectively. Under all investigated conditions, vortex breakdown was established downstream of the area expansion. This led to the typical flowfield of swirl-stabilized combustors, which consists of an inner recirculation zone (IRZ), enveloped by an annular jet, and an outer recirculation zone between the annular jet and the bounding walls.

In the absence of AI ($\chi = 0\%$), the IRZ extended upstream to the nozzle outlet (Fig. 5a). The line of zero axial velocity, indicated by the solid black line, was, on the central axis, located directly at the nozzle exit at $x/D < 0.1$. The flowfield inside the mixing tube exhibited a

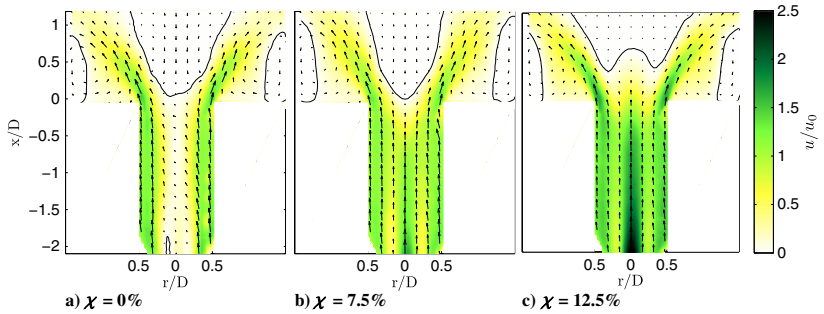

Fig. 5 Time-averaged flowfields at increasing AI rates for configuration 4, with solid lines indicating zero axial velocity obtained in the water test rig.

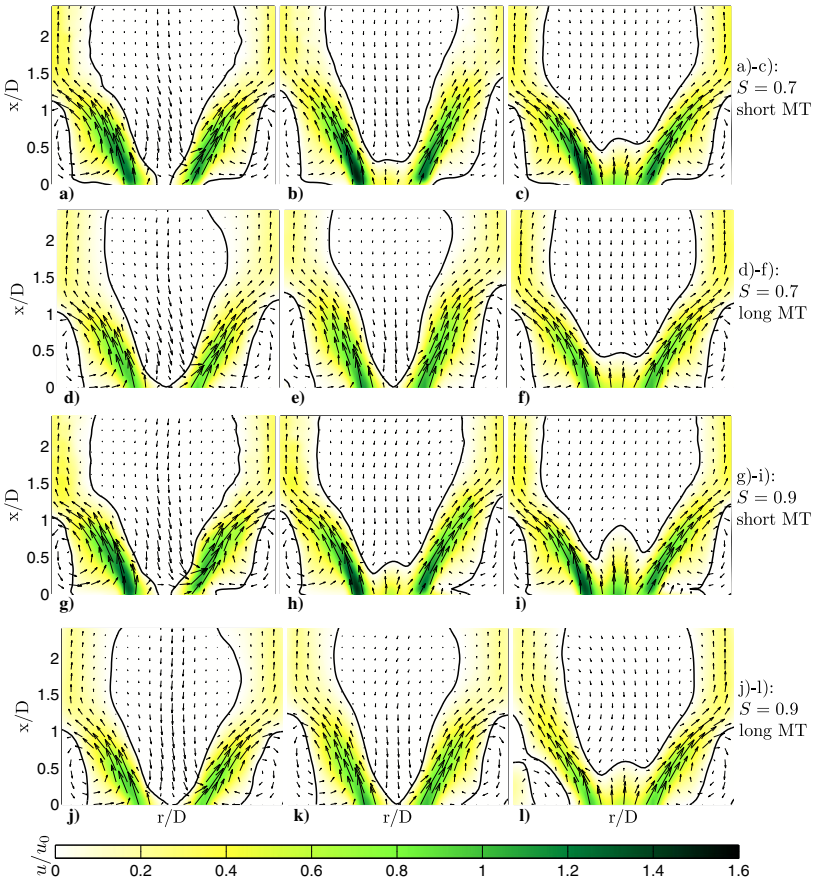

Fig. 6 Time-averaged flowfields at increasing AI rates for configuration 1–4 (from top to bottom). From left to right, $\chi = 0$, 7.5, and 12.5% obtained in the water test rig.

deficit in axial velocity toward the centerline for the entire length of the mixing tube. Reacting tests reported in Sec. III.B revealed that such a flowfield did not allow for flame stabilization downstream of the nozzle exit when the burner is operated with premixed hydrogen.

In case of a medium amount of AI ($\chi = 7.5\%$), the flowfield in the combustion chamber of configuration 4 remained nearly unaffected. The opening angle of the CRZ was slightly reduced, which is attributed to the slightly reduced swirl number due to AI. However, strong changes were observed in the mixing tube. There, the deficit in axial velocity on the central axis was overcome, and the axial injection yielded a more homogeneous radial distribution of axial velocity along the mixing tube.

Further increasing the amount of AI to $\chi = 12.5\%$ led to additional flowfield changes in the combustion chamber. As desired for FB resistance, a downstream shift of the stagnation point on the central axis to $x/D = 0.7$ was observed. Inside the mixing tube, strong radial gradients in axial velocity due to the central jet were detected, which, however, declined along the path through the premixing section, achieving the desired plug-flow shape at the mixing tube exit.

A similar effect of AI was also observed for configurations 1–3, representing varied swirl numbers and mixing tube lengths. A comprehensive overview of configurations 1–4 is given in Fig. 6. The results indicate two interesting findings. First, for a long mixing tube, only an AI rate of $\chi = 12.5\%$ achieved the plug-flow shaped velocity profile at the mixing tube outlet, which is desired for FB resistance. Second, for a short mixing tube, a medium AI rate of $\chi = 7.5\%$ might be sufficient to suppress FB. For the short mixing tube and a high AI rate ($\chi = 12.5\%$), an axial velocity overshoot was observed (see Fig. 6i), which potentially degrades both flame stability and fuel–air mixing, as is further investigated in the next section. In a next step, the postulated increased FB resistance is evaluated from the combustors stability limits for varied AI rates, which were recorded in the atmospheric combustion test rig.

B. Stability Maps Obtained from Reacting Tests

Configurations 1–4 were investigated in reacting tests to, first, confirm the predicted FB resistance and, second, record NO_x emissions for correlation with the respective unmixedness parameters obtained from the water-tunnel tests (Sec. III.E). Note that, for all configurations, at least a medium AI rate ($\chi = 7.5\%$) was necessary to operate on a high-reactivity fuel such as premixed hydrogen. For $\chi = 0\%$, the onset of FB limited the operational range so much that the recording of a proper stability map was not possible.

Applying a medium rate of AI ($\chi = 7.5\%$) sufficiently increased the FB resistance to allow stability maps to be recorded (left column, Fig. 7). Only mass flows within the range $22 < m_{air} < 50\,g/s$ for $T_{in} = 620\,K$ (below $\dot{m}_{air} < 66\,g/s$ for 450 K) were investigated due to the limitation of the test rig to provide the respective inlet temperature outside of this mass flow range. All configurations were capable of operating at $\phi = 1$ without FB. For these conditions, OH* imaging confirms that the flame remained anchored in the combustion chamber (Fig. 8). In the shear layer, the flame burns closer to the burner rim; however, the upstream flame front on the central burner axis is located well downstream of the mixing tube outlet, which was previously reported as a positive estimator for FB resistance [25]. The lower limits of all configurations revealed a strong dependence on the air mass flow rate and stem from either LBO or FB.

For $\chi = 7.5\%$, only for configurations 2 and 4, at the highest investigated air mass flow $\dot{m} = 66\,g/s$, the lower limit was caused by LBO at an equivalence ratio as low as $\phi = 0.2$ (symbol ◁). For all other configurations and air mass flows, the lower limit occurred due to FB, although no FB occurred at the higher equivalence ratios (symbol ◀). At first glance, it might surprise that a higher equivalence ratio at constant air mass flow achieves higher FB resistance, even though turbulent burning velocities of lean hydrogen–air mixtures are known to increase with equivalence ratio. However, a previous study of the authors [25] revealed the high volumetric fuel flow rates of hydrogen to cause significant changes in the combustor flowfield already at moderate equivalence ratios. Similar to increasing AI rates, an increasing equivalence ratio increases the axial velocities and homogenizes their

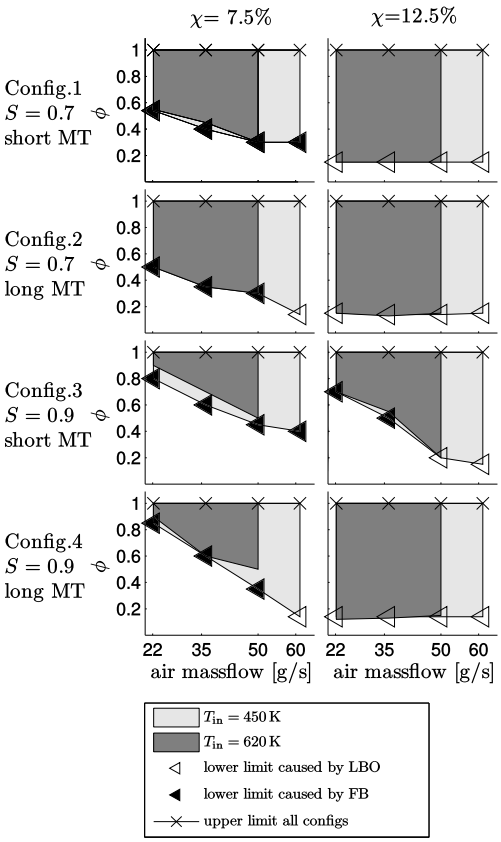

Fig. 7 Combustor operational range for medium ($\chi = 7.5\%$, left column) and high ($\chi = 12.5\%$, right column) AI rates at two air preheat temperatures; not tested for $\phi > 1$.

radial distribution. The elevated axial velocities due to the increased equivalence ratio were shown to outweigh any parallel augmentation in turbulent burning velocity, which manifests in a downstream shift of the flame front and results in increased FB resistance.

Because of the occurrence of FB as the lower stability limit, the $\chi = 7.5\%$ case allows to identify the impact of geometric parameters and operating conditions on FB limits (e.g., swirl number S, mixing tube length l_{mt}, and preheat temperature T_{in}). Generally, the lower swirl number $S = 0.7$ results in higher axial velocities at the mixing tube outlet compared to $S = 0.9$ (Fig. 6). This explains the extended lower stability limit of configuration 1 compared to 3 and configuration 2 compared to 4.

The larger mixing tube length l_{mt} has a positive effect as it slightly extends the FB limits. This is assumed to stem, on the one hand, from the homogenization of axial velocity gradients in radial direction at the mixing tube outlet with larger l_{mt} (compare Figs. 6i and 6l). On the other hand, increasing l_{mt} also improves fuel–air mixing and, therefore, prevents fuel-rich pockets, which otherwise would locally increase the burning velocity and, thus, increase FB propensity (compare Figs. 9i and 9l).

Increasing the air preheat temperature, generally, could extend the LBO limits. However, in the current case, where the lower stability limits is posed by FB instead of LBO, the increasing burning velocity of the combustible mixture with increased temperature promotes an earlier occurrence of FB and leads to the reduced stability limits at higher preheat temperatures.

Increasing the AI rate to ($\chi = 12.5\%$) further increased the FB resistance and substantially extended the operational range of all

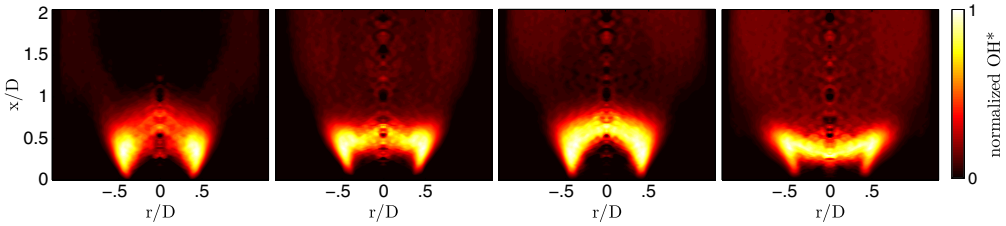

Fig. 8 Time-averaged, Abel-deconvoluted OH* images of configurations 1–4 ($\phi = 1, \chi = 12.5\%, T_{in} = 620$ K).

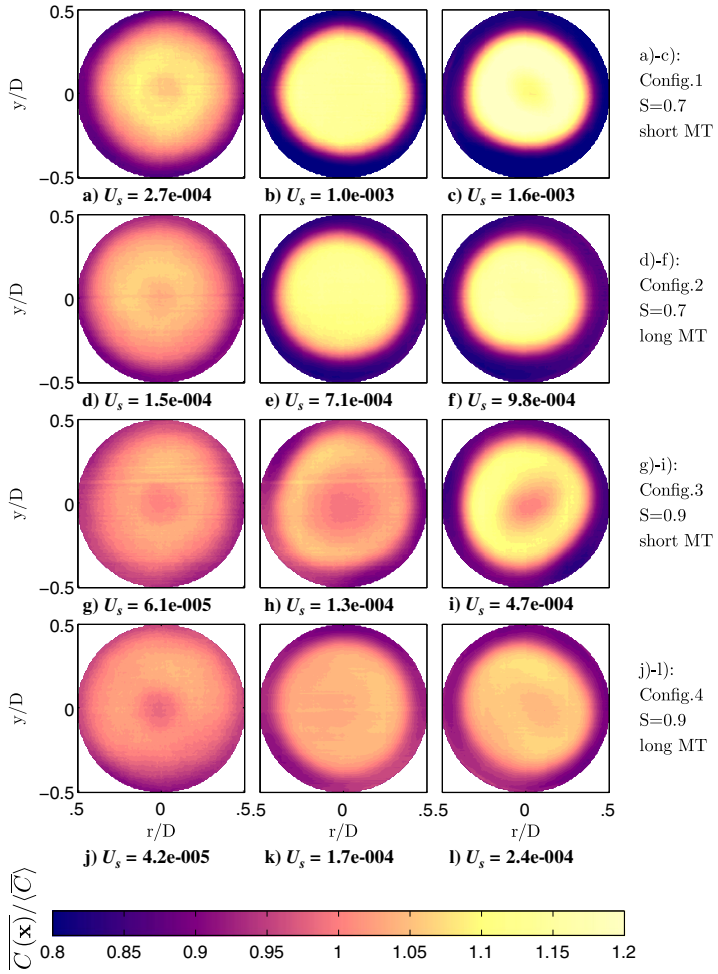

Fig. 9 Mean normalized fuel concentration obtained in the water test rig. From left to right, $\chi = 0$, 7.5, and 12.5%. Configurations 1–4 are shown from top to bottom.

investigated configurations and preheat temperatures (right column, Fig. 7). For configurations 1, 2, and 4, no FB occurred on the entire investigated operational range. The LBO limits were extended to an equivalence ratio as low as $\phi = 0.15$. For configuration 3, the increased AI rate also extended the operational range. However, the lower limit of the operational range remained restricted by FB for mass flow rates below $\dot{m}_{air} = 50\,g/s$. The reduced operational range of configuration 3 is attributed to the combination of high swirl and a short mixing tube; under these conditions, the axial velocity increase due to the AI was limited to a narrow region on the central axis, which manifests in the velocity overshoot reported in Fig. 6i. These results underline the importance of a radially homogeneous, plug-flow-like velocity distribution for FB resistance.

In summary, an increase in AI rate is shown to result in a significantly extended operational range. In a next step, the impact of AI on the fuel–air mixing quality is investigated by the means of PLIF. This investigation aims to confirm that the extended operational range is achieved without affecting mixing quality.

C. Impact of AI on Fuel–Air Mixing Quality

1. Spatial Unmixedness Obtained in the Water Rest Rig

Figure 9 presents the spatial distribution of the normalized mean concentration of the fuel agent $\overline{C(\boldsymbol{x})}/\langle\overline{C}\rangle$ for varied AI rates obtained from the PLIF measurements in the water tunnel. The results are arranged in the same manner as the velocity data in Fig. 6. Above each plot, we provide the spatial unmixedness U_s for comparison of the numeric values, which are displayed collectively for all investigated configurations and AI rates in Fig. 10a. According to the latter figure, the spatial unmixedness U_s increased with increasing AI rate. This effect was more pronounced for the lower swirl number $S = 0.7$, whereas a higher swirl number preserved lower spatial unmixedness U_s at high AI rates. A long mixing tube further reduced U_s independent of the swirl number.

A closer look at the spatial distribution of the mean fuel concentration in the absence of AI ($\chi = 0\%$, left column in Fig. 9) reveals a quite homogeneous distribution, which, however, exhibited a distinct axially centered deficit, which was more distinct in case of $S = 0.7$. By increasing the AI rate to $\chi = 7.5\%$ (center column in Fig. 9), for a swirl number of $S = 0.7$, the central fuel deficit disappeared and turned into a fuel overshoot of up to 20% above the mean concentration. For $S = 0.9$, the central fuel deficit remained present, although it appeared less pronounced. If the AI rate was further increased to $\chi = 12.5\%$ (right column in Fig. 9), again an axially centered fuel deficit appeared, only, however, in the case of a short mixing tube (configurations 1 and 3).

To understand how AI affects the spatial fuel–air distribution, one has to take into account how AI changes the time-mean flowfield and, thus, also affects self-excited flow instabilities. We argue that a helical self-excited flow instability featuring a precessing vortex core and its suppression in the presence of a medium AI rate ($\chi = 7.5\%$) were the driving mechanism for the observed behavior in the spatial and temporal mixing that is discussed and verified in Sec. III.D.

2. Temporal Unmixedness Obtained in the Water Rest Rig

Figure 11 presents the spatial distribution of the normalized standard deviation of the concentration of the fuel agent $\sigma_t'^2/\sigma_0^2$. Above each plot, the temporal unmixedness U_t is provided for comparison of the numeric values, which are displayed collectively for the investigated configurations and AI rates in Fig. 10b. The latter figure reveals that, although for $\chi = 0\%$, the spatial parameter U_s was minimum, the temporal unmixedness U_t was maximum in the absence of AI for all configurations. Increasing the AI rate to $\chi = 7.5\%$ significantly reduced U_t, whereas a further increase of the AI rate to $\chi = 12.5\%$ barely affected the temporal unmixedness. Independent of the AI rate, a higher swirl number achieved lower temporal unmixedness U_t, which was further reduced when combined with a long mixing tube.

A closer look at the spatial distribution of the normalized concentration standard deviation without AI reveals a small, circular ($r = 0.13D$) minimum on the central axis, surrounded by a ring-shaped area of local maximum (left column, Fig. 11). In both cases, AI rates of $\chi = 7.5\%$ and $\chi = 12.5\%$ (center and right columns, Fig. 11), the central nonswirling jet significantly altered the $\sigma_t'^2/\sigma_0^2$ distribution. The small minimum on the central axis disappeared, and a much bigger region of very low temporal fluctuations, extending up to $r = 0.38D$, was observed. This distinct change in the standard deviation distribution is related to a coherent structure, which constitutes a precessing fuel-rich pattern, which remained for $\chi = 0\%$ and was suppressed for AI rates $\chi \geq 7.5\%$ (see Sec. III.D).

It is concluded that configuration 4 (high swirl, long mixing tube) with a high AI rate is the most promising setup with respect to

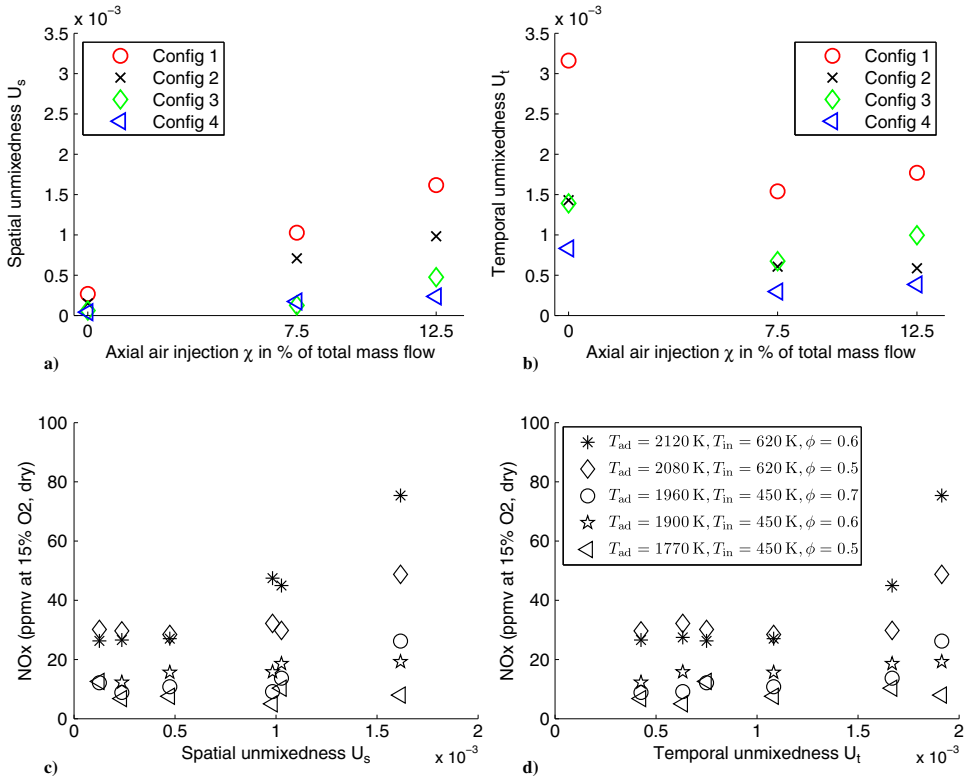

Fig. 10 Top: summary of a) spatial unmixedness, and b) temporal unmixedness, for configurations 1–4 and increasing AI rates obtained in the water test rig. Bottom: NO_x emissions from reacting tests over c) temporal unmixedness, and d) spatial unmixedness.

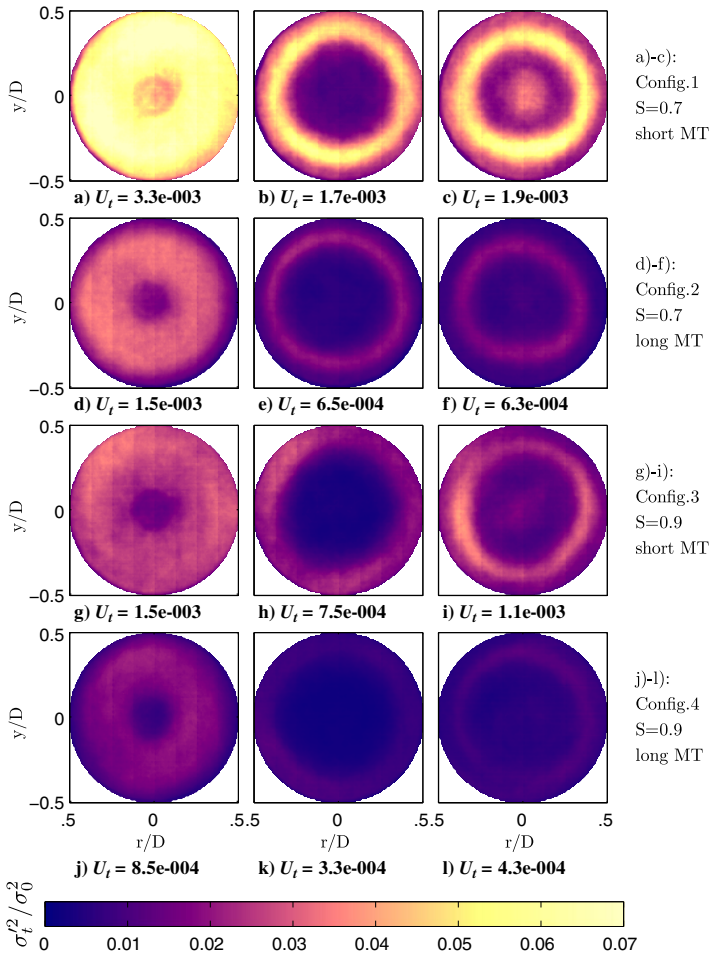

Fig. 11 Spatial distribution of $\sigma_t'^2/\sigma_0^2$, obtained in the water test rig. From left to right, $\chi = 0$, 7.5, and 12.5%. Configurations 1–4 are shown from top to bottom.

minimizing NO_x emissions. This setup significantly decreased U_t (Fig. 10b) while simultaneously causing only a negligible increase in U_s (Fig. 10b). Slightly lower absolute values of U_s and U_t are found for $\chi = 7.5\%$. However, the superior FB resistance at $\chi = 12.5\%$ fully compensates for this matter.

D. Occurrence and Suppression of the Coherent Structure

In this section, flow instabilities and unsteady mixing characteristics are identified based on the flowfield and concentration field $C(\boldsymbol{x}, t)$ obtained in the water test rig by PIV and PLIF, respectively. It is now argued that the characteristics observed in the spatial and temporal mixing distributions described in the previous section are closely related to the occurrence of a coherent structure in the absence of AI and its suppression for AI rates $\chi \geq 7.5\%$. Such a coherent flow structure was previously observed by Galley et al. [34] in a similar combustor setup. Fuel is trapped in the center of the strongly swirling flow inside the mixing tube. However, upon exiting the mixing tube, this fuel-rich core is displaced from the central axis and describes a precessing motion, following the coherent structure referred to as PVC. This leads to a precessing mixing pattern, which is depicted in Fig. 12. One can clearly identify the fuel-rich pattern describing an off-center, counterclockwise precessing motion. This pattern is very similar to the one observed by Galley et al. [34], which they described to look like a "comma". This mixing pattern, on average, is least likely located in the center but rather precessing on higher radii with a fixed frequency, which explains the central concentration deficit and the high temporal concentration fluctuations for $\chi = 0\%$. To allow for identification of the precessing mixing pattern in Fig. 12, the snapshot PLIF images were phase-averaged. The phase-averaging was conducted with respect to the frequency of the distinct peak in the power spectral density (PSD) of the recorded concentration $C(x, t)$ (Fig. 13a). Hereby, the PSD was computed according to Welch's method [46]. The link of the mixing pattern to the PVC can be established by the PSD of the radial velocity from the PIV measurements, which is shown to contain the same underlying frequency originating from the coherent structure (Fig. 13a).

A medium AI rate of $\chi = 7.5\%$ causes significant flowfield changes in the mixing tube and combustion chamber (Fig. 5b), which result in a suppression of the coherent structure and thus of the precessing mixing pattern. Such a suppression of a coherent structure by a nonswirling axial jet was previously reported by other authors [37–40]. In the current study, the disappearance of the distinct peaks for $\chi \geq 7.5\%$ in the spectra of both the concentration as well as the radial velocity (Fig. 13b) validate the suppression of the coherent structure and of the comma-shaped mixing pattern. The absence of the precessing mixing pattern explains the

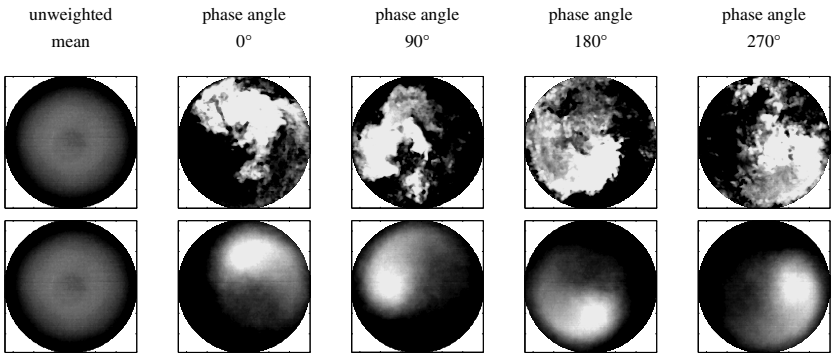

Fig. 12 Instantaneous (top) and phase-averaged (bottom) PLIF images ($\chi = 0\%$, configuration 4) in a plane 2 mm downstream of the burner outlet obtained in the water rest rig.

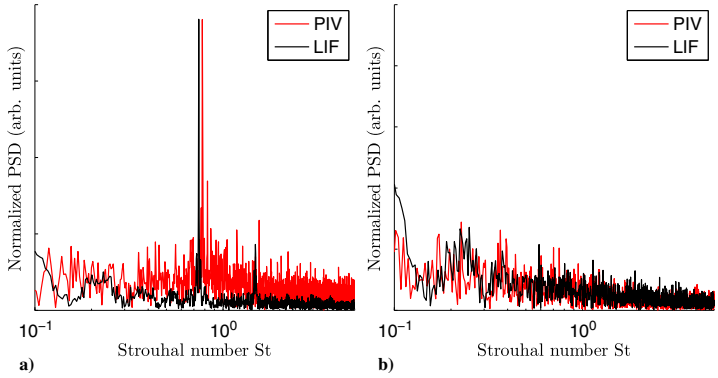

Fig. 13 Spectra of fuel concentration $C(x,t)$ (LIF) and radial velocity u_r (PIV) at an arbitrarily chosen point in the shear layer $x/D = 0.5, r/D = 0.25$ in a) absence ($\chi = 0\%$), and b) presence ($\chi = 12.5\%$), of AI for configuration 4.

disappearance of the axially centered deficit in the mean concentration distribution (Fig. 9, center column) as well as the significant reduction in the temporal unmixedness for all configurations (Fig. 10b).

The repeated occurrence of the central concentration deficit for short mixing tubes at $\chi = 12.5\%$ is not related to the hydrodynamic instability but is identified as the footprint of the fuel-less central air jet, which persists at the mixing tube outlet in the case of a short mixing tube. Two facts support this assumption. First, the distinct axial velocity overshoot at the mixing tube outlet for high AI rates (Figs. 6c and 6i), and second, the suppression of the coherent structure in the presence of AI, which excludes the precessing mixing pattern as the source of the local deficit.

In summary, the aforementioned flowfield changes along with the suppression of the precessing mixing pattern are the mechanisms by which AI determines the fuel–air mixing characteristics. Quantitatively, AI positively affects the temporal mixing quality while only negligibly decreasing spatial mixing quality. The direct effect on NO_x emissions of these changes in unmixedness parameters are discussed in the next section.

E. Correlation of Unmixedness and NO_x Emissions

Figures 10c and 10d provide the dependence of NO_x emissions on spatial and temporal unmixedness, respectively. To this end, the global NO_x data obtained from reacting tests are plotted against the unmixedness data obtained from the mixing investigations in the water tunnel. The different levels of unmixedness correspond to configurations 1–4 at $\chi = 7.5\%$ and $\chi = 12.5\%$.

On the investigated range of unmixedness, below a calculated adiabatic flame temperature of $T_{ad} = 1800$ K, the NO_x emissions are independent of both spatial and temporal unmixedness. This is expected because the thermal NO path proceeds at a significant rate only above primary zone flame temperatures of 1850 K [47]. Note that, because of the unavailability of the actual flame temperature, the calculated adiabatic flame temperature T_{ad} is used to differentiate between operating conditions. Because T_{ad} neglects heat loss, it represents an overestimation of the actual flame temperature.

For flame temperatures well above 2000 K, the NO_x emissions are shown to be independent of the unmixedness below a threshold of $U_s < 0.5 \times 10^{-3}$ and $U_t < 1.1 \times 10^{-3}$. Above these thresholds, emissions and unmixedness are correlated, and the NO_x emissions increase with both spatial and temporal unmixedness (Figs. 10c and 10d). A higher adiabatic flame temperature leads to a steeper increase in NO_x with increased unmixedness. Even in the case of high AI rates, the unmixedness of configurations with a long mixing tube (2 and 4) remains well below the thresholds of U_s and U_t (Figs. 10c and 10d). In the case of a short mixing tube, only the unmixedness of the high swirl configuration 3 is low enough to remain uncorrelated with NO_x emissions. Configuration 1, with low swirl and short mixing tube, exceeds these thresholds, which thus indicates elevated NO_x emissions above adiabatic flame temperatures of 2000 K.

It is concluded that, for all configurations, to prevent a deterioration of NO_x emissions in the presence of AI, a sufficiently high initial swirl number or mixing tube length is required to ensure a high level of fuel–air mixing. This was achieved for configurations 2–4. For these configurations, the NO_x emissions are shown to remain well below 10 ppm up to adiabatic flame temperatures of nearly 2000 K (Fig. 14).

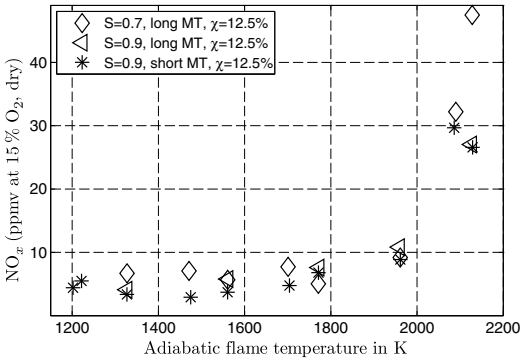

Fig. 14 NO_x emissions (dry) over calculated adiabatic flame temperature for two swirl numbers at $\chi = 12.5\%$, $l_{mt} = 60$ mm.

IV. Conclusions

An approach to tailor the flowfield of a lean, premixed, swirl-stabilized hydrogen combustor to suppress flashback (FB) by means of axial injection (AI) was investigated and validated. Therefore, the impact of AI on the flowfield, with respect to varying swirl number and mixing tube length, is revealed by isothermal particle image velocimetry measurements in a water tunnel. Subsequent reacting tests confirm that increasing the AI rate up to $\chi = 12.5\%$ significantly extends the operational range. Operating the burner on undiluted hydrogen requires at least a medium amount of axial injection ($\chi = 7.5\%$). For a high AI rate ($\chi = 12.5\%$) and a long mixing tube, FB was fully suppressed at the investigated conditions, namely inlet temperatures up to 620 K and stoichiometric conditions. Comparison of the isothermal flowfields and stability maps underlined the importance of a radially homogeneous, plug-flow-like velocity distribution for FB resistance. The water-tunnel flowfield observations were shown to allow for a fair prediction of the FB resistance of a combustor geometry.

AI maintains excellent fuel–air mixing quality and very low NO_x emissions. It is revealed that, given a sufficiently high swirl number or mixing tube length, even for high AI rates, the levels of both U_t and U_s are well below the threshold where unmixedness and NO_x emissions are correlated. For configurations 2–4, the NO_x emissions are shown to remain well below 10 ppm up to adiabatic flame temperatures of nearly 2000 K. It is concluded that AI significantly extends the operational range of the combustor without increasing the NO_x emissions.

Acknowledgments

The research leading to these results has received funding from the European Union FP7 (2007–2013) under grant agreement Advanced Hybrid Engines for Aircraft Development (AHEAD) and the European Research Council under grant agreement 247322 Gas Turbine Combustion with Reduced Emissions Employing Extreme Steam Injection (GREENEST).

References

[1] Brewer, G. D., "The Prospects for Liquid Hydrogen Fueled Aircraft," *International Journal of Hydrogen Energy*, Vol. 7, No. 1, 1982, pp. 21–41.
doi:10.1016/0360-3199(82)90205-1

[2] Pohl, H. W., and Malychev, V. V., "Hydrogen in Future Civil Aviation," *International Journal of Hydrogen Energy*, Vol. 22, No. 10, 1997, pp. 1061–1069.
doi:10.1016/S0360-3199(95)00140-9

[3] Brand, J., Sampath, S., and Shum, F., "Potential Use of Hydrogen in Air Propulsion," *AIAA/ICAS International Air and Space Symposium and Exposition: The Next 100 Years*, AIAA Paper 2003-2879, July 2003.
doi:10.2514/6.2003-2879

[4] Rao, A. G., Yin, F., van Buijtenen, J. P., and Isikveren, A., "A Hybrid Engine Concept for Multi-Fuel Blended Wing Body," *Aircraft Engineering and Aerospace Technology*, Vol. 86, No. 6, 2014, pp. 483–493.
doi:10.1108/AEAT-04-2014-0054

[5] Levy, Y., Sherbaum, V., and Arfi, P., "Basic Thermodynamics of FLOXCOM, the Low-NOx Gas Turbines Adiabatic Combustor," *Applied Thermal Engineering*, Vol. 24, No. 11, 2004, pp. 1593–1605.
doi:10.1016/j.applthermaleng.2003.11.022

[6] Ziemann, J., "Low-NO_x Combustors for Hydrogen Fueled Aero Engine," *International Journal of Hydrogen Energy*, Vol. 23, No. 4, 1998, pp. 281–288.
doi:10.1016/S0360-3199(97)00054-2

[7] Schefer, R. W., "Hydrogen Enrichment for Improved Lean Flame Stability," *International Journal of Hydrogen Energy*, Vol. 28, No. 10, 2003, pp. 1131–1141.
doi:10.1016/S0360-3199(02)00199-4

[8] Griebel, P., Boschek, E., and Jansohn, P., "Lean Blowout Limits and NOx Emissions of Turbulent, Lean Premixed, Hydrogen-Enriched Methane/Air Flames at High Pressure," *Journal of Engineering for Gas Turbines and Power*, Vol. 129, No. 2, 2006, pp. 404–410.
doi:10.1115/1.2436568

[9] Plee, S. L., and Mellor, A. M., "Review of Flashback Reported in Prevaporizing/Premixing Combustors," *Combustion and Flame*, Vol. 32, 1978, pp. 193–203.
doi:10.1016/0010-2180(78)90093-7

[10] Schefer, R., Wicksall, D., and Agrawal, A., "Combustion of Hydrogen-Enriched Methane in a Lean Premixed Swirl-Stabilized Burner," *Proceedings of the Combustion Institute*, Vol. 29, No. 1, 2002, pp. 843–851.
doi:10.1016/S1540-7489(02)80108-0

[11] Strakey, P., Sidwell, T., and Ontko, J., "Investigation of the Effects of Hydrogen Addition on Lean Extinction in a Swirl Stabilized Combustor," *Proceedings of the Combustion Institute*, Vol. 31, No. 2, 2007, pp. 3173–3180.
doi:10.1016/j.proci.2006.07.077

[12] Lieuwen, T., McDonell, V., Santavicca, D., and Sattelmayer, T., "Burner Development and Operability Issues Associated with Steady Flowing Syngas Fired Combustors," *Combustion Science and Technology*, Vol. 180, No. 6, 2008, pp. 1169–1192.
doi:10.1080/00102200801963375

[13] Syred, N., Abdulsada, M., Griffiths, A., O'Doherty, T., and Bowen, P., "The Effect of Hydrogen Containing Fuel Blends Upon Flashback in Swirl Burners," *Applied Energy*, Vol. 89, No. 1, 2012, pp. 106–110.
doi:10.1016/j.apenergy.2011.01.057

[14] Emadi, M., Karkow, D., Salameh, T., Gohil, A., and Ratner, A., "Flame Structure Changes Resulting from Hydrogen-Enrichment and Pressurization for Low-Swirl Premixed Methane–Air Flames," *International Journal of Hydrogen Energy*, Vol. 37, No. 13, 2012, pp. 10397–10404.
doi:10.1016/j.ijhydene.2012.04.017

[15] Syred, N., Giles, A., Lewis, J., Abdulsada, M., Valera Medina, A., Marsh, R., Bowen, P. J., and Griffiths, A. J., "Effect of Inlet and Outlet Configurations on Blow-Off and Flashback with Premixed Combustion for Methane and a High Hydrogen Content Fuel in a Generic Swirl Burner," *Applied Energy*, Vol. 116, March 2014, pp. 288–296.
doi:10.1016/j.apenergy.2013.11.071

[16] Sayad, P., Schönborn, A., and Klingmann, J., "Experimental Investigation of the Stability Limits of Premixed Syngas-Air Flames at Two Moderate Swirl Numbers," *Combustion and Flame*, Vol. 164, Feb. 2016, pp. 270–282.
doi:10.1016/j.combustflame.2015.11.026

[17] Schönborn, A., Sayad, P., Konnov, A. A., and Klingmann, J., "Autoignition of Dimethyl Ether and Air in an Optical Flow-Reactor," *Energy Fuels*, Vol. 28, No. 6, 2014, pp. 4130–4138.
doi:10.1021/ef402476r

[18] Marek, J. C., Smith, T. D., and Kundu, K., "Low Emission Hydrogen Combustors for Gas Turbines Using Lean Direct Injection," *41st AIAA/ASME/SAE/ASEE Joint Propulsion Conference & Exhibit*, AIAA Paper 2005-3776, July 2005.

[19] Döbbeling, K., and Hellat, J., "25 Years of BBC/ABB/Alstom Lean Premix Combustion Technologies," *Journal of Engineering for Gas Turbines and Power*, Vol. 129, No. 1, 2007, pp. 2–0.
doi:10.1115/1.2181183

[20] Mayer, C., Sangl, J., Sattelmayer, T., Lachaux, T., and Bernero, S., "Study on the Operational Window of a Swirl Stabilized Syngas Burner Under Atmospheric and High Pressure Conditions," *Journal of Engineering for Gas Turbines and Power*, Vol. 134, No. 3, 2012, Paper 031506.
doi:10.1115/1.4004255

[21] Kröner, M., Fritz, J., and Sattelmayer, T., "Flashback Limits for Combustion Induced Vortex Breakdown in a Swirl Burner," *Journal of Engineering for Gas Turbines and Power*, Vol. 125, No. 3, 2003, p. 693. doi:10.1115/1.1582498

[22] Burmberger, S., and Sattelmayer, T., "Optimization of the Aerodynamic Flame Stabilization for Fuel Flexible Gas Turbine Premix Burners," *Journal of Engineering for Gas Turbines and Power*, Vol. 133, No. 10, 2011, Paper 101501. doi:10.1115/1.4003164

[23] Reichel, T. G., Terhaar, S., and Paschereit, O., "Increasing Flashback Resistance in Lean Premixed Swirl-Stabilized Hydrogen Combustion by Axial Air Injection," *Journal of Engineering for Gas Turbines and Power*, Vol. 137, No. 7, 2015, Paper 071503. doi:10.1115/1.4029119

[24] Reichel, T. G., Goeckeler, K., and Paschereit, O., "Investigation of Lean Premixed Swirl-Stabilized Hydrogen Burner with Axial Air Injection Using OH-PLIF Imaging," *Journal of Engineering for Gas Turbines and Power*, Vol. 137, No. 11, 2015, Paper 111513. doi:10.1115/1.4031181

[25] Reichel, T. G., and Paschereit, C. O., "Interaction Mechanisms of Fuel Momentum with Flashback Limits in Lean-Premixed Combustion of Hydrogen," *International Journal of Hydrogen Energy*, Vol. 42, No. 7, 2017, pp. 4518–4529. doi:10.1016/j.ijhydene.2016.11.018

[26] Fric, T. F., "Effects of Fuel-Air Unmixedness on NO(x) Emissions," *Journal of Propulsion and Power*, Vol. 9, No. 5, 1993, pp. 708–713. doi:10.2514/3.23679

[27] Danckwerts, P. V., "The Definition and Measurement of Some Characteristics of Mixtures," *Applied Scientific Research*, Vol. 3, No. 4, 1952, pp. 279–296. doi:10.1007/BF03184936

[28] Biagioli, F., and Güthe, F., "Effect of Pressure and Fuel–Air Unmixedness on NOx Emissions from Industrial Gas Turbine Burners," *Combustion and Flame*, Vol. 151, Nos. 1–2, 2007, pp. 274–288. doi:10.1016/j.combustflame.2007.04.007

[29] Dederichs, S., Zarzalis, N., Habisreuther, P., Beck, C., Prade, B., and Krebs, W., "Assessment of a Gas Turbine NOx Reduction Potential Based on a Spatiotemporal Unmixedness Parameter," *Journal of Engineering for Gas Turbines and Power*, Vol. 135, No. 11, 2013, Paper 111504. doi:10.1115/1.4025078

[30] Zajadatz, M., Lachner, R., Bernero, S., Motz, C., and Flohr, P., "Development and Design of Alstom's Staged Fuel Gas Injection EV Burner for NOx Reduction," *Proceedings of the ASME Turbo Expo 2007: Power for Land, Sea, and Air*, ASME Paper GT2007-27730, 2007, pp. 559–567. doi:10.1115/GT2007-27730

[31] Lacarelle, A., and Paschereit, C. O., "Increasing the Passive Scalar Mixing Quality of Jets in Crossflow with Fluidics Actuators," *Journal of Engineering for Gas Turbines and Power*, Vol. 134, No. 2, 2012, Paper 021503. doi:10.1115/1.4004373

[32] Sangl, J., Mayer, C., and Sattelmayer, T., "Prediction of the NOx Emissions of a Swirl Burner in Partially and Fully Premixed Mode on the Basis of Water Channel Laser Induced Fluorescence and Particle Image Velocimetry Measurements," *Journal of Engineering for Gas Turbines and Power*, Vol. 136, No. 6, 2014, Paper 061503. doi:10.1115/1.4025071

[33] Estefanos, W., "Effects of the Fuel-Air Mixing on Combustion Instabilities and NOx Emissions in Lean Premixed Combustion," Ph.D. Thesis, Univ. of Cincinnati, Cincinnati, OH, 2016.

[34] Galley, D., Ducruix, S., Lacas, F., and Veynante, D., "Mixing and Stabilization Study of a Partially Premixed Swirling Flame Using Laser Induced Fluorescence," *Combustion and Flame*, Vol. 158, No. 1, 2011, pp. 155–171. doi:10.1016/j.combustflame.2010.08.004

[35] Syred, N., "A Review of Oscillation Mechanisms and the Role of the Precessing Vortex Core (PVC) in Swirl Combustion Systems," *Progress in Energy and Combustion Science*, Vol. 32, No. 2, 2006, pp. 93–161. doi:10.1016/j.pecs.2005.10.002

[36] Paschereit, C. O., Gutmark, E., and Weisenstein, W., "Coherent Structures in Swirling Flows and Their Role in Acoustic Combustion Control," *Physics of Fluids*, Vol. 11, No. 9, 1999, pp. 2667–2678. doi:10.1063/1.870128

[37] Jochmann, P., Sinigersky, A., Koch, R., and Bauer, H.-J., "URANS Prediction of Flow Instabilities of a Novel Atomizer Combustor Configuration," *Proceedings of the ASME Turbo Expo 2005: Power for Land, Sea, and Air*, ASME Paper GT2005-68072, 2005, pp. 19–27. doi:10.1115/GT2005-68072

[38] Spencer, A., McGuirk, J. J., and Midgley, K., "Vortex Breakdown in Swirling Fuel Injector Flows," *Journal of Engineering for Gas Turbines and Power*, Vol. 130, No. 2, 2008, Paper 021503. doi:10.1115/1.2799530

[39] Midgley, K., Spencer, A., and McGuirk, J. J., "Unsteady Flow Structures in Radial Swirler Fed Fuel Injectors," *Journal of Engineering for Gas Turbines and Power*, Vol. 127, No. 4, 2005, p. 755. doi:10.1115/1.1925638

[40] Terhaar, S., Reichel, T. G., Schrödinger, C., Rukes, L., Paschereit, C. O., and Oberleithner, K., "Vortex Breakdown Types and Global Modes in Swirling Combustor Flows with Axial Injection," *Journal of Propulsion and Power*, Vol. 31, No. 1, 2015, pp. 219–229. doi:10.2514/1.B35217

[41] Göke, S., Schimek, S., Terhaar, S., Reichel, T., Göckeler, K., Krüger, O., Fleck, J., Griebel, P., and Oliver Paschereit, C., "Influence of Pressure and Steam Dilution on NOx and CO Emissions in a Premixed Natural Gas Flame," *Journal of Engineering for Gas Turbines and Power*, Vol. 136, No. 9, 2014, Paper 091508. doi:10.1115/1.4026942

[42] Kuhn, P., Terhaar, S., Reichel, T., and Paschereit, C. O., "Design and Assessment of a Fuel-Flexible Low Emission Combustor for Dry and Steam-Diluted Conditions," *Proceedings of the ASME Turbo Expo 2015: Turbine Technical Conference and Exposition*, June 2015, Paper V04BT04A024. doi:10.1115/GT2015-43375

[43] Beér, J. M., and Chigier, N. A., *Combustion Aerodynamics*, Applied Science Publishers, London, 1972, p. 76.

[44] Tanneberger, T., Reichel, T. G., Krüger, O., Terhaar, S., and Paschereit, C. O., "Numerical Investigation of the Flow Field and Mixing in a Swirl-Stabilized Burner with a Non-Swirling Axial Jet," *Proceedings of the ASME Turbo Expo 2015*, ASME Paper GT2015-43382, 2015. doi:10.1115/GT2015-43382

[45] Lacarelle, A., "Modeling, Control, and Optimization of Fuel, Air Mixing in a Lean Premixed Swirl Combustor Using Fuel Staging to Reduce Pressure Pulsations and NOx Emissions," Ph.D. Thesis, Technical Univ. of Berlin, Berlin, 2011.

[46] Welch, P., "The Use of Fast Fourier Transform for the Estimation of Power Spectra: A Method Based on Time Averaging over Short, Modified Periodograms," *IEEE Transactions on Audio and Electroacoustics*, Vol. 15, No. 2, 1967, pp. 70–73. doi:10.1109/TAU.1967.1161901

[47] Lefebvre, A. H., and Ballal, D. R., *Gas Turbine Combustion: Alternative Fuels and Emissions*, 3rd ed., CRC Press, Boca Raton, FL, 2010, p. 374.

G. Richards
Associate Editor

2.2 Second Publication[1]

Increasing Flashback Resistance in Lean Premixed Swirl-Stabilized Hydrogen Combustion by Axial Air Injection

Thoralf G. Reichel[1]
Chair of Fluid Dynamics,
Hermann-Föttinger-Institut,
Technische Universität Berlin,
Müller-Breslau-Str. 8,
Berlin 10623, Germany
e-mail: thoralf.reichel@tu-berlin.de

Steffen Terhaar
Chair of Fluid Dynamics,
Hermann-Föttinger-Institut,
Technische Universität Berlin,
Müller-Breslau-Str. 8,
Berlin 10623, Germany

Oliver Paschereit
Chair of Fluid Dynamics,
Hermann-Föttinger-Institut,
Technische Universität Berlin,
Müller-Breslau-Str. 8,
Berlin 10623, Germany

Since lean premixed combustion allows for fuel-efficiency and low emissions, it is nowadays state of the art in stationary gas turbines. In the long term, it is also a promising approach for aero engines, when safety issues like lean blowout (LBO) and flame flashback in the premixer can be overcome. While for the use of hydrogen the LBO limits are extended, the flashback propensity is increased. Thus, axial air injection is applied in order to eliminate flashback in a swirl-stabilized combustor burning premixed hydrogen. Axial injection constitutes a nonswirling jet on the central axis of the radial swirl generator which influences the vortex breakdown (VB) position. In the present work, changes in the flow field and their impact on flashback limits of a model combustor are evaluated. First, a parametric study is conducted under isothermal test conditions in a water tunnel employing particle image velocimetry (PIV). The varied parameters are the amount of axially injected air and swirl number. Subsequently, flashback safety is evaluated in the presence of axial air injection in an atmospheric combustor test rig and a stability map is recorded. The flame structure is measured using high-speed OH chemiluminescence imaging. Simultaneous high-speed PIV measurements of the reacting flow provide insight in the time-resolved reacting flow field and indicate the flame location by evaluating the Mie scattering of the raw PIV images by means of the qualitative light sheet (QLS) technique. The isothermal tests identify the potential of axial air injection to overcome the axial velocity deficits at the nozzle outlet, which is considered crucial in order to provide flashback safety. This effect of axial air injection is shown to prevail in the presence of a flame. Generally, flashback safety is shown to benefit from an elevated amount of axial air injection and a lower swirl number. Note that the latter also leads to increased NO_x emissions, while axial air injection does not. Additionally, fuel momentum is indicated to positively influence flashback resistance, although based on a different mechanism, an explanation of which is suggested. In summary, flashback-proof operation of the burner with a high amount of axial air injection is achieved on the whole operating range of the test rig at inlet temperatures of 620 K and up to stoichiometric conditions while maintaining single digit NO_x emissions below a flame temperature of 2000 K.*
[DOI: 10.1115/1.4029119]

Introduction

Future demands on air transport systems dictate that aircraft should be less polluting, less noisy, and more fuel efficient. In the long term, alternative fuels like bio fuels and hydrogen are likely to replace traditional jet fuel [1–3]. Experimental tests on a low NO_x hydrogen combustor for aero engines have been conducted within the European Union supported FP7 project Advanced Hybrid Engines for Aircraft Development (AHEAD). The concept proposed in the AHEAD project is a contra-rotating turbofan engine with sequential dual hybrid combustors, using two different fuels [4]. The engine is operated on pure hydrogen in the first stage and bio fuel under flameless conditions [5] in the second stage, aiming to reduce CO_2 and NO_x emission, respectively. This study focuses on the hydrogen combustion carried out in the first stage.

Lean premixed combustion is chosen as the preferred combustion mode since the low flame temperature and high mixing quality offer potential to very low NO_x emissions. Alternative concepts for NO_x reduction include flame miniaturization [6] or rich-quench-lean (RQL) [7] combustion. For lean premixed combustion, with increasing fuel reactivity lean blow out limits are extended but flashback disposition is increased. Hence, the design of a flashback-proof burner is particularly challenging in the case of hydrogen fuel.

Evaluating lean hydrogen combustion concepts for aero engines, Ziemann [8] indicated the low NO_x potential of an aerodynamically stabilized high swirl burner from preliminary tests. Lean premixed concepts applying low swirl combustion [9] have also been suggested. Similar to other modern premixer concepts [10], in the current investigation a center body-less mixing tube and swirl-induced, VB flame stabilization is applied. Such a setup promises enhanced mixing and creates a central recirculation zone that provides for recirculation of hot gases and, thus, flame stability (Gupta et al. [11]).

To prevent recirculation in the premixing section which degrades flashback safety, Burmberger and Sattelmayer [12,13]

[1]Corresponding author.

Contributed by the Combustion and Fuels Committee of ASME for publication in the Journal of Engineering for Gas Turbines and Power. Manuscript received September 1, 2014; final manuscript received October 30, 2014; published online December 23, 2014. Editor: David Wisler.

1 Republished with permission of American Society of Mechanical Engineers ASME, from Increasing Flashback Resistance in Lean Premixed Swirl-Stabilized Hydrogen Combustion by Axial Air Injection, Reichel et. al, *Journal of Engineering for Gas Turbines and Power*, Bd. 137 (2015) (7): 071503; permission conveyed through Copyright Clearance Center, Inc.

suggested to influence the position of the VB by a nonswirling air flow exiting on the central axis of the radial swirl generator. Burmberger et al. [14] proved that a burner, designed by this concept, allows for flashback-free operation of stoichiometric methane-diluted hydrogen mixtures under unconfined conditions. However, the study is limited to perfectly premixed combustion and omits the challenges related to achieving flashback safety as well as low NO_x emissions for pure hydrogen in a technically premixed case, where the premixing section is limited.

Previous investigations revealed that in the presence of a high momentum [15–17] or low momentum [18] nonswirling jet the flow field is less prone to exhibit self-excited flow oscillations. Such hydrodynamic instabilities tend to trap the fuel in a precessing vortex core and lead to strong temporal fuel concentration fluctuations (Galley et al. [19]). Consequently, axial air injection, by suppressing the hydrodynamic instability, increases the temporal mixing quality, without deteriorating spatial mixing quality, as was proven by Reichel et al. [20] from mixing investigations in a water tunnel. Terhaar et al. [18] recorded isothermal and reacting flow field data for methane in the presence of varied amounts of axial air injection, which were controlled by a mass flow meter. They present a correlation where, depending on the combination of primary swirl number and amount of axial air injection, the hydrodynamic instability is suppressed. This suppression is observed to coincide with a change in VB type from bubble type to cone type (compare Billant et al. [21]). Whereas the bubble type VB exhibits a local minimum in axial velocity in the plane upstream of VB, the cone type VB does not and is therefore preferred for flashback safety.

The works of Mayer et al. [22] and Sangl et al. [23] both applied a nonswirling, axial fuel jet, making use of the additional fuel momentum of hydrogen fuel in comparison to, e.g., methane. By shifting the fuel injection mode from trailing edge injection in the radial swirler vanes toward the axial fuel jet they reported an extension of the flashback limits but also highly increased NO_x emissions.

In the current study, axial air injection is applied with the intention to create a plug flowlike velocity profile at the nozzle exit and shift the stagnation point downstream. Furthermore, the fuel injection is arranged through 16 circumferentially distributed, streamwise orientated, injection holes. This allows to take advantage of the additional fuel momentum while simultaneously optimizing the spatial distribution of the fuel. The dependency of fuel momentum on inlet conditions is quantified and an explanation is suggested of how the impact of fuel momentum is different compared to axial air injection.

The remainder of the paper is structured as follows. First, the effect of varied amounts of axial injection on the isothermal flow field in the premixing section and combustion chamber is revealed from PIV measurements in a water tunnel. Subsequently, reacting tests in the atmospheric test rig prove the ability of axial air injection to allow for flashback-proof hydrogen combustion. A stability map and NO_x emissions are recorded for different burner configurations given in Table 1. Moreover, PIV measurements of the reacting flow are conducted to examine the impact of axial air injection as well as fuel momentum on the flow field in the combustion chamber. Finally, OH* images and the Mie scattering of the reacting flow are evaluated to determine the flame location in dependency on axial air injection and equivalence ratio.

Table 1 Overview of investigated configurations

Configuration	Swirl number S	Orifice diameter D_{or} (mm)	Injection ratio χ
1	0.7	8.0	0.07
2	0.7	8.8	0.12
3	0.9	8.0	0.08
4	0.9	8.8	0.13

Theoretical Considerations

Characterization of Flashback. One major challenge of premixed combustion is the hazard of flame stabilization in the premixing section, where fuel and air are mixed before entering the combustion chamber, referred to as flashback. According to Lieuwen et al. [24], four generally different types of flashback are distinguished which may lead to fast upstream flame propagation:

The first type is flashback due to combustion instabilities and should not occur during regular, stable combustor operation. For the operation with hydrogen no combustion instabilities were encountered for the investigated configurations and this flashback type was, thus, not observed. The second type is flashback in the boundary layer. Measures against this type of flashback are implemented during the design of the burner: The design is adapted to keep boundary layers thin and avoid local separation. Additionally, dilution holes are applied to lean out the near-wall region of the mixing tube. In order to avoid flashback due to type three and four, turbulent flame propagation in the core flow and combustion induced vortex breakdown (CIVB [25]), "a major design criterion for nozzle aerodynamics is that the axial velocity must be as high and as uniform as possible and free of strong wakes" [24]. Therefore, it is intended to apply axial air injection and make use of the additional fuel momentum.

Quantification of Additional Fuel Momentum. Generally, additional fuel momentum stems from the high fuel volume flow due to its low density and low volumetric heat density. The exact amount of additional fuel momentum strongly depends on the air–fuel temperature ratio T_{in}/T_{fuel} which strongly varies between typical test rig conditions (air temperature $T_{in} = 450 - 620\,K$) and engine conditions (air temperature up to $T_{in} = 900\,K$). In both cases, the fuel temperature is very low. While in the test rig fuel is supplied at ambient temperature, the fuel temperature at engine conditions is even lower due to its cryogenic storage. According to Haglind and Singh [3], the fuel temperature is assumed to be $T_{fuel} = 250\,K$. Consequently, whereas the conditions in the test rig correspond to $T_{in}/T_{fuel} = 1.5 - 2.1$, the air–fuel temperature ratio at engine conditions is estimated to $T_{in}/T_{fuel} = 3.6$.

Two relevant parameters depend on both air–fuel temperature ratio T_{in}/T_{fuel} and equivalence ratio (Fig. 1). First, and most importantly, the fuel air momentum ratio J, which is defined as

$$J = \frac{\rho_{fuel} u_{fuel}^2}{\rho_{air} u_{air}^2}$$

As the fuel is injected in axial direction, an increase in J reduces the swirl number, since it increases the axial momentum flux while the tangential momentum flux remains constant.

Second, the bulk outlet velocity of the reacting case $u_0(\phi)$ normalized by $u_0(\phi = 0)$ of the isothermal case which is observed to increase 10–20% at moderate equivalence ratios ($\phi = 0.4 - 0.6$) for test rig conditions. The bulk outlet velocity is not the governing parameter for flashback safety. It is given anyway, since it provides a vivid impression of how the additional fuel momentum impacts the overall velocity level. Both parameters' dependence on the air–fuel temperature ratio T_{in}/T_{fuel} is given in Fig. 1 in order to estimate the remaining impact at engine conditions. The impact of fuel momentum deducted from the test rig results is, thus, slightly overestimated with respect to engine conditions (u_0: less then 5%; J by a factor of 1.7).

Experimental Setup and Diagnostics

Burner Model. Figure 2 provides a schematic of the investigated swirl burner. There are two ways for the main air flow to enter the cylindrical mixing tube. First, through the radial swirl generator, whereby a certain amount of swirl is imposed on the flow, depending on the number of blocking rings. Second, through

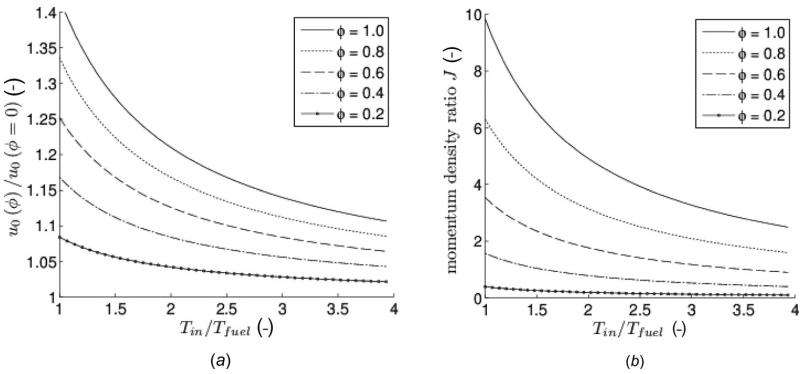

Fig. 1 Increase of both, (*a*) bulk outlet velocity $u_0(\phi)$ and (*b*) momentum ratio *J*, with equivalence ratio strongly depends on ratio of inlet air to fuel temperature (T_{in}/T_{fuel})

an orifice of the diameter D_{or} on the central axis, constituting the axial air injection. The amount of axially injected air is not metered but adjusted only by the ratio of pressure loss between the swirl generator and axial injection orifice. Therefore, varying the orifice diameter D_{or} allows to adjust the axial volume flow $\dot{V}_{ax}$. The orifice is either left open ($D_{or} = 8.8$ mm) or blocked by a variable size orifice $D_{or} = 5.0 - 8.0$ mm. The resulting ratio of axial to total volume flow is defined as $\chi = \dot{V}_{ax}/(\dot{V}_{ax} + \dot{V}_{swirl})$ and is determined from a comparison of the velocity field to previous measurements with metered axial air injection. Table 1 gives the axial injection volume flow for the investigated configurations 1–4. The fuel is injected into the premixing section through 16 injection ports located on an annular ring around the truncated center body. The mixing tube is located downstream of the swirl generator and has an inner diameter of $D = 34$ mm. A short ($l_{mt} = 40$ mm, displayed in the schematic) and a long ($l_{mt} = 60$ mm) mixing tube variant are tested. Auto ignition has been considered in the design process and the residence times in the premixing section are designed to remain below the auto-ignition delay times determined by Beerer and McDonnell [26]. The purpose of the circumferentially distributed dilution holes at $x/D = -0.7$ in the mixing tube, is to reduce the near-wall equivalence ratio in order to prevent boundary layer flashback. Since strong acceleration of the flow, appearing in converging nozzles, prevents a relocation of the flame in the combustion chamber in case of flashback, a cylindrical shape of the mixing tube was chosen. For the water tunnel experiments a plexi glass model of the burner was designed that, in addition to the combustion chamber, also provided full optical access to the mixing tube.

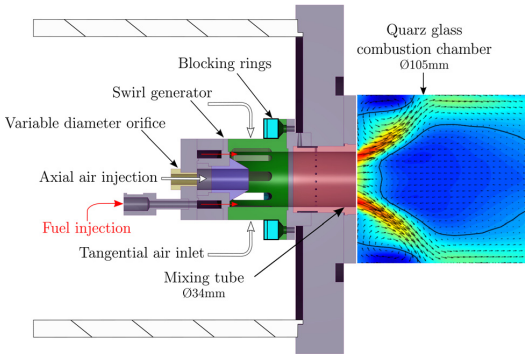

Fig. 2 Schematic of burner model, indicating different volume flow pathways through swirl generator or axial injection

Velocity Measurements. Initially, water tunnel experiments were conducted in order to characterize the impact of axial injection on the velocity field in the mixing tube (optically accessible only in water tunnel) as well as in the combustion chamber. The vertical test section of the water tunnel, which geometrically resembles the atmospheric test rig, allows for optical access to the streamwise plane from four sides (see Ref. [27] for a detailed description of the water test rig). In agreement with the gas-fired tests, the Reynolds number is set to $Re = 40{,}000$ with respect to the diameter of the mixing tube *D*. High-speed PIV, a nonintrusive optical method to obtain instantaneous 2D velocity data from seeding particles illuminated by a double pulsed Nd:YLF laser (0.75 kHz) with a wavelength of 527 nm and a pulse energy of 30 mJ per pulse, is applied. Two cylindrical lenses are used to form a light sheet of 2 mm thickness illuminating the streamwise plane downstream of the burner exit. For seeding of the flow, silver coated hollow glass spheres with a nominal diameter of 15 μm are added to the water. The scattered light is detected by a high-speed CMOS camera (Photron SA 1). The pulse separation is set to 0.1 and to 0.2 ms depending on the water volume flow. For the cross-correlation, an interrogation area of 16×16 pixels and 50% overlapping is selected. The velocity fields are averaged over 1000 image pairs and normalized with the bulk velocity at the burner exit u_o.

A schematic drawing of the atmospheric combustor test rig used for the present investigations is given in Fig. 3. The air entering the swirl generator is preheated up to $T_{in} = 620$ K. Located downstream of the burner model is the 105 mm diameter combustion chamber. It is made of quartz glass and, hence, optically accessible. For the PIV measurements, the same laser and high-speed camera (3 kHz) are used as in the water tunnel. The

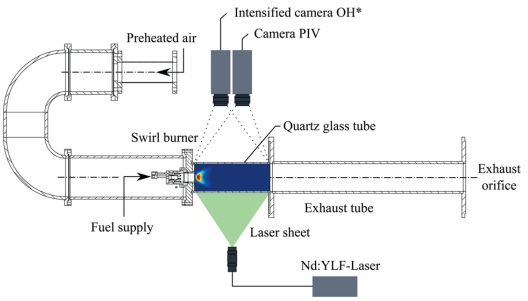

Fig. 3 Experimental setup for simultaneous PIV and OH* measurements in atmospheric combustion test rig

combustor air was seeded with Zirconium dioxide particles of 2 μm diameter. The pulse separation was set to 5–10 μs depending on mass flow and preheating temperature. The Reynolds number with respect to the mixing tube diameter is Re = 40,000 for comparison to the water tunnel experiments and is later increased up to Re = 75,000 for the recording of the stability map.

Flame Localization

OH Chemiluminescence Measurements.* The location of the flame is captured using a bandpass filtered intensified camera for the chemiluminescence of the OH* radical, which qualitatively correlates with the location of heat release and the intensity of the chemical reaction. Since the obtained images are line of sight-integrated the Abel-deconvolution algorithm is applied which assumes rotational symmetry in order to calculate the section view. Therefore, only time-averaged images can be Abel-deconvoluted. Although the OH* images are recorded at 3 kHz, the inverse Abel transform uses only the time-averaged information.

Quantitative Light Sheet Technique. The distribution of the density field inside the combustor is estimated using the QLS [28,29]. The advantage of QLS over alternatives, such as Raman or Rayleigh scattering, is the simplicity of the setup which is almost identical to the PIV setup and makes the QLS technique very suitable to be used simultaneously to PIV measurements. The QLS technique is used to derive the spatial distribution of the seeding density $P(x, y)$ from the amount of scattered light $I(x, y)$ which can be correlated to the fluid density $\rho(x, y)$. With the known homogeneous light intensity distribution $I_h(x, y)$ and the light intensity of an unseeded background image $I_b(x, y)$, for a measured light intensity distribution $I(x, y)$ the particle density ratio $P(x, y)/P_h$ can be obtained:

$$P(x,y)/P_h = (I(x,y) - I_b(x,y))/(I_h(x,y) - I_b(x,y)) \quad (1)$$

With the fluid density of the homogeneous image P_h which is calculated from the isothermal test rig inlet conditions, Eq. (2) yields the desired density distribution $\rho(x,y)$:

$$\rho(x,y) = \rho_h P(x,y)/P_h \quad (2)$$

Due to dilatation of the fluid, a sudden decrease in density is present over the flame front. The fluid density decreases from the unburnt density at the exit ρ_0 to the burnt density ρ_{burnt} downstream of the flame. Gradients in a single picture are very sharp and allow to differentiate between burnt and unburnt regions. The arithmetic mean between unburnt and burnt density is defined as a threshold $\rho_{thresh} = 1/2(\rho_0 + \rho_{burnt})$ which is used to pixelwise determine burnt $\alpha(x, y) = 1$ and unburnt regions $\alpha(x, y) = 0$ in every snapshot of the recorded time-resolved data.

$$\alpha = \begin{cases} 1 & if,\ \rho_{thresh} < \rho_0 \\ 0 & if,\ \rho_{thresh} > \rho_0 \end{cases} \quad (3)$$

Eventually, averaging over all recorded images at one location yields the flame probability $\bar{\alpha}(x, y) \in [0, 1]$, which is assumed as the probability of this region being filled with burnt or unburnt fluid. The flame probability $\bar{\alpha}(x, y)$, hence, allows to determine the upstream front of the flame. The downstream front can not be resolved since all fluid downstream of the flame front nearly assumes the same density ρ_{burnt}. With the QLS technique, in contrast to OH*, also instantaneous information about the flame front can be extracted. The flame location is resolved from an actual section view obtained by a laser sheet and at a rate of 3 kHz delivering time-resolved information about the flame location.

Emissions. Exhaust gas is extracted 850 mm downstream of the burner outlet and transported through a heated tube to a cold steam trap to remove humidity, before it is analyzed for NO, NO_2, and O_2 on a dry basis. For the investigated conditions of $\dot{m}_{air} = 180$ kg/h and a combustor power ranging from 35 to 80 kW this leads to a bulk hot gas residence time ranging from 0.07 to 0.035 s.

Results

Isothermal Velocity Field. The velocity field inside the mixing tube and the combustion chamber is investigated in a water tunnel in order to assess the impact of axial injection. Characteristics of the flow field in the absence and presence of a medium ($D_{or} = 8.0$ mm) and high amount ($D_{or} = 8.8$ mm) of axial air injection for a swirl number of $S = 0.9$ are presented in Fig. 4. For all investigated conditions, VB is established downstream of the area expansion. This leads to the typical flow field of swirl-stabilized combustors, which constitutes in an inner recirculation zone (IRZ), enveloped by an annular jet, and an outer recirculation zone (ORZ) between the annular jet and the bounding walls. It is observed that in the absence of axial air injection, the IRZ extends up to the nozzle outlet (Fig. 5, left). The line of zero axial

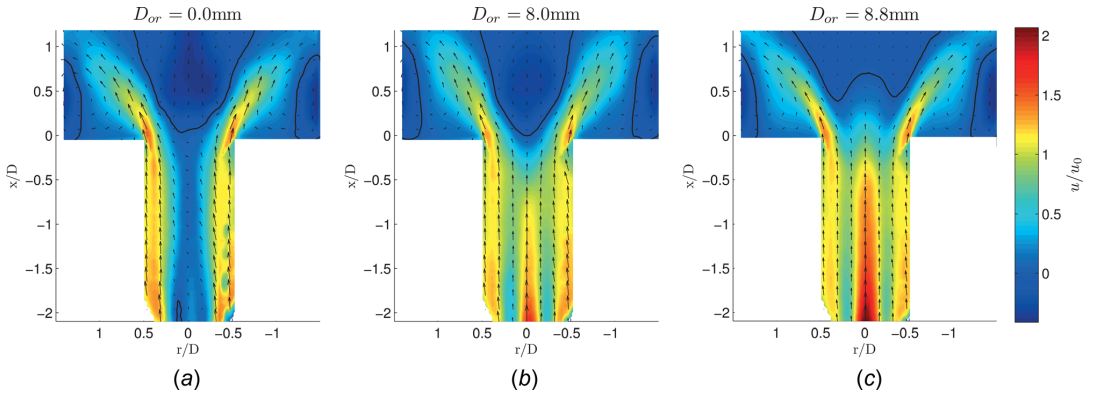

Fig. 4 Velocity vectors superimposed on normalized mean axial velocity of the isothermal flow field in the (*a*) absence ($D_{or} = 0$ mm) and (*b*) presence of a medium ($D_{or} = 8.0$ mm), and (*c*) high ($D_{or} = 8.8$ mm) amount of axial air injection (long mixing tube; $S = 0.9$), solid lines indicating zero axial velocity

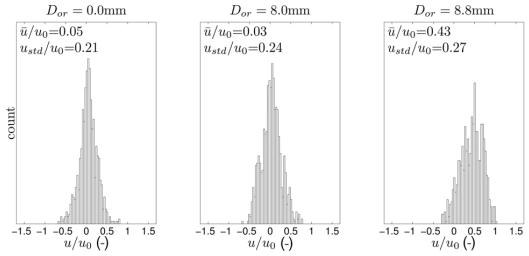

Fig. 5 Histogram of axial velocity at ($x/D = 0.1$, $r/D = 0$) for isothermal conditions in the absence ($D_{or} = 0$ mm) and presence of a medium ($D_{or} = 8.0$ mm) and high ($D_{or} = 8.8$ mm) amount of axial air injection (Re = 68,000)

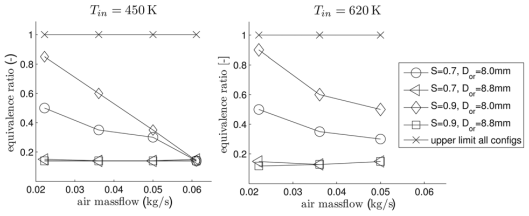

Fig. 6 Stability limits for varied air mass flows at two inlet temperatures; configurations 1–4 operated at stoichiometric conditions without flashback (symbol ×, not tested above stoichiometric). Hence, only the lower stability limits are displayed for each configuration.

velocity, indicated by the solid black line, is, on the central axis, located directly at the nozzle exit at $x/D < 0.1$. The flow field inside the mixing tube exhibits a deficit in axial velocity toward the center line for the entire length of the mixing tube. As revealed in the gas-fired tests reported below, when combusting hydrogen, such a flow field does not allow for permanent flame stabilization in the combustion chamber.

In case of a medium amount of axial air injection (Fig. 5, center), the flow field in the combustion chamber remains nearly unaffected. Merely, the opening angle of the annular jet is slightly reduced. This effect is assumed to appear due to the reduced swirl number when applying axial injection. However, strong changes are observed in the mixing tube. Here the deficit in axial velocity on the central axis is overcome and the axial injection yields a more homogenous radial distribution of axial velocity along the mixing tube.

Further increasing the amount of axial air injection to a high amount (Fig. 5, right) eventually yields flow field changes in the combustion chamber. As desired for flashback resistance, a downstream-shift of the stagnation point on the central axis is observed, from $x/D < 0.1$ to $x/D = 0.7$. Moreover, the opening angle of the annular jet significantly increases, contrarily to the further reduction of resulting swirl which can, hence, not be the only aspect influencing the opening angle. Terhaar et al. [18] suggest a link of the jet divergence to the cone and bubble type VB first observed by Billant et al. [21]. Inside the mixing tube, strong radial gradients in axial velocity due to the central jet are detected which, decline along the path through the premixing section, nearly achieving a plug flow shape at the nozzle exit. Generally, the effect of varied amounts of axial air injection is slightly different for varied swirl numbers and mixing tube lengths, a detailed overview of which is provided by previous work the authors [20]. Nevertheless, the general characteristics of the flow field remain the same as reported above.

A histogram of the axial velocity at ($x/D = 0.1$, $r/D = 0$), recorded in the atmospheric test rig, provides insight into the temporal velocity distribution. In accordance with the water tunnel tests, a medium amount of axial injection yields a minor reduction in mean velocity $\bar{u}$, due to the IRZ moving slightly upstream. The turbulence on the central axis is slightly increased indicated by the increase in normalized standard deviation. In the presence of a high amount of axial air injection, the desired downstream shift of the IRZ causes a strong increase in mean velocity to $\bar{u}/u_0 = 0.43$. Nevertheless, for some times t the instantaneous velocity $u(\boldsymbol{x}, t)$ is still $u(\boldsymbol{x}, t) < 0$ due to the normalized standard deviation being further increased with increased axial air injection.

Atmospheric Test Rig

Operational Limits and Stability Map. For operation with hydrogen without axial air injection, none of the configurations provides a satisfying operation range without flashback. However, applying a medium or high amount of axial air injection, all configurations are capable of operating at stoichiometric conditions (Fig. 6). The results reveal that for $D_{or} = 8.8$ mm at inlet temperatures up to $T_{in} = 620$ K no flashback occurs over the whole operating range of the test rig. The lower stability limit is the LBO limit which is observed to be as low as $\phi = 0.15$, irrespective of the swirl number.

For $D_{or} = 8.0$ mm and an air mass flow of $\dot{m} = 0.06$ kg/s, the stable equivalence ratios range from stoichiometric to LBO at $\phi = 0.15$. With decreasing air mass flow below $\dot{m} = 0.06$ kg/s this range of stable equivalence ratios becomes narrower. The smaller the air mass flow, the higher the equivalence ratio of the lower limit. The upper limit remains at $\phi = 1.0$. Additionally, it is observed that at identical inlet conditions the lower swirl ($S = 0.7$) exhibits a wider operating window than the higher swirl ($S = 0.9$). Other then in case of high axial air injection, the lower limit is not caused by LBO but rather by the flame flashing back in the premixing section.

It can be summarized that for high axial air injection ($D_{or} = 8.8$ mm) no flashback occurred at all. Moreover, although the isothermal velocity field of $D_{or} = 8.0$ mm did not exhibit the desired plug flow like velocity profile at the nozzle exit, it could still be operated at stoichiometric conditions. However, flashback occurred below a certain equivalence ratio at mass flows lower then $\dot{m} = 0.06$ kg/s, despite the fact that the laminar burning velocity of lean hydrogen air mixtures decreases with equivalence ratio. Consequently, the ability to withstand flashback of the $D_{or} = 8.0$ mm configurations is assumed to stem from the additional fuel momentum, whose impact can be derived from the PIV measurements of the reacting flow.

Reacting Velocity Field—Observation. It is observed that for a high amount of axial injection (Fig. 7, top row) the stagnation point on the central axis is shifted downstream with increasing equivalence ratio; from $x/D = 0.6$ at isothermal conditions to $x/D = 1.4$ and $x/D = 2.0$ for $\phi = 0.4$ and $\phi = 0.8$, respectively. Such a downstream shift is not observed for methane [18] and is hence attributed to both, the additional fuel momentum and increased dilatation due to increased heat addition. Additionally, the overall velocity level is elevated with increasing equivalence ratio for the same reasons. Due to its wide opening angle and the plug flowlike velocity profile at the nozzle exit, the VB type in the presence of a high amount of axial air injection is identified as cone type VB [21].

Evaluating the histogram of axial velocity at ($x/D = 0.1$, $r/D = 0$) shows the significant increase in normalized mean velocity with equivalence ratio. Moreover, the standard deviation of axial velocity is reduced, which can be explained by the lower resulting swirl number in the presence of axially injected fuel. For a medium amount of axial air injection (Fig. 7, bottom row) the isothermal case features a much narrower IRZ opening angle than for a high amount of axial injection and exhibits an axial velocity deficit in the nozzle exit plane. The VB is, thus, identified to be of

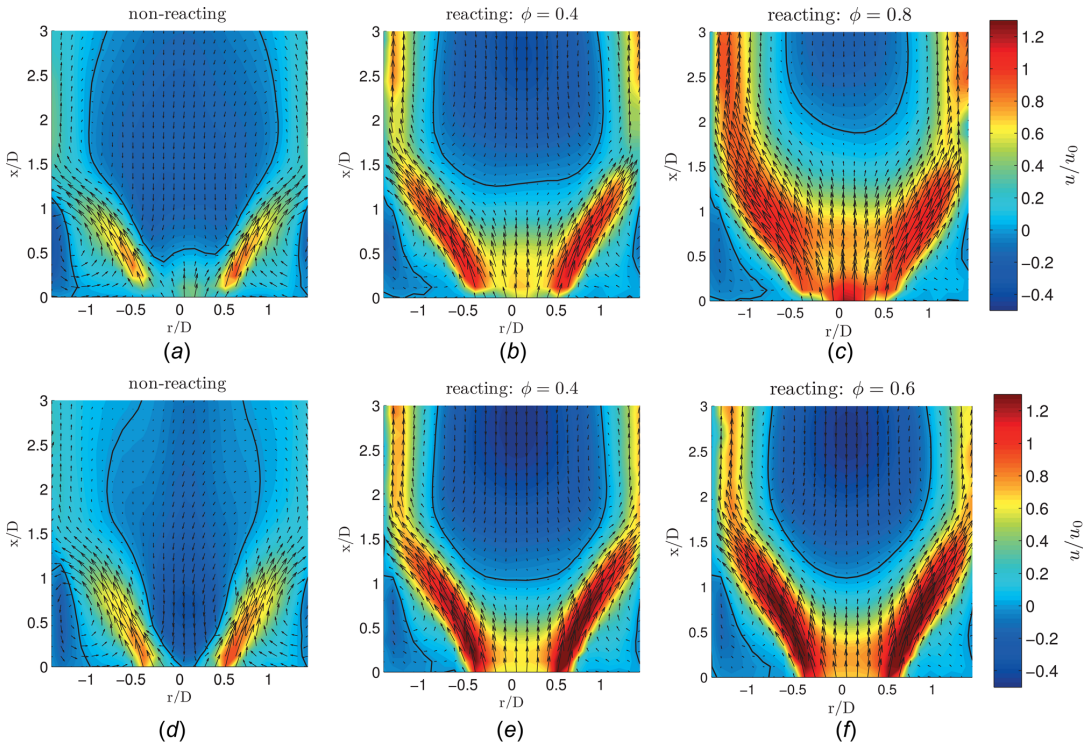

Fig. 7 Impact of increased equivalence ratio for the reacting flow ($\dot{m} = 180$ kg/h, $t_{in} = 450$ k) for a high ((*a*)–(*c*), $\phi = 0$, 0.4, and 0.8) and medium ((*d*)–(*f*), $\phi = 0$, 0.4, and 0.6) amount of axial air injection. Solid lines indicate zero axial velocity.

bubble type. However, for the reacting cases at $\phi = 0.4$ and 0.6 the stagnation point is shifted significantly to $x/D = 1.1$ and 1.2, respectively. Moreover, the IRZ opening angle widens and the axial velocity deficit is overcome. The VB is, thus, changed to cone type VB.

It is summarized that the fuel momentum and dilatation due to heat addition have a strong impact on the velocity field and are capable of creating the desired plug flow-shaped velocity profile at the nozzle outlet, in case this is not achieved yet, due to an only medium amount of axial air injection. This leads to the observed flashback safety at high equivalence ratios. On the other hand, a lack of fuel momentum and dilatation due to heat addition explains the occurring flashback for leaner mixtures in the presence of only a medium amount of axial injection. The type of flashback is identified as CIVB, since, for a high amount of axial injection, turbulent flame propagation in the core flow does not occur even at much lower mass flows and bulk velocities (Fig. 8 for $D_{or} = 8.8$ mm).

However, for high amounts of axial air injection the flow field is sufficiently conditioned to allow for flashback-proof operation for equivalence ratios ranging from $\phi = 0.15$ (LBO) to stoichiometric, at inlet temperatures up to $T_{in} = 620$ K, and mass flows as low as $\dot{m}_{air} = 0.02$ kg/s, which corresponds to the complete operating range of the atmospheric test rig.

Reacting Velocity Field—Explanation. Although both measures, additional fuel momentum and axial air injection, have a similar effect, a downstream shift of the VB, the underlying mechanism is different. Both measures substantially differ in the location where they are applied and in their working principle. Axial air injection is applied on the central axis ($r/D = 0$) with the aim to prevent a loss of azimuthal velocity in streamwise direction on the center line, which according to Burmberger and Sattelmayer

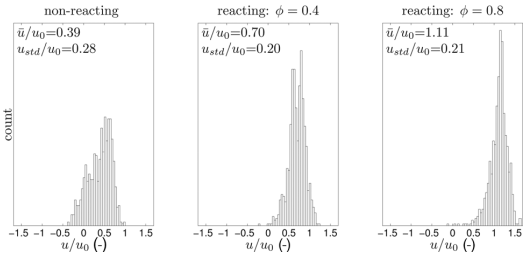

Fig. 8 Histogram of axial velocity at ($x/D = 0.1$, $r/D = 0$) revealing impact of fuel momentum in the presence of high ($D_{or} = 8.8$ mm) amount of axial air injection (Re = 75,000)

[13] leads to the a delay of VB. The resulting swirl number S_{res}, which is measured at the nozzle outlet, is slightly reduced. The governing parameter is the axial air injection ratio χ.

Axial fuel injection, on the other hand, is applied on a high radius ($r/D = 0.46$), where it directly interferes with the air entering through the radial swirl generator. Right at the bottom of the mixing tube, the injected fuel adds axial momentum to the air entering the premixing section and hence reduces the primary swirl number S_{prim}, which is the swirl number before interacting with the axial nonswirling jet. The impact of fuel momentum is quantified by the fuel–air momentum ratio J.

To visualize the difference in character of the two measures and their influence on the flow field, we refer to the diagram suggested by Terhaar et al. [18] given in Fig. 9. The diagram pictures the decrease of primary swirl number S_{prim} to the resulting swirl number S_{res} in the presence of axial air injection. It was found that

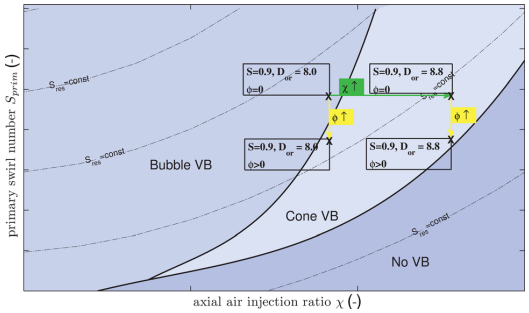

Fig. 9 Observed VB types during PIV measurements of configurations 3 and 4 transferred to schematic in Ref. [18], in order to explain difference in character of axial air injection ($\chi \uparrow$) and fuel momentum ($\phi \uparrow$)

below a critical resulting swirl number of S_{crit}, no VB is established. Above the critical resulting swirl number, two types of VB are distinguished: The bubble and cone type VB [21]. Their occurrence is not related to a certain resulting swirl number, but rather to a certain combination of primary swirl number S_{prim} and axial injection ratio χ. High primary swirl numbers at high rates of axial injection result in a plug flowlike velocity distribution at the combustor inlet and promote the cone type VB, which is desired flow flashback safety. The bubble type VB occurs for low rates of axial injection and is characterized by a narrow IRZ and an axial velocity deficit in the combustor inlet plane. This velocity deficit makes the bubble type VB prone to flashback. As was shown by the PIV results of the reacting flow (Fig. 7), fuel momentum has the capability to alter the bubble type to cone type VB and, thus, decrease flashback propensity. This behavior is intended to be explained and predicted by the use of the diagram.

The diagram was obtained for a setup with an identical premixing section, i.e., axial air injection and fuel injection, but a different radial swirl generator. Consequently, the operating conditions in the different setups do not exactly coincide and no quantitative statements but qualitative trends can be derived. The operating points of the PIV measurement from Fig. 7 are added to the diagram Fig. 9. Furthermore, the effect of the increased axial injection χ and equivalence ration ϕ is indicated. Other than for increased χ, which resembles a right shift, for increased ϕ the points are shifted down. As explained above, this is due to the decreased primary swirl number. In agreement with the observations from the PIV measurements, the diagram predicts a change from bubble to cone type VB for the medium axial air injection ($D_{or} = 8.0$ mm). For a high amount of axial air injection ($D_{or} = 8.8$ mm) the diagram agrees with the measurements by predicting the VB to be of cone type, remain there in the presence of additional fuel momentum but get close to the region of no VB, which can be inferred from the shrinking IRZ in the PIV results.

In summary, the diagram succeeds in correctly reproducing and predicting the VB types in a qualitative manner. The VB type determines the combustor inlet plane velocity distribution and, thus, flashback propensity. Consequently, the diagram allows for the prediction of flashback safety for burner configurations with respect to swirl number S, axial air injection χ, and equivalence ratio ϕ.

However, in order to obtain quantitative predictions, the diagram, i.e., the critical resulting swirl numbers for a change from cone to bubble type VB, would have to be recorded for this specific burner geometry, which is planned as future work.

Flame Localization. According to the results from the recorded stability map, configuration 4 exhibits flashback safety over the whole operating range and is, thus, investigated further to determine the flame location corresponding to the velocity fields in Fig. 7. The results from the QLS and OH* chemiluminescence measurements are given in Figs. 10 and 11, respectively.

Both measurement techniques agree in resolving a flame detached from the burner exit for $T_{in} = 450$ K and equivalence from $\phi = 0.4 - 0.8$. For the QLS image at $\phi = 0.8$ the flame probability in the shear layer of the jet is slightly overpredicted. This is due to the fuel momentum reducing the swirl number and, hence, the jet angle in comparison to the isothermal case which was used to obtain the homogeneous intensity reference image. The OH* intensity distribution in Fig. 11 for the same condition proves the flame not to propagate in the shear layer.

However, the flame location on the central axis is shown, by both techniques, to be slightly shifted downstream with increasing equivalence ratio. On the one hand, this effect contradicts the increase in laminar burning velocity with increasing equivalence ratio which actually promotes an upstream travel of the flame. On the other hand, the additional fuel momentum at $\phi = 0.4$ and $\phi = 0.8$, which is shown to alter the flow field by shifting the stagnation point and increases the overall velocity level, seems to outweigh the increase in burning velocity. This results in the observed slight downstream shift of the flame front.

Emissions. The NO_x concentration for the hydrogen combustion plotted with respect to the calculated adiabatic flame temperature is presented in Fig. 12. For a high amount of axial air injection, irrespective of swirl number ($S = 0.7 - 0.9$) and mixing tube length ($l_{mt} = 40 - 60$ mm), the burner's emissions remain below 10 ppm (dry at 15% O_2) up to a calculated adiabatic flame temperature of $T_b = 2000$ K.

It is, thus, proven that the concept of axial air injection allows to increase flashback safety and extend the operational range while maintaining single digit NO_x emissions. These findings are in line with the results from a previous work of the authors which showed the positive impact of axial air injection on spatial and

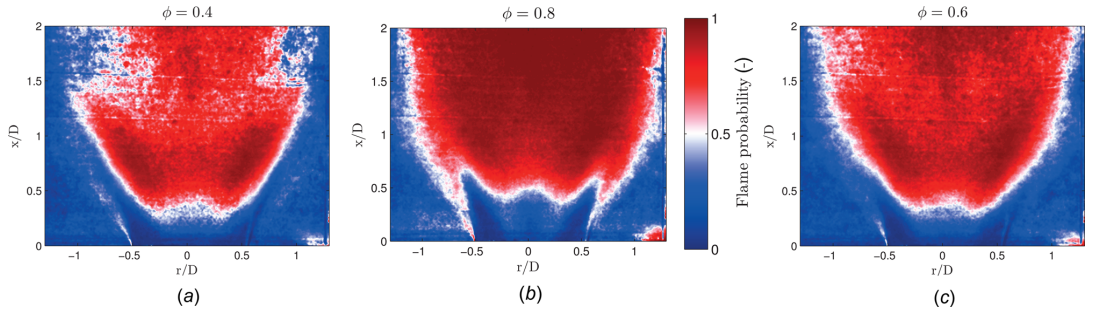

Fig. 10 Flame probability indicating the likelihood of the flame to appear in a certain region, hence, allowing to determine the upstream flame shape (Re = 75,000)

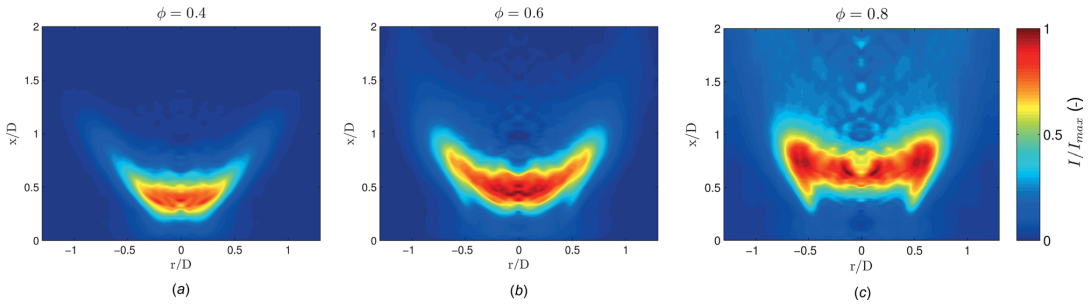

Fig. 11 ABEL-deconvoluted OH* images normalized to the maximum intensity of the image at $\phi = 0.8$ (Re = 75,000)

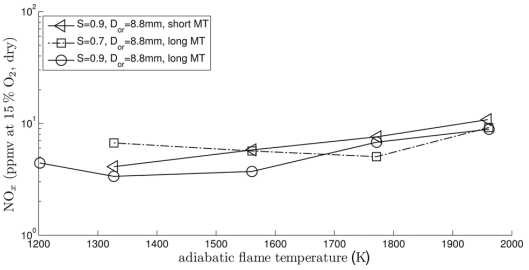

Fig. 12 NO_x emissions (dry) over calculated adiabatic flame temperature for high axial air injection

temporal fuel air mixing in a water tunnel, due to the suppression of a helical flow instability [20].

Conclusion

The flow field of a swirl-stabilized burner operating on lean premixed hydrogen is successfully tailored by means of axial air injection to fulfill the requirements for flashback-proof operation. A detailed comparison of the effect of different amounts of axially injected air on the isothermal and reacting flow field is provided. The desired effect of a high amount of axial air injection, a plug flowlike velocity profile at the nozzle exit, is observed to remain present and be even enforced under reacting conditions. The enforcement of the effect is assigned to the additional fuel momentum, stemming from the high fuel volume flow, which already occurs at moderate equivalence ratios. The impact of additional fuel momentum as a function of inlet conditions and equivalence ratio is quantified (Fig. 1). Moreover, an explanation on how axial air injection and fuel momentum influence the occurrence of VB type is provided, concluding that the cone type VB is superior over the bubble type VB in terms of flashback safety.

Furthermore, we recorded a stability map for four configurations which vary with respect to swirl number and amount of axial air injection. These gas-fired tests revealed that the concept of axial air injection allows for flashback-proof swirl-stabilized combustion of technically premixed hydrogen mixtures. It was noted that at least a medium amount of axial injection was mandatory to achieve a satisfying operation of the burner on undiluted hydrogen. However, in the presence of a high amount of axial air injection, no occurrence of flashback was observed on the whole operating range of the atmospheric test rig, with inlet temperatures ranging up to 620 K and up to stoichiometric conditions.

NO_x emissions in the presence of a high amount of axial air injection have been shown to remain below 10 ppm (dry at 15% O_2) up to a calculated adiabatic flame temperature of 2000 K. At a swirl number of $S = 0.9$, irrespective of the flame temperature, the NO_x emissions of a high amount of axial air injection are always lower compared to a medium amount. OH* chemiluminescence and the QLS measurement techniques have been used to determine the location of flame anchoring. For a high amount of axial air injection, the flame is proven to remain anchored in the combustion chamber under all operating conditions. While detached from the rim, the lift off height of the flame is noted to slightly increase with equivalence ratio, which is explained with the additional fuel momentum. An increase in fuel momentum causes both, a reduction in primary swirl number and elevation of the overall velocity level, resulting in a slight downstream shift of the flame front.

The results prove axial air injection to significantly increase flashback safety and hence the operational range of lean premixed hydrogen combustion. At high amounts of axial air injection no flashback occurred while maintaining single digit NO_x emissions below a calculated adiabatic flame temperature of $T_b = 2000$ K.

Acknowledgment

The research leading to these results has received funding from the European Union Seventh Framework Program (FP7/2007-2013) under Grant agreement No. 284636 and the European Research Council under the ERC Grant agreement No. 247322, GREENEST.

Nomenclature

D = burner outlet diameter
D_{or} = orifice diameter for axial air injection
IRZ = inner recirculation zone
J = momentum ratio
l_{mt} = length of mixing tube
ORZ = outer recirculation zone
Re = Reynolds number
S = geometric swirl number
S_{crit} = critical swirl number for occurrence of VB
S_{prim} = primary swirl number for $\chi = 0$
S_{res} = resulting swirl number for $\chi > 0$
T_b = adiabatic flame temperature K
T_{fuel} = fuel inlet temperature K
T_{in} = air inlet temperature in K
u = axial velocity
u_0 = bulk outlet velocity for $\phi = 0$
$\dot{V}_{ax}$ = air volume flow through axial injection
$\dot{V}_{swirl}$ = air volume flow through radial swirl generator
VB = vortex breakdown
$\bar{\alpha}$ = flame probability
ρ_{air} = air density
ρ_{fuel} = fuel density
ϕ = equivalence ratio
χ = axial injection ratio $\chi = \dot{V}_{ax}/(\dot{V}_{ax} + \dot{V}_{swirl})$

References

[1] Brand, J., Sampath, S., and Shum, F., 2003, "Potential Use of Hydrogen in Air Propulsion," AIAA Paper No. 2003–2879.

[2] Corchero, G., and Montañés, J. L., 2005, "An Approach to the Use of Hydrogen for Commercial Aircraft Engines," Proc. Inst. Mech. Eng., Part G., **219**(1), pp. 35–44.
[3] Haglind, F., and Singh, R., 2006, "Design of Aero Gas Turbines Using Hydrogen," ASME J. Eng. Gas Turbines Power, **128**(4), pp. 754–764.
[4] Yin, F., Rao, A. G., and van Buijtenen, J., 2013, "Performance Cycle Analysis for a Multi-Fuel Hybrid Engine," ASME Paper No. GT2013-94601.
[5] Levy, Y., Sherbaum, V., and Arfi, P., 2004, "Basic Thermodynamics of FLOXCOM, the Low-NO_x Gas Turbines Adiabatic Combustor," Appl. Therm. Eng., **24**(11), pp. 1593–1605.
[6] Boerner, S., Funke, H. H.-W., Hendrick, P., Recker, E., and Elsing, R., 2011, "Development and Integration of a Scalable Low NO_x Combustion Chamber for a Hydrogen-Fueled Aerogas Turbine," Prog. Propuls. Phys., **4**, pp. 357–372.
[7] Lefebvre, A. H., and Ballal, D. R., 2010, *Gas Turbine Combustion: Alternative Fuels and Emissions*, 3rd ed., Taylor & Francis, Boca Raton, FL.
[8] Ziemann, J., 1998, "Low-NO_x Combustors for Hydrogen Fueled Aero Engine," Int. J. Hydrogen Energy, **23**(4), pp. 281–288.
[9] Beerer, D., McDonnell, V., Therkelsen, P. L., and Cheng, R. K., 2012, "Flashback, Blow Out, Emissions and Turbulent Displacement Flame Speed Measurements in a Hydrogen and Methane Fired Low-Swirl Injector at Elevated Temperatures and Pressures," ASME Paper No. GT2012-68216.
[10] Döbbeling, K., and Hellat, J., 2007, "25 Years of BBC/ABB/Alstom Lean Premix Combustion Technologies," ASME J. Eng. Gas Turbines Power, **129**(1), pp. 2–12.
[11] Gupta, A. K., Lilley, D. G., and Syred, N., 1984, *Swirl Flows*, Abacus, Tunbridge Wells and Kent, UK.
[12] Burmberger, S., Hirsch, C., and Sattelmayer, T., 2006, "Designing a Radial Swirler Vortex Breakdown Burner," ASME Paper No. GT2006-90497.
[13] Burmberger, S., and Sattelmayer, T., 2011, "Optimization of the Aerodynamic Flame Stabilization for Fuel Flexible Gas Turbine Premix Burners," ASME J. Eng. Gas Turbines Power, **133**(10), p. 101501.
[14] Burmberger, S., Hirsch, C., and Sattelmayer, T., "Design Rules for the Velocity Field of Vortex Breakdown Swirl Burners," ASME Paper No. GT2006-90495.
[15] Jochmann, P., Sinigersky, A., Koch, R., and Bauer, H.-J., "URANS Prediction of Flow Instabilities of a Novel Atomizer Combustor Configuration," ASME Paper No. GT2006-90495.
[16] Spencer, A., McGuirk, J. J., and Midgley, K., 2008, "Vortex Breakdown in Swirling Fuel Injector Flows," ASME J. Eng. Gas Turbines Power, **130**(2), p. 021503.
[17] Midgley, K., Spencer, A., and McGuirk, J. J., 2005, "Unsteady Flow Structures in Radial Swirler Fed Fuel Injectors," ASME J. Eng. Gas Turbines Power, **127**(4), pp. 755–764.
[18] Terhaar, S., Reichel, T. G., Schrödinger, C., Rukes, L., Paschereit, C. O., and Oberleitner, K., 2013, "Vortex Breakdown and Global Modes in Swirling Combustor Flows With Axial Air Injection," AIAA Paper No. 0748-4658.
[19] Galley, D., Ducruix, S., Lacas, F., and Veynante, D., 2011, "Mixing and Stabilization Study of a Partially Premixed Swirling Flame Using Laser Induced Fluorescence," Combust. Flame, **158**(1), pp. 155–171.
[20] Reichel, T. G., Terhaar, S., and Paschereit, C. O., 2013, "Flow Field Manipulation by Axial Air Injection to Achieve Flashback Resistance and Its Impact on Mixing Quality," AIAA Paper No. 2013-2603.
[21] Billant, P., Chomaz, J.-M., and Huerre, P., 1998, "Experimental Study of Vortex Breakdown in Swirling Jets," J. Fluid Mech., **376**, pp. 183–219.
[22] Mayer, C., Sangl, J., Sattelmayer, T., Lachaux, T., and Bernero, S., 2012, "Study on the Operational Window of a Swirl Stabilized Syngas Burner Under Atmospheric and High Pressure Conditions," ASME J. Eng. Gas Turbines Power, **134**(3), p. 031506.
[23] Sangl, J., Mayer, C., and Sattelmayer, T., "Dynamic Adaptation of Aerodynamic Flame Stabilization of a Premix Swirl Burner to Fuel Reactivity Using Fuel Momentum," ASME Paper No. GT2010-22340.
[24] Lieuwen, T., McDonell, V., Petersen, E., and Santavicca, D., 2008, "Fuel Flexibility Influences on Premixed Combustor Blowout, Flashback, Autoignition, and Stability," ASME J. Eng. Gas Turbines Power, **130**(1), p. 011506.
[25] Kröner, M., Fritz, J., and Sattelmayer, T., 2003, "Flashback Limits for Combustion Induced Vortex Breakdown in a Swirl Burner," ASME J. Eng. Gas Turbines Power, **125**(3), pp. 693–700.
[26] Beerer, D. J., and McDonell, V. G., 2008, "Autoignition of Hydrogen and Air Inside a Continuous Flow Reactor With Application to Lean Premixed Combustion," ASME J. Eng. Gas Turbines Power, **130**(5), p. 051507.
[27] Lacarelle, A., and Paschereit, C. O., 2012, "Increasing the Passive Scalar Mixing Quality of Jets in Crossflow With Fluidics Actuators," ASME J. Eng. Gas Turbines Power, **134**(2), p. 021503.
[28] Roehle, I., Schodl, R., Voigt, P., and Willert, C., 2000, "Recent Developments and Applications of Quantitative Laser Light Sheet Measuring Techniques in Turbomachinery Components," Meas. Sci. Technol., **11**(7), pp. 1023–1035.
[29] Terhaar, S., and Paschereit, C., 2012, "High-Speed PIV Investigation of Coherent Structures in a Swirl-Stabilized Combustor Operating at Dry and Steam-Diluted Conditions," 16th International Symposium on Applications of Laser Techniques to Fluid Mechanics, Lisbon, Portugal, July 9–12, pp. 37–48.

2.3 Third Publication[1]

Investigation of Lean Premixed Swirl-Stabilized Hydrogen Burner With Axial Air Injection Using OH-PLIF Imaging

Thoralf G. Reichel[1]
Chair of Fluid Dynamics,
Hermann-Föttinger-Institut,
Technische Universität Berlin,
Müller-Breslau-Str. 8,
Berlin 10623, Germany
e-mail: thoralf.reichel@tu-berlin.de

Katharina Goeckeler
Chair of Fluid Dynamics,
Hermann-Föttinger-Institut,
Technische Universität Berlin,
Müller-Breslau-Str. 8,
Berlin 10623, Germany

Oliver Paschereit
Chair of Fluid Dynamics,
Hermann-Föttinger-Institut,
Technische Universität Berlin,
Müller-Breslau-Str. 8,
Berlin 10623, Germany

In the context of lean premixed combustion, the prevention of upstream flame propagation in the premixing zone, referred to as flashback (FB), is a crucial challenge related to the application of hydrogen as a fuel for gas turbines. The location of flame anchoring and its impact on FB tendencies in a technically premixed, swirl-stabilized hydrogen burner are investigated experimentally at atmospheric pressure conditions using planar laser-induced fluorescence of hydroxyl radicals (OH-PLIF). The inlet conditions are systematically varied with respect to equivalence ratio ($\phi = 0.2 - 1.0$), bulk air velocity $u_0 = 30–90\,m/s$, and burner preheat temperature ranging from 300 K to 700 K. The burner is mounted in an atmospheric combustion test rig, firing at a power of up to 220 kW into a 105 mm diameter quartz cylinder, which provides optical access to the flame region. The experiments were performed using an in-house burner design that previously proved to be highly resistant against FB occurrence by applying the axial air injection strategy. Axial air injection constitutes a nonswirling air jet on the central axis of the radial swirl generator. While a high rate of axial air injection yields excellent FB resistance, reduced rates of air injection are utilized to trigger FB, which allowed to investigate the near FB flame behavior. Results show that both, fuel momentum of hydrogen and axial air injection, alter the isothermal flow field as they cause a downstream shift of vortex breakdown and, thus, the axial flame front location. Such a shift is proven beneficial for FB resistance from the recorded FB limits. This effect was quantified by applying an edge detection algorithm to the OH-PLIF images, in order to extract the location of maximum flame front probability x_F. By these means, it was revealed that for hydrogen x_F is shifted downstream with increasing equivalence ratio due to the added momentum of the fuel flow, superseding any parallel augmentation in the turbulent flame speed. The parameter x_F is identified to be governed by J, the momentum ratio between fuel and air flow, over a wide range of inlet conditions. These results contribute to the understanding of the sensitivity of FB to changes in the flow field, stemming from geometry changes or specific fuel properties. [DOI: 10.1115/1.4031181]

Introduction

Future demands on air transport systems dictate that aircraft should be less polluting, less noisy, and more fuel efficient. In the long term, alternative fuels like biofuels and hydrogen are likely to replace traditional jet fuel [1–3]. Experimental tests on a low NO_x hydrogen combustor for aero engines have been conducted within the European Union supported FP7 project *Advanced Hybrid Engines for Aircraft Development (AHEAD)*. The concept proposed in the *AHEAD* project is a contrarotating turbofan engine with sequential dual hybrid combustors, using two different fuels [4]. The engine is operated on pure hydrogen in the first stage and biofuel under flameless conditions [5] in the second stage, aiming to reduce CO_2 and NO_x emission, respectively. This study focuses on the hydrogen combustion carried out in the first stage.

Similar to other modern premixer concepts [6], in the current investigation, a center body-less mixing tube and lean premixed, swirl-stabilized combustion are applied. Such a setup promises enhanced mixing and creates a central recirculation zone (CRZ) that provides for locally reduced flow velocities, recirculation of hot gases and, thus, flame stability [7]. For lean premixed combustion, with increasing fuel reactivity lean blow out (LBO) limits are extended but FB disposition is increased [8]. FB terms the upstream propagation of a flame in a combustible mixture into regions not designed for flame holding. Common measures against FB are an increase in bulk air velocity or a decrease in swirl intensity. These measures come with a significant tradeoff in terms of increased pressure loss and degraded fuel air-mixing [9], respectively. While increased pressure loss reduces the engine efficiency, decreased fuel air-mixing quality increases NO_x emissions [10]. Another approach with less tradeoff is to inject an air film to lean out the wall-near boundary layer, which is particularly susceptible to flame propagation, due its low velocity level [11]. This approach is successfully used in the current setup to suppress wall boundary layer FB. Additionally, the burner applies axial air injection, which constitutes a nonswirling air jet on the central axis of the radial swirl generator. The application of such low-momentum air jet to increase the FB resistance when operating with syngases was first suggested by Burmberger and Sattelmayer [12]. It is applied with the intention to create a plug flowlike axial velocity profile at the nozzle exit and shift the stagnation point downstream. This technique vastly extends the current burners operational range. At a high amount of axial air injection, FB is suppressed on the whole operational range of the atmospheric test

[1]Corresponding author.

Contributed by the Combustion and Fuels Committee of ASME for publication in the Journal of Engineering for Gas Turbines and Power. Manuscript received July 13, 2015; final manuscript received July 20, 2015; published online September 18, 2015. Editor: David Wisler.

1 Republished with permission of American Society of Mechanical Engineers ASME, from Investigation of Lean Premixed Swirl-Stabilized Hydrogen Burner With Axial Air Injection Using OH-PLIF Imaging, Reichel et. al, *Journal of Engineering for Gas Turbines and Power*, Bd. 137 (2015) (11): 111513; permission conveyed through Copyright Clearance Center, Inc.

rig (compare Fig. 1). At the same time, single-digit NO_x emissions up to adiabatic flame temperatures of $T_{ad} = 2000$ K could be maintained [13].

In case of hydrogen fuel, a significant amount of additional momentum is introduced in the premixing section, which stems from the high volumetric flow rates associated to hydrogen fuel (see next section, Quantification of Additional Fuel Momentum). In case of technically premixed systems, like in the current study, this effect has to be taken into consideration in the context of fuel injection location. The works of Mayer et al. [14] and Sangl et al. [15] both applied a nonswirling, axial fuel jet, making use of the additional fuel momentum of hydrogen. By shifting the fuel injection mode from trailing edge injection in the radial swirler vanes toward the axial fuel jet, they reported an extension of the FB limits but also highly increased NO_x emissions.

The current setup's fuel injection is arranged through 16 circumferentially distributed, streamwise orientated, injection holes. This allows for taking advantage of the additional fuel momentum while simultaneously optimizing the spatial distribution of the fuel and maintaining single-digit NO_x emissions, which were reported in a previous study of the authors [13].

These previous atmospheric tests on the current combustor configuration report a very high FB safety margin for the setup employing high axial air injection. For inlet temperatures up to $T_{in} = 700$ K and stoichiometric conditions, no FB occurs over the whole operating range of the test rig (Fig. 1, square symbols). The lower stability limit is the LBO limit which is observed to be as low as $\phi = 0.15$. For a medium amount of axial air injection, the FB safety margin is reduced. FB occurred when the equivalence ratio was reduced below a certain value at mass flows lower then $\dot{m} = 0.06$ kg/s, although the burner could be operated up to stoichiometric conditions (Fig. 1, circle symbols). This may appear counter-intuitive, since the laminar burning velocity of lean hydrogen–air mixtures increases with increased equivalence ratio. However, it can be shown that the ability of this configuration to withstand FB stems from the flow field changes inferred by the additional fuel momentum, which outweighs the increase in flame speed. To support this statement, the fuel momentum's impact on the isothermal velocity field is documented in the Results section below. The impact of fuel momentum on the reacting flow field for both, medium and high rates of axial air injection, reportedly prevails at reacting conditions [13,16].

Both axial air injection and fuel momentum impact the flow field and, hence, the flame position. The axial position of the flame front is reported to travel upstream when approaching conditions where FB occurs [13,17,18]. It is therefore considered as an indicator of the FB safety margin for the respective condition and investigated by means of OH-PLIF. A number of studies have previously applied OH-PLIF to hydrogen enriched methane or syngas mixtures [18–21]. However, OH-PLIF data of lean premixed hydrogen flames are scarcely published [17,22] and cannot be found for swirl-stabilized hydrogen flames in literature.

In the current study, the axial flame front location is investigated as a function of axial air injection and fuel momentum for a variety of inlet parameters. Therefore, inlet conditions were varied with respect to equivalence ratio ($\phi = 0.2 - 1.0$), bulk air velocity $u_0 = 30$–90 m/s, and burner preheat temperature ranging from 300 K to 700 K. OH-PLIF is applied in order to extract the instantaneous flame front from a set of snap shots and to calculate the axial location of maximum flame front probability x_F. This parameter is then used as an estimator of the safety margin to FB for the respective configuration.

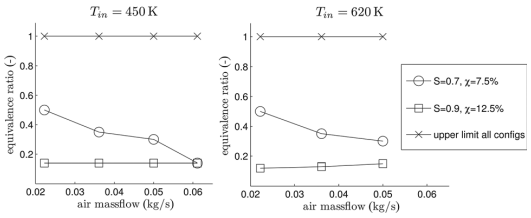

Fig. 1 Stability limits (from Ref. [13]) for $\chi = 12.5\%$ and $\chi = 7.5\%$; both configurations operated at $\phi = 1$ without FB (symbol ×, $\phi > 1$ not tested). Hence, only the lower stability limits are displayed.

The remainder of the paper is structured as follows. First, the effect of both, varied amounts of axial air injection and fuel mass flows on the isothermal flow field in the premixing section and combustion chamber, is studied from particle image velocimetry (PIV) measurements in a water tunnel. Subsequently, instantaneous OH-PLIF recordings and mean OH signal probability distributions yield a qualitative overview of the flame characteristics for two selected configurations, representing a high and very low FB safety margin. Next, the parameter x_F, which is considered an estimator for the FB safety margin, is evaluated at all investigated conditions detailed in Table 1. The results are utilized to identify the governing parameters for x_F with respect to varied inlet conditions.

Quantification of Additional Fuel Momentum. In order to achieve a desired power output from hydrogen, about 3.5 times higher volumetric fuel flow rates in comparison to methane are required, due to hydrogen's low energy content per unit volume. Therefore, a considerable amount of additional volume flow is introduced into the system, causing both, changes in the flow field and an increase in bulk mixture velocity $u_0(\phi)$ [23]. Two different parameters can be used to describe the impact of fuel momentum. First, and most importantly, the fuel air momentum ratio J, which is defined as

$$J = \frac{\rho_{\text{fuel}} u_{\text{fuel}}^2}{\rho_{\text{air}} u_{\text{air}}^2} \tag{1}$$

Second, the bulk mixture velocity of the reacting case $u_0(\phi)$ normalized by $u_0(\phi = 0)$, which is observed to increase up to 20% already at moderate equivalence ratios ($\phi = 0.4 - 0.6$) for typical test rig conditions. Both parameters strongly depend on

Table 1 Investigated conditions for hydrogen; last column indicates whether the lower stability limit was LBO or FB

#	χ (%)	T_{in} (K)	u_0 (m/s)	$\dot{m}_{air}$ (kg/hr)	Re… 10^{-3}	ϕ
1–9	12.5	310	35	130	70	∈ [LBO, 1]
10–19			50	184	100	
20–29			60	220	120	
30–39			70	255	135	
40–49			80	295	160	
50–59		450	30	80	35	
60–69			50	130	55	
70–79			60	150	60	
80–89			70	180	75	
90–99			80	205	85	
100–109			90	230	95	
110–119		620	50	93	30	
120–129			60	110	35	
130–139			70	130	45	
140–149			80	148	50	
150–159		700	50	82	25	
160–169			60	100	30	
170–179			70	116	35	
180–189			80	133	40	
190–199	7.5	310	70	255	135	∈ [*FB*, 1]
201–209		420	70	180	75	∈ [*FB*, 1]
211–219		620	70	130	40	∈ [*FB*, 1]
221–229		700	70	116	35	∈ [*FB*, 1]

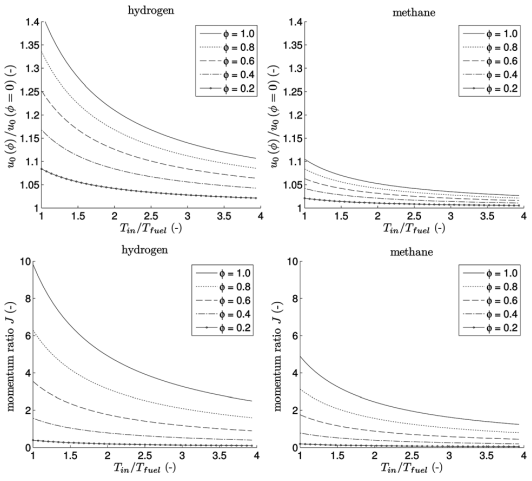

Fig. 2 Bulk outlet velocity $u_0(\phi)$, top, and momentum ratio J, bottom, at constant air mass flow $\dot{m}_{air}$ with respect to varied equivalence ratio ϕ and ratio of inlet air to fuel temperature (T_{in}/T_{fuel}) for hydrogen, left, and methane, right

equivalence ratio ϕ and air–fuel temperature ratio T_{in}/T_{fuel}. To visualize the stronger impact of fuel momentum for hydrogen, both parameters are given for methane (Fig. 2). The fuel temperature T_{fuel} in T_{in}/T_{fuel}, which is required to calculate J and $u_0(\phi)$, significantly varies for typical test rig conditions depending on the amount of air preheating. This stems from the fuel plenum and piping being exposed to the preheated air. T_{fuel} could not be measured for all conditions and is therefore modeled below (see Discussion section).

Experimental Setup and Diagnostics

Burner Model. Figure 3 provides a schematic of the investigated swirl burner. There are two ways for the main air flow to enter the cylindrical mixing tube. First, through the radial swirl generator, whereby a certain amount of swirl is imposed on the flow, depending on the number of blocking rings. Second, through an orifice of the diameter D_{or} on the central axis, constituting the axial air injection. The amount of axially injected air is not metered but adjusted only by the ratio of pressure loss between the swirl generator and axial injection orifice. Therefore, varying the orifice diameter D_{or} allows to adjust the axial to total volume flow ratio $\chi = \dot{V}_{ax}/(\dot{V}_{ax} + \dot{V}_{swirl})$. The values for χ of the unmetered case are determined from a comparison of the isothermal velocity field to the metered case and additional pressure measurements. The fuel split is, moreover, validated by a numerical investigation using Reynolds-averaged Navier–Stokes (RANS) and large eddy simulation (LES) [24].

The fuel is injected into the premixing section through sixteen injection ports located on an annular ring around the truncated center body. The mixing tube is located downstream of the swirl generator and has an inner diameter of $D = 34$ mm. The purpose of the circumferentially distributed dilution holes at $x/D = -0.7$ in the mixing tube is to reduce the near-wall equivalence ratio in order to prevent boundary layer FB. Note that the fuel plenum and supply pipes are exposed to the preheated air. Consequently, the amount of preheating impacts the fuel temperature T_{fuel} which is required for the calculation of the momentum ratio J. This effect is addressed in more detail in the Discussion section.

Water Tunnel. Water tunnel experiments were conducted in order to characterize the impact of both, axial air injection and fuel momentum on the velocity field in the mixing tube and the combustion chamber. In fact, the flow field is altered under reacting conditions due to heat release, as was documented in previous studies on the same test rig [13,16,25]. However, heat release mainly influences the region downstream of the flame front. For investigation of the FB resistance of a flow field, the velocity distribution just upstream of the flame front is of utmost importance. This velocity distribution is almost identical for isothermal and reacting conditions, thus, justifying the investigation of the isothermal flow field.

A plexiglass model of the burner was designed that provided optical access to the mixing tube. The vertical test section of the water tunnel, which geometrically resembles the atmospheric test rig, allows for optical access to the streamwise plane from four sides (see Ref. [26] for a detailed description of the water test rig). Reynolds number is set to Re = 40,000 with respect to the diameter of the mixing tube D. High-speed particle image velocimetry utilizing a double pulsed Nd:YLF laser (0.75 kHz) with a wavelength of 527 nm and a pulse energy of 30 mJ per pulse is applied. Two cylindrical lenses are used to form a light sheet of 2 mm thickness illuminating the streamwise plane downstream of the burner exit. For seeding of the flow, silver coated hollow glass spheres with a nominal diameter of 15 μm are added to the water. The scattered light is detected by a high-speed CMOS camera. The pulse separation is set to 0.1 and to 0.2 ms depending on the water volume flow. For the cross-correlation, an interrogation area of 16×16 pixels and 50% overlapping is selected. The velocity fields are averaged over 1000 image pairs and normalized with the bulk velocity at the burner exit u_o. For the sake of clarity, the number of displayed velocity vectors is reduced and does not represent the spatial resolution of the measurement.

Reynolds similarity was maintained in order to allow for comparison of the investigated velocity fields in the water tunnel and the atmospheric combustion test rig. Moreover, the density ratio between fuel and air in the atmospheric test rig deviates from the density ratio of the two water flows representing air and fuel in the water channel. Therefore, the momentum ratio J was kept constant to achieve similarity between the experiments of both platforms.

Atmospheric Test Rig. A schematic drawing of the atmospheric combustor test rig used for the present investigations is given in Fig. 3. The air entering the swirl generator is preheated up to $T_{in} = 700$ K. The burner fires into a 105 mm diameter combustion chamber at a power of up to $P = 220$ kW. The chamber is made of quartz glass and, hence, optically accessible.

The Reynolds number with respect to the mixing tube diameter is Re = 40,000 for comparison to the water tunnel experiments and is later varied in the range of Re = 25,000–160,000 for the recording of the FB limits. However, the isothermal flow field normalized with u_0 is expected to be self-similar in the investigated

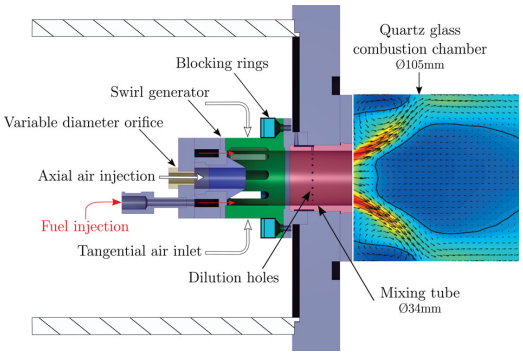

Fig. 3 Schematic of burner model, indicating different volume flow pathways through swirl generator or axial injection

Re number range, as was previously shown for a similar burner geometry [27].

OH-PLIF System. The OH-PLIF system consisted of a frequency-doubled dye laser pumped by a Nd:YAG laser, and an intensified, 5 Hz frame rate CCD camera. The dye laser used Rhodamine-6 G in ethanol and produced approximately 8 mJ/pulse at 283 nm at a rate of 5 Hz. The output wavelength (566 nm) of the dye laser was frequency doubled and tuned to approximately 283 nm to excite the Q1(8) transition of OH in the $\nu'' = 1$, $\nu' = 1$ vibrational band of the $A^2\Sigma^+ - X^2\Pi$ system. OH fluorescence in the $\nu'' = 1$, $\nu' = 1$ and $\nu'' = 0$, $\nu' = 0$ bands near 310 nm was detected through an interference filter in the wavelength region 295–340 nm. The experimental setup is detailed in Fig. 4.

The laser beam was formed, using a cylindrical lens and a spherical lens, into an approximately 50 mm wide and 500 μm thick laser sheet. The laser sheet was guided into the combustion chamber via an articulated laser arm and aligned through the center plane of the burner. The resulting OH fluorescence signal was detected perpendicular to the laser sheet by an image-intensified CCD camera equipped with a UV sensitive camera lens (f/2, $f = 105$ mm) recording with a resolution of 10 pixels/mm. The image intensifier of the CCD camera was set to an exposure time of 50 ns to further limit the background contribution from flame chemiluminescence. For each flame condition, 300 single-shot images were collected.

Intensity Correction. For very high OH densities, the laser is often observed to be attenuated along the beam path, resulting in degraded signal-to-noise ratio with increasing path length. This effect is observed for the hydrogen fuel to occur at equivalence ratios $\phi > 0.6$. In order to correct for the attenuation, the laser sheet absorption was modeled according to the Beer–Lambert law [28].

$$\frac{I}{I_0} = \exp(-\hat{\alpha} l N)$$

where I and I_0 represent the incident and transmitted beam intensity, respectively, $\hat{\alpha}$ is the absorption coefficient of the gas, l is the path length through the medium, and N is the number density of absorbing molecules. In order to model the laser absorption, the OH distribution across the combustor is approximated by the mean axisymmetric OH distribution, as suggested by Boxx et al. [29]. The modeled laser absorption can be used to normalize individual OH-PLIF images, which significantly improves contrast on this side of the OH-PLIF images facing away from the laser, in a physically plausible fashion. As indicated above, the correction became necessary only at conditions above $\phi = 0.6$. No corrections for signal trapping or laser sheet energy distribution were applied.

Results

Isothermal Flow Field. Figure 5 provides the isothermal velocity field inside the mixing tube and the combustion chamber

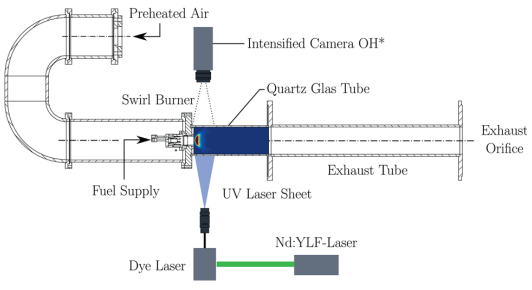

Fig. 4 Experimental setup for OH-PLIF measurements in atmospheric combustion test rig

in order to assess the impact of both, axial air injection and the additional fuel momentum. First, the characteristics of the flow field without fuel injection ($J = 0$, first row Fig. 5) in the absence and presence of a medium ($\chi = 7.5\%$) and high amount ($\chi = 12.5\%$) of axial air injection are presented. For all investigated conditions, vortex breakdown is established downstream of the area expansion. This leads to the typical flow field of swirl-stabilized combustors, which constitutes in a CRZ, enveloped by an annular jet, and an ORZ between the annular jet and the bounding walls. It is observed that in the absence of axial air injection (Fig. 5, left), the CRZ extends up to $x/D < 0.1$ toward the nozzle outlet. The flow field inside the mixing tube exhibits a deficit in axial velocity toward the center line for the entire length of the mixing tube. Such a flow field does not allow for permanent flame stabilization in the combustion chamber. In case of a medium amount of axial air injection (Fig. 5, center), the flow field in the combustion chamber remains nearly unaffected. However, strong changes are observed in the mixing tube. Here, the deficit in axial velocity on the central axis is overcome, and the axial injection yields a more homogenous radial distribution of axial velocity along the mixing tube. A high amount of axial air injection (Fig. 5, right) eventually yields flow field changes in the combustion chamber. As desired for FB resistance, a downstream shift of the stagnation point on the central axis is observed, from $x/D < 0.1$ to $x/D = 0.7$. Inside the mixing tube, strong radial gradients in axial velocity due to the central jet are detected which, decline along the path through the premixing section, nearly achieving a plug flow shape at the nozzle exit.

An increase in fuel flow to $J = 3$ and $J = 6$ (second and third row in Fig. 5), which is equivalent to a moderate and elevated hydrogen fuel flow of $\phi = 0.4$ and $\phi = 0.6$, respectively (compare Fig. 2), obviously impacts the flow field in both, mixing tube and combustion chamber.

In the absence of axial injection, this impact is very small. Also with increasing fuel momentum, a velocity increase is only observed on high radii ($r > 0.3$), whereas the axial velocity deficit on the axis is not overcome. Thus, the flow field remains unsuited for high reactivity fuels like hydrogen. For a medium amount of axial injection ($\chi = 7.5\%$), the increase of axial velocity with increasing J is evenly distributed over all radii, resulting in a slight downstream shift of the vortex breakdown location to $x/D = 0.3$ at $J = 6$. This shift explains the observed increase in FB resistance toward higher equivalence ratios, documented in Fig. 1. For the case of high axial injection ($\chi = 12.5\%$), the strongest axial velocity increase is perceived in the central jet. The axial velocities at the nozzle outlet are increased, and their radial distribution is homogenized. These changes are considered beneficial for FB resistance, providing an explanation for the observed wide operational range at atmospheric conditions (Fig. 1).

OH-PLIF. The actual flame, which represents the area of heat release, is not detectable using OH-PLIF. As OH persists in post-combustion gases of premixed flames over a time-scale significantly longer than that of the heat-releasing reactions, it is not a direct marker of the flame location [29]. Nonetheless, it is possible to extract the flame front from OH-PLIF images. It has been shown in Refs. [30,31] that in premixed flames, the reaction zone is identifiable by regions of high OH-PLIF signal-gradient.

A representative raw intensity distribution obtained from the OH-PLIF measurement is given in Fig. 6(*a*). In this figure, the dark region directly downstream of the burner outlet represents the unburned mixture of fuel and air. The subsequent bright area stems from super-equilibrium OH generated in the reaction zone, and OH present in the post flame zone. The decay of OH signal further downstream is associated to dilution of the OH concentration with recirculating exhaust gas. The upstream edge of OH signal exhibits a very sharp OH-PLIF signal-gradient which is used as indicator of the upstream flame front.

Applying [2 × 2] binning, median filtering, and a Canny edge detection algorithm, this gradient is extracted from a snap shot

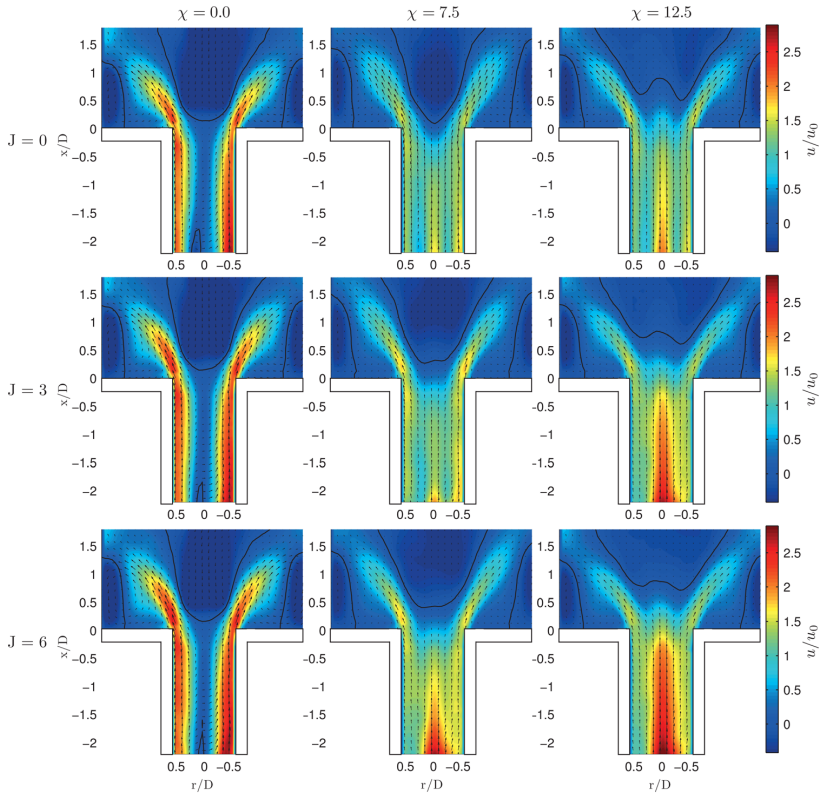

Fig. 5 Isothermal flow field in the absence ($\chi = 0\%$, left column) and presence of a medium ($\chi = 7.5\%$, center column) and high ($\chi = 12.5\%$, right column) amount of axial air injection. Additionally, the effect of injected fuel is presented at $J = 3$ (center row) and $J = 6$ (bottom row); (Re = 40,000, $S = 0.9$, and $u_0 = \text{const.}$); solid lines indicating $u/u_0 = 0$.

OH-PLIF image (Fig. 6(*b*)). In spite of a much lower OH-PLIF signal-gradient at the downstream edge, it is yet detectable by the algorithm. As discussed above, only the upstream part of the obtained curve represents the flame front. Plotting the mean gradient curves obtained from an ensemble of 300 images yields Fig. 6(*c*).

The distance of the flame front from the nozzle exit is considered a crucial parameter for FB resistance. It is quantified by the axial location of maximum flame front probability density x_F. In order to extract x_F, only the region just downstream of the nozzle exit, indicated by the rectangle in Fig. 6(*c*), is evaluated. First, spatial averaging from $y/D = -0.3$ to $y/D = +0.3$ is conducted. This is motivated by the strong wrinkling of the upstream flame front which makes a single point hardly representative for the hole flame front. Next, x_F can be extracted as location of the maximum in the plot of the mean OH-PLIF signal-gradient curve, whose upstream distribution represents the flame front (Fig. 6(*d*)). By these means, a robust method is found to extract a distinct parameter x_F, according to which a range of different conditions, geometries, and fuels can be compared.

Additionally, the snap shot images (Fig. 6(*b*)) were binarized pixelwise, according to whether or not a pixel was inside the region with OH signal

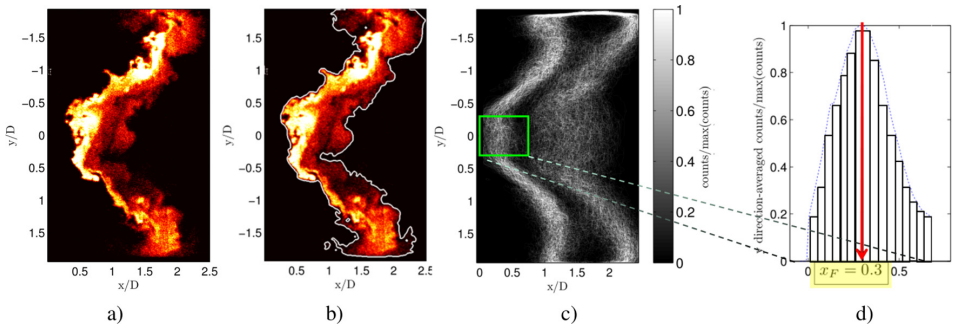

Fig. 6 Extraction method for axial location of maximum flame front probability x_F from a series of OH PLIF snapshots ($T_{in} = 450$ K, $u_0 = 70$ m/s, and ϕ=0.3)

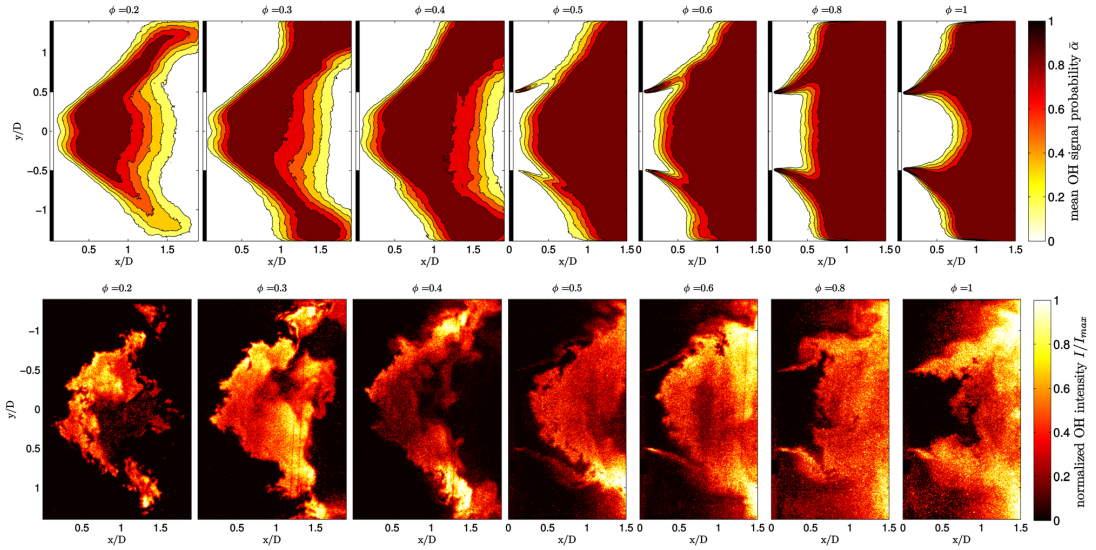

Fig. 7 Mean OH signal probability (top row) and instant OH-PLIF images (bottom row) in the presence of high axial air injection ($\chi = 12.5\%$) recorded at $T_{in} = 453$ K and $u_0 = 70$ m/s

$$\alpha(x_i, y_j) = \begin{cases} 1 & \text{if, } \in \text{ OH signal region} \\ 0 & \text{if, } \notin \text{ OH signal region} \end{cases} \quad (2)$$

Eventually, averaging over all recorded images at one location yields the mean OH signal probability $\bar{\alpha}(x, y) \in [0, 1]$. The upstream front of the $\bar{\alpha}(x, y)$ distribution provides information about the time-averaged location of the flame front. The obtained $\bar{\alpha}(x, y)$ distributions allow for easy comparison of a range of operating conditions, since they are independent of signal intensity.

Time-Averaged OH Signal Probability. The mean OH signal probability $\bar{\alpha}$ and an instant OH-PLIF recording for configurations employing high and medium axial air injection are provided by Figs. 7 and 8, respectively. As discussed in the previous section,

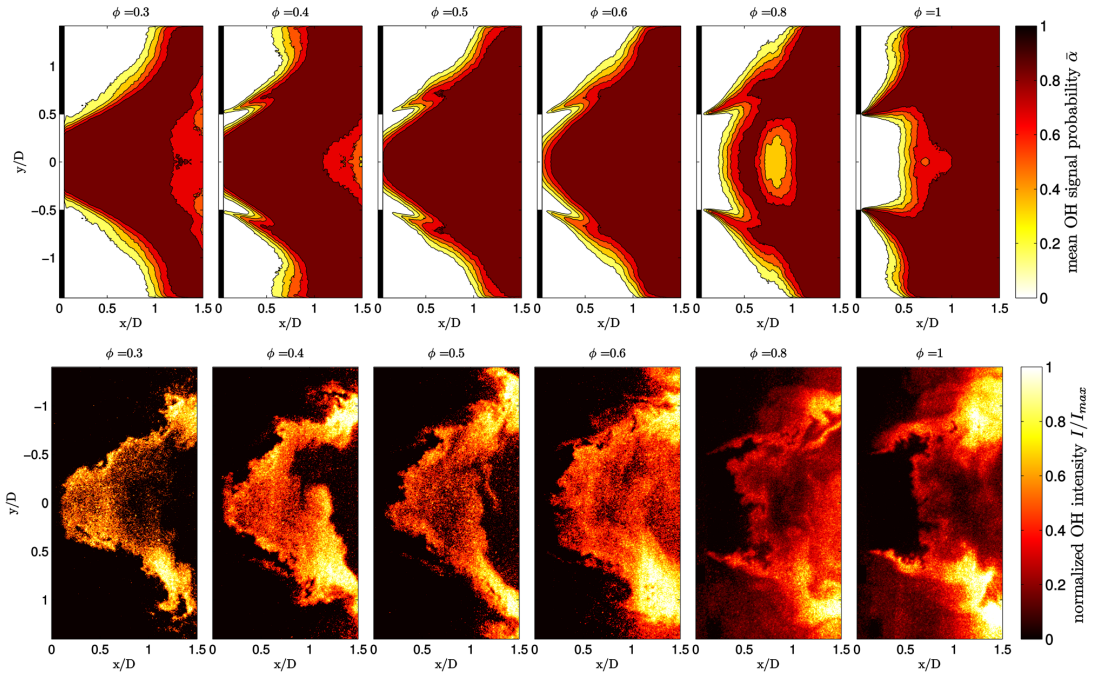

Fig. 8 Mean OH signal probability (top row) and instant OH-PLIF images (bottom row) in the presence of medium axial air injection ($\chi = 7.5\%$) recorded at $T_{in} = 453$ K and $u_0 = 70$ m/s

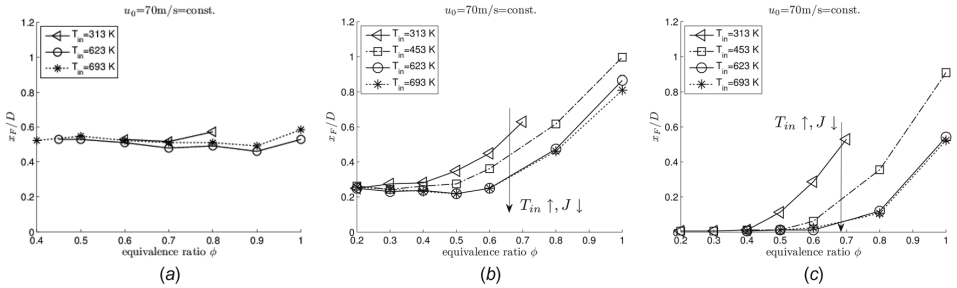

Fig. 9 Location of maximum flame front likelihood x_F over equivalence ratio ϕ for varied air preheat temperatures T_{in} for methane (left, $\chi = 12.5\%$) and hydrogen (center, $\chi = 12.5\%$ and right $\chi = 7.5\%$); all points recorded at a constant bulk air velocity $u_0 = 70$ m/s

Isothermal Flow Field, $\chi = 12.5\%$ constitutes a high FB resistance, while for $\chi = 7.5\%$ FB is reported for low equivalence ratios (compare Fig. 1).

In the presence of a high amount of axial air injection (Fig. 7), a V-shaped, lifted-off flame is observed for equivalence ratios $\phi \leq 0.5$. The flame stabilizes in the shear layer between the emanating swirling jet and the CRZ. With increasing equivalence ratio above $\phi = 0.5$, the reaction zone on the central axis is shifted downstream, while the flame remains attached in the shear layer. This downstream shift of the reaction zone with increased ϕ, in spite of the associated increase in burning velocity, is even more obvious in the case of $\chi = 7.5\%$ and is discussed below. Note that the CRZ reduces in size, but remains present for all equivalence ratios. Therefore, the characterization as swirl-stabilized, vortex breakdown flame remains valid, as was reported in a previous study by the authors [13].

In case of a medium amount of axial air injection (Fig. 8), FB occurs at an equivalence ratio of $\phi < 0.3$. The reaction zone at $\phi = 0.3$ already extends into the premixing section, although the flame does not attach to the burner rim, indicating the impending FB in case of further fuel reduction. For $\phi = 0.4$, the flame is stabilized in the shear layer and the flame base is still located upstream of the nozzle exit. An increase to $\phi = 0.5$ and above leads to a further downstream shift of the reaction zone on the central axis. This shift stems from the velocity field changes, associated to the increased equivalence ratio reported in the isothermal tests. This effect of the additional fuel momentum outweighs the increase is burning velocity, which would promote an upstream propagation of the flame.

The observation, that the flame would penetrate upstream the nozzle outlet prior to FB, was repeated for all FB occurrences. On the other hand, FB was never observed for a situation, where the flame was located downstream of the nozzle exit, in spite of the flame anchoring to the burner rim and operating at stoichiometric conditions. Based on this experience, the axial flame front location x_F is chosen as an estimator for the FB safety margin.

Quantitative Flame Front Localization. The mean OH signal probability results and OH-PLIF snap shots provide an excellent qualitative impression of the impact of both, axial air injection and fuel momentum. In the following, applying the extraction algorithm detailed above, the flame front location x_F is extracted for a variety of inlet conditions. The dependence of x_F is quantified in terms of air preheat temperatures T_{in}, equivalence ratio ϕ, bulk air velocities u_0, and axial air injection χ.

Equivalence Ratio Dependence of x_F. Figures 9(*a*)–9(*c*) reveal the characteristics of x_F with respect to equivalence ratio and preheat temperature at a fixed bulk air velocity of $u_0 = 70$ m/s. These are given for methane at $\chi = 12.5\%$ (left), for hydrogen at $\chi = 12.5\%$ (center), and $\chi = 7.5\%$ (right).

In case of methane (Fig. 9(*a*)), x_F is slightly reduced for increasing ϕ, which is attributed to the increased flame speed. This observation agrees with the statement from the Introduction that in case of methane, the additional fuel flow does not cause any flow field changes, and thus no increase in x_F was expected. The level of x_F for methane is higher than for low equivalence ratios of hydrogen, where the isothermal flow field is not yet altered due to fuel momentum. This stems from the much lower flame speeds of methane/air in comparison to hydrogen/air mixtures.

In case of high axial air injection and hydrogen fuel (Fig. 9(*b*)), x_F is strongly dependent on equivalence ratio. Two effects can be distinguished: First, a slight decrease of x_F with equivalence ratio, which dominates for $\phi < 0.5$. Analog to the methane case, this is caused by the increased flame speed. Second, a significant downstream shift of the reaction zone on the central axis, which is associated to the increase of fuel volume flow and thus momentum introduced by the fuel which alters the flow field. This effect dominates above $\phi = 0.5$.

Note that, for a fixed equivalence ratio, the lowest x_F is observed for the highest air preheat temperature T_{in}. This stems from the fact that, for increased preheating, the air momentum is increased while the fuel momentum remains nearly constant. Thus, the momentum ratio J is decreased which alters the flow field in a less favorable manner (Fig. 5) and causes the flame to anchor closer to the outlet; x_F is reduced. Generally, an increase in flame speed with air preheat temperature might also contribute to the reduced values of x_F. However, the latter effect is small compared to the former, as will become evident in the next section, Dependence of xF on Bulk Mixture Velocity.

Reducing the amount of axial air injection to a medium amount (Fig. 9(*c*)) significantly reduces x_F for all investigated conditions. This emphasizes the outstanding ability of axial air injection to influence flame location. Close to the lowest equivalence ratio before FB occurrence ($\phi = 0.3 - 0.4$), the flame tip reaches into the mixing tube. Therefore, the effect of decreased x_F with increased ϕ, reported for high axial injection at low equivalence ratios cannot be reproduced. However, analog to $\chi = 12.5$ above a threshold equivalence ratio, which coincides with the equivalence ratio of burner attachment, x_F is significantly shifted downstream with increasing equivalence ratio. Likewise, the strong dependence of x_F on air preheat temperature and, thus, the momentum ratio J is observed and can be explained in the same manner as above.

Dependence of x_F on Bulk Mixture Velocity $u_0(\phi)$. An increase in equivalence ratio results in both, changes in the flow field and an increase in bulk mixture velocity $u_0(\phi)$ (compare Fig. 2). At the investigated conditions above, the bulk air velocity was kept constant. However, the bulk mixture velocity $u_0(\phi)$ could not be kept constant at the same time since it varies with ϕ. Therefore, in order to separate both effects, Fig. 10 presents x_F as a function of $u_0(\phi)$ for a variety of inlet temperatures at a constant equivalence ratio of $\phi = 0.4$ (left) and $\phi = 0.6$ (right).

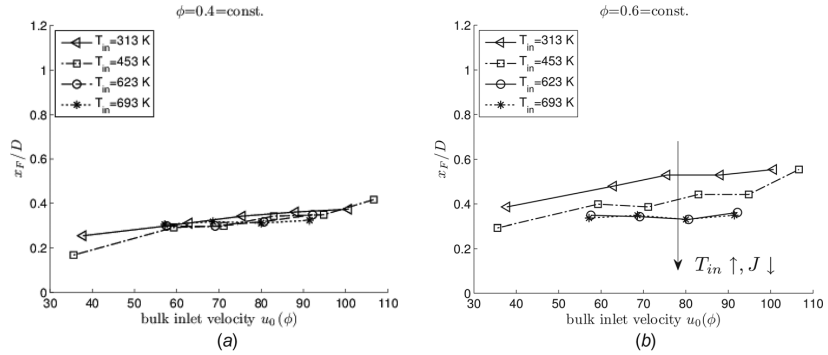

Fig. 10 Location of maximum flame front likelihood x_F over bulk air velocity u_0 for varied air preheat temperatures T_{in} for hydrogen at $\chi = 12.5\%$ for ϕ=0.4 (left) and ϕ=0.6 (right)

For both equivalence ratios, x_F exhibits a very weak dependence on the bulk mixture velocity $u_0(\phi)$. This can be explained with the self-similarity of the isothermal flow field normalized by u_0 over the investigated Re number range. An increase in bulk mixture velocity does not alter the general characteristics of the flow.

In line with the results at constant bulk velocity, it is observed for $\phi = 0.6$ that x_F is sensitive to the level of air preheating. At a constant $u_0(\phi)$, with increased preheating x_F is reduced. Since this behavior is not observed at the lower equivalence ratio $\phi = 0.4$, it cannot be attributed to an increase in flame speed. Instead, the behavior stems from the flow field changes associated with the decreased momentum ratio J.

At $\phi = 0.4$, the momentum ratio is reduced from $J = 1.8$ to $J = 1.0$ due to air preheating from $T_{\text{in}} = 313\,\text{K}$ to $T_{\text{in}} = 693\,\text{K}$. As discussed above, preheating increases the air momentum, while the fuel momentum remains nearly constant, thus, reducing the momentum ratio J. No changes in the isothermal flow field are present for such low values of J (Fig. 5) and, thus, no change in x_F is observed.

At the elevated fuel flow of $\phi = 0.6$, the momentum ratio range is increased to $J = 3.8 - 2.0$, which stems from the inlet temperature variation from $T_{\text{in}} = 313\,\text{K}$ to $T_{\text{in}} = 693\,\text{K}$. For such high levels of J, strong flow field changes have been reported (Fig. 5). These flow field changes cause the decrease in x_F with increased air preheating.

It turns out, the momentum density ratio is very well-suited to express the impact of fuel momentum on x_F across a range of air preheat temperatures and equivalence ratios. This option is further explored in the next section, Discussion and Modeling.

Discussion and Modeling

In order to obtain the momentum ratio J, Eq. (1) is considered. Rewriting this equation with respect to inlet parameters and the individual air and fuel inlet geometries yields

$$J = J(\phi, T_{\text{in}}/T_{\text{fuel}}) = \frac{\dot{m}^2_{\text{fuel}}}{\phi^2 \cdot \left(\dot{m}^2_{\text{air}}\right)_{\text{stoichmetric}}} \cdot \frac{\left(\rho_{\text{air}}(T_{\text{in}}) \cdot A^2_{\text{air}}\right)}{\left(\rho_{\text{fuel}}(T_{\text{fuel}}) \cdot A^2_{\text{fuel}}\right)} \tag{3}$$

The only required parameter which cannot be considered a standard inlet parameter, that is always available, is the fuel temperature T_{fuel}, required to calculate ρ_{fuel}. Thermocouple readings from the fuel plenum, just upstream of the fuel injection ports, have only been recorded at selected conditions. In order to allow for the calculation of J at all conditions, the fuel temperature is modeled as a function of air preheat temperature T_{in} and equivalence ratio ϕ. This model takes into account, that the fuel temperature increases with air preheat temperature, due to the fuel pipes and plenum being exposed to the preheated air. Moreover, a dependence on fuel mass flow is captured.

The increase in fuel enthalpy h_{fuel}, due to the heat flux $\dot{Q}$ from preheated air over the fuel pipe wall (surface area A and conductivity k) to the fuel, is described with the Fourier law of heat transfer.

$$\dot{Q} = \dot{m}_{\text{fuel}}(h_{\text{fuel}} - h_{\text{fuel0}}) \tag{4}$$

$$kA(T_{\text{in}} - T_m) = \dot{m}_{\text{fuel}} c_{p_{\text{fuel}}}(T_{\text{fuel}} - T_{\text{fuel0}}) \tag{5}$$

where $T_m = 1/2(T_{\text{fuel}} + T_{\text{fuel0}})$ is the arithmetic mean of the fuel temperature. Solving Eq. (5) for the fuel temperature after the heat transfer T_{fuel} yields Eq. (6), where $a = kA$ and $b = T_{\text{fuel0}}$.

$$T_{\text{fuel}} = \frac{aT_{\text{in}} + b(m_{\text{fuel}} c_{p_{\text{fuel}}} - 0.5a)}{0.5a + m_{\text{fuel}} c_{p_{\text{fuel}}}} \tag{6}$$

The model parameters $a = 1.40$ and $b = 34.9$ are obtained from a least square fit with the experimental data. The excellent agreement of the model with experimental data is shown in Fig. 11. Although fitted to experimental data using hydrogen, the model also reliably predicts the fuel temperature of methane. With the model and Eq. (3), the momentum ratio J can now be calculated for all investigated conditions.

Consequently, the flame front location x_F can be replotted with respect to the actual governing parameter, as a function of J.

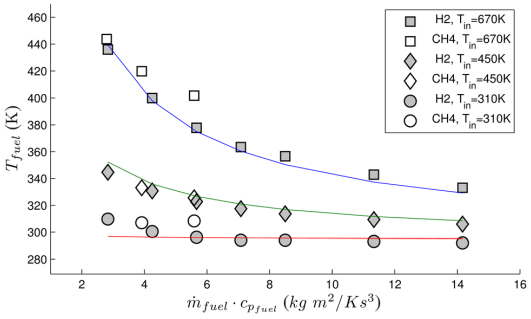

Fig. 11 Measured (symbols) and modeled (lines) fuel temperature as a function of air preheat temperature T_{in} and equivalence ratio at constant $u_0 = 70$ m/s

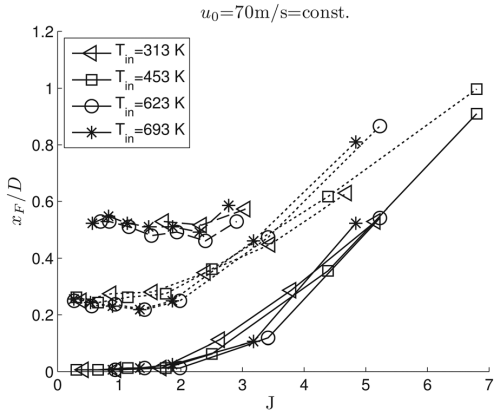

Fig. 12 x_F over J with varied T_{in} and ϕ for hydrogen at $\chi = 7.5\%$ (solid), $\chi = 12.5\%$ (dotted), and methane at $\chi = 12.5\%$ (dashed line)

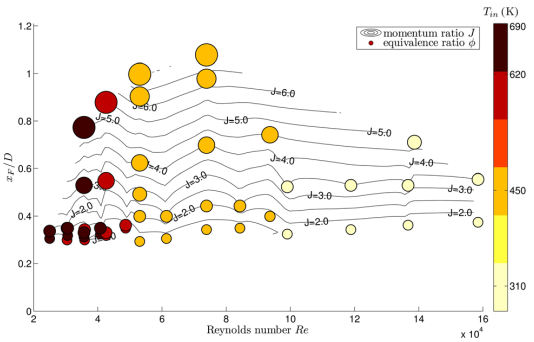

Fig. 13 Location of maximum flame front likelihood x_F over Reynolds number, varying T_{in} (circle color) and ϕ=0.2−1.0 (circle diameter) yields different levels of momentum ratio J, recorded for hydrogen at $\chi = 12.5\%$

Figure 12 summarizes all configurations ($\chi = 12.5\%$ and $\chi = 7.5\%$) and fuels (hydrogen and methane) previously given in Fig. 9. As predicted from the isothermal flow field data, below $J = 2$, the additional fuel momentum does not alter the flow field. Hence, x_F remains constant. As the flow field is altered by the additional fuel momentum for values above $J = 2.5$, this results in an increase in x_F. Note, that in contrast to the equivalence ratio, when plotted over J all air preheat temperatures nicely collapse on one curve. It is concluded that J is identified as the governing parameter to describe the dependence of x_F with respect to equivalence ratio and preheat temperature over a range of varied axial air injection ratios and even two fuel types.

Figure 12 proves this statement for a constant bulk air velocity. However, as indicated above, the bulk air velocity has a marginal impact on x_F. Figure 13 yields x_F over a wide range of Reynolds numbers, which was achieved by varying both, air preheat temperature T_{in} and bulk air velocity u_0. It can be seen that even for vastly varied Reynolds numbers, representing a variety of inlet conditions, the level of x_F is governed by the momentum ratio J.

Conclusion

The current study investigates the impact of varied inlet conditions (air preheat temperature, equivalence ratio, and bulk air velocity), varied burner geometries (medium and high axial air injection), and fuel types (methane and hydrogen) on the FB safety margin of a swirl-stabilized combustor. The FB safety margin is estimated by the axial flame front location x_F, which is obtained from a set of OH-PLIF images.

The additional momentum from the fuel is argued to play an important role, only in case of hydrogen. The effects of additional momentum from the fuel are to alter the flow field, depending on the momentum ratio J, and to increase the bulk mixture velocity $u_0(\phi)$ (Fig. 2). The changes in the isothermal flow field as results of both, increasing axial air injection and momentum ratio J, are reported in Fig. 5. An onset of changes in the mean flow field stemming from fuel injection is observed for $J > 2$. An increase in $u_0(\phi)$ does not alter the general characteristics of the flow field, since it exhibits self-similarity for a wide range of Re numbers.

Furthermore, instantaneous OH-PLIF images and mean OH signal probability distributions provide a qualitative insight in the impact additional fuel momentum on flame structure and flame front location. It was observed from these measurements, that a decrease of the axial flame front location to $x/D = 0$ is a necessary predecessor for FB occurrence. Based on this observation, the axial location of maximum flame front likelihood x_F was identified as an estimator of FB safety margin. A quantitative survey of the axial flame front location x_F with respect to varied equivalence ratio ($\phi = 0.2 - 1.0$), bulk air velocity $u_0 = 30$–90 m/s, and burner preheat temperature $T_{in} = 300$–700 K was conducted for hydrogen fuel a with high axial air injection. At distinct conditions, x_F was additionally recorded for hydrogen at $\chi = 7.5\%$ and methane at $\chi = 12.5\%$.

A strong increase in x_F and the onset of changes in the isothermal flow field due to additional fuel momentum are shown to coincide, as they occur at the same momentum ratio range, above $J = 2$. In this region, an increase in momentum ratio due to increased ϕ will result in a downstream shift of the flame front, superseding any parallel augmentation in flame speed. A decrease in momentum ratio, which occurs in case of increased preheating, will results in a reduction of x_F, an upstream shift of the flame. Again the momentum ratios impact is shown to outweigh influence of the flame speed. Therefore, J is identified as the governing parameter to describe the characteristics of x_F with respect to varied equivalence ratio and air preheat temperatures. This was shown to be valid over an extensive Reynolds number range, axial air injection ratios, and even fuel types.

It is concluded that the momentum ratio J is a mandatory parameter to be taken into account during combustor design for systems operating with pure hydrogen or high-hydrogen content fuel blends.

Acknowledgment

The research leading to these results has received funding from the European Union Seventh Framework Program (FP7/2007-2013) under Grant Agreement No. 284636 and the European Research Council under the ERC Grant Agreement No. 247322, GREENEST. The authors thankfully acknowledge the support of Philip Buschmann during the experiments.

Nomenclature

D = burner outlet diameter
J = momentum ratio
S = geometric swirl number
T_{fuel} = fuel inlet temperature in K
T_{in} = air inlet temperature in K
u_0 = bulk air velocity for $\phi = 0$ and $D = 34$ mm
$u_0(\phi)$ = bulk air–fuel mixture velocity for $\phi > 0$ and $D = 34$ mm
$\dot{V}_{ax}$ = air volume flow through axial injection
$\dot{V}_{swirl}$ = air volume flow through radial swirl generator
$\bar{\alpha}$ = time-averaged OH signal probability
ρ_{air} = air density

ρ_{fuel} = fuel density
ϕ = equivalence ratio
χ = axial injection ratio $\chi = \dot{V}_{\text{ax}}/(\dot{V}_{\text{ax}} + \dot{V}_{\text{swirl}})$

References

[1] Brand, J., Sampath, S., and Shum, F., 2003, "Potential Use of Hydrogen in Air Propulsion," AIAA Paper No. 2003-2879.
[2] Corchero, G., and Montañés, J. L., 2005, "An Approach to the Use of Hydrogen for Commercial Aircraft Engines," Proc. Inst. Mech. Eng., Part G, **219**(1), pp. 35–44.
[3] Haglind, F., and Singh, R., 2006, "Design of Aero Gas Turbines Using Hydrogen," ASME J. Eng. Gas Turbines Power, **128**(4), pp. 754–764.
[4] Rao, A. G., Yin, F., and van Buijtenen, J. P., 2014, "A Hybrid Engine Concept for Multi-Fuel Blended Wing Body," Aircr. Eng. Aerosp. Technol., **86**(6), pp. 483–493.
[5] Levy, Y., Sherbaum, V., and Arfi, P., 2004, "Basic Thermodynamics of FLOXCOM, the Low-NOx Gas Turbines Adiabatic Combustor," Appl. Therm. Eng., **24**(11), pp. 1593–1605.
[6] Döbbeling, K., and Hellat, J., 2007, "25 Years of BBC/ABB/Alstom Lean Premix Combustion Technologies," ASME J. Eng. Gas Turbines Power, **129**(1), pp. 2–12.
[7] Gupta, A. K., Lilley, D. G., and Syred, N., 1984, *Swirl Flows*, Abacus Press, Tunbridge Wells, UK.
[8] Schefer, R., Smith, T. D., and Marek, J. C., 2002, "Evaluation of NASA Lean Premixed Hydrogen Burner," Sandia National Laboratories, Livermore, CA, Report No. SAND2002-8609.
[9] Reichel, T. G., Terhaar, S., and Paschereit, C. O., 2013, "Flow Field Manipulation by Axial Air Injection to Achieve Flashback Resistance and Its Impact on Mixing Quality," AIAA Paper No. 2013-2603.
[10] Fric, T. F., 1993, "Effects of Fuel-Air Unmixedness on NO(x) Emissions," J. Propul. Power, **9**(5), pp. 708–713.
[11] Baumgartner, G., and Sattelmayer, T., 2013, "Experimental Investigation on the Effect of Boundary Layer Fluid Injection on the Flashback Propensity of Premixed Hydrogen-Air Flames," ASME Paper No. GT2013-94266.
[12] Burmberger, S., and Sattelmayer, T., 2011, "Optimization of the Aerodynamic Flame Stabilization for Fuel Flexible Gas Turbine Premix Burners," ASME J. Eng. Gas Turbines Power, **133**(10), p. 101501.
[13] Reichel, T., Terhaar, S., and Paschereit, C. O., 2014, "Increasing Flashback Resistance in Lean Premixed Swirl-Stabilized Hydrogen Combustion by Axial Air Injection," ASME J. Eng. Gas Turbines Power, **137**(7), p. 071503.
[14] Mayer, C., Sangl, J., Sattelmayer, T., Lachaux, T., and Bernero, S., 2012, "Study on the Operational Window of a Swirl Stabilized Syngas Burner Under Atmospheric and High Pressure Conditions," ASME J. Eng. Gas Turbines Power, **134**(3), p. 031506.
[15] Sangl, J., Mayer, C., and Sattelmayer, T., 2010, "Dynamic Adaptation of Aerodynamic Flame Stabilization of a Premix Swirl Burner to Fuel Reactivity Using Fuel Momentum," ASME J. Eng. Gas Turbines Power, **133**(7), p. 071501.
[16] Terhaar, S., Reichel, T. G., Schrödinger, C., Rukes, L., Paschereit, C. O., and Oberleithner, K., 2015, "Vortex Breakdown Types and Global Modes in Swirling Combustor Flows With Axial Injection," J. Propul. Power, **31**(1), pp. 219–229.
[17] Schefer, R., Wicksall, D., and Agrawal, A., 2002, "Combustion of Hydrogen-Enriched Methane in a Lean Premixed Swirl-Stabilized Burner," Proc. Combust. Inst., **29**(1), pp. 843–851.
[18] Lantz, A., Collin, R., Aldén, M., Lindholm, A., Larfeldt, J., and Lörstad, D., 2014, "Investigation of Hydrogen Enriched Natural Gas Flames in a SGT-700/800 Burner Using OH PLIF and Chemiluminescence Imaging," ASME Paper No. GT2014-26293.
[19] Sadanandan, R., Lückerath, R., Meier, W., and Wahl, C., 2011, "Flame Characteristics and Emissions in Flameless Combustion Under Gas Turbine Relevant Conditions," J. Propul. Power, **27**(5), pp. 970–980.
[20] Emadi, M., Karkow, D., Salameh, T., Gohil, A., and Ratner, A., 2012, "Flame Structure Changes Resulting From Hydrogen-Enrichment and Pressurization for Low-Swirl Premixed Methane–Air Flames," Int. J. Hydrogen Energy, **37**(13), pp. 10397–10404.
[21] Göckeler, K., Krüger, O., and Paschereit, C. O., 2015, "Laminar Burning Velocities and Emissions of Hydrogen–Methane–Air–Steam Mixtures," ASME J. Eng. Gas Turbines Power, **137**(3), p. 031503.
[22] Strakey, P. A., Woodruff, S. D., Williams, T. C., and Schefer, R. W., 2008, "OH-Planar Fluorescence Measurements of Pressurized, Hydrogen Premixed Flames in the SimVal Combustor," AIAA J., **46**(7), pp. 1604–1613.
[23] Tuncer, O., Acharya, S., and Uhm, J., 2009, "Dynamics, NOx and Flashback Characteristics of Confined Premixed Hydrogen-Enriched Methane Flames," Int. J. Hydrogen Energy, **34**(1), pp. 496–506.
[24] Tanneberger, T., Reichel, T. G., Krüger, O., Terhaar, S., and Paschereit, C. O., 2015, "Numerical Investigation of the Flow Field and Mixing in a Swirl-Stabilized Burner With a Non-Swirling Axial Jet," ASME Paper No. GT2015-43382.
[25] Terhaar, S., Krüger, O., and Paschereit, C. O., 2015, "Flow Field and Flame Dynamics of Swirling Methane and Hydrogen Flames at Dry and Steam Diluted Conditions," ASME J. Eng. Gas Turbines Power, **137**(4), p. 041503.
[26] Lacarelle, A., and Paschereit, C. O., 2012, "Increasing the Passive Scalar Mixing Quality of Jets in Crossflow With Fluidics Actuators," ASME J. Eng. Gas Turbines Power, **134**(2), p. 021503.
[27] Göckeler, K., Göke, S., Schimek, S., and Paschereit, C. O., 2010, "Enhanced Recirculation in the Cold Flow Field of a Swirl-Stabilized Burner for Ultra Wet Combustion," International Conference Jets, Wakes Separated Flows (ICJWSF-2010), Cincinnati, OH, Sept. 27–30.
[28] Eckbreth, A. C., 1996, *Laser Diagnostics for Combustion Temperature and Species*, Vol. 3, CRC Press, Boca Raton, FL.
[29] Boxx, I., Slabaugh, C., Kutne, P., Lucht, R., and Meier, W., 2014, "3 kHz PIV/OH-PLIF Measurements in a Gas Turbine Combustor at Elevated Pressure," Proc. Combust. Inst., **35**(3), pp. 3793–3802.
[30] Donbar, J. M., Driscoll, J. F., and Carter, C. D., 2000, "Reaction Zone Structure in Turbulent Nonpremixed Jet Flames—From CH-OH PLIF Images," Combust. Flame, **122**(1–2), pp. 1–19.
[31] Sadanandan, R., Stöhr, M., and Meier, W., 2008, "Simultaneous OH-PLIF and PIV Measurements in a Gas Turbine Model Combustor," Appl. Phys. B, **90**(3–4), pp. 609–618.

2.4 Fourth Publication

INTERNATIONAL JOURNAL OF HYDROGEN ENERGY 42 (2017) 4518–4529

Available online at www.sciencedirect.com

ScienceDirect

journal homepage: www.elsevier.com/locate/he

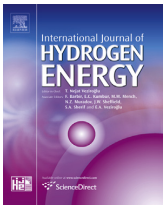

Interaction mechanisms of fuel momentum with flashback limits in lean-premixed combustion of hydrogen

Thoralf G. Reichel[*], *Christian Oliver Paschereit*

Chair of Fluid Dynamics, Hermann-Föttinger-Institut, Müller-Breslau-Str. 8, 10623 Berlin, Germany

ARTICLE INFO

Article history:
Received 18 August 2016
Received in revised form
1 November 2016
Accepted 2 November 2016
Available online 24 November 2016

Keywords:
Hydrogen–air combustion
Turbulent lean-premixed flames
Swirl-stabilized
Fuel momentum
Flashback
OH-PLIF

ABSTRACT

The impact of fuel momentum on the combustor flow field is studied experimentally in a swirl-stabilized, technically premixed hydrogen flame. The volumetric heating value of hydrogen is about 3.5 times lower compared to natural gas, which leads to significantly higher volumetric fuel flow rates at the same power level. This additional fuel momentum significantly alters the combustor flow field. Therefore, the fuel momentum also affects the combustor stability limits. Previous studies were mostly conducted at perfectly premixed conditions, where the fuel momentum does not alter the combustor flow field. In the current study, non-reacting and reacting combustor flow fields of a technically premixed model combustor injecting fuel in axial direction are recorded. Results reveal a strong impact of fuel momentum on axial velocity distribution at the mixing tube outlet and, thus, on the stability limits. Additionally, OH-PLIF recordings for different flow rates, air preheat temperatures, and equivalence ratios show that the axial location of the upstream flame front, x_f, poses a telling estimator for flashback resistance. No flashback was observed when the upstream flame front was located downstream of the mixing tube. However, the flame tip always located upstream of the mixing tube outlet prior to flashback. A high value of x_f was, thus, identified as a sufficient condition for flashback resistance. At the investigated conditions, x_f is shifted downstream with increasing equivalence ratio due to the added momentum of the fuel flow, thereby superseding any parallel augmentation in the turbulent flame speed. This has been identified as the driving mechanism affecting the combustor stability limit.

Introduction

Future demands on air transport systems dictate that aircraft should be less polluting, less noisy, and more fuel efficient. In the long term, alternative fuels, such as bio fuels and hydrogen, are likely to replace traditional jet fuel [1–3]. Experimental tests on a low NO_x hydrogen combustor for aero engines have been conducted within the European Union-supported FP7 project Advanced Hybrid Engines for Aircraft Development (AHEAD). The concept proposed in the AHEAD project is a contra-rotating turbofan engine with sequential dual hybrid combustors using two different fuels [4]. The engine is operated on pure hydrogen in the first stage and bio

* *Corresponding author.*
E-mail address: thoralf.reichel@tu-berlin.de (T.G. Reichel).
http://dx.doi.org/10.1016/j.ijhydene.2016.11.018

INTERNATIONAL JOURNAL OF HYDROGEN ENERGY 42 (2017) 4518–4529

fuel under flameless conditions [5] in the second stage, aiming to reduce CO_2 and NO_x emissions, respectively. This study focuses on the lean-premixed, swirl-stabilized hydrogen combustion of the first stage. It is, therefore, also relevant to syngas combustion in IGCC cycles, where the burned syngases are mainly composed of CO, CH_4, and H_2 with an H_2 content of up to 50% by volume. Pure hydrogen is, thus, a meaningful test case for flashback (FB) resistance of a burner geometry.

The scope of the study is to describe the mechanisms by which the fuel momentum of hydrogen impacts the FB limits of a swirl-stabilized, technically premixed model combustor. Other aspects limiting the operational range of swirl-stabilized combustors are intensively detailed in the work by Huang and Yang [6] and Lieuwen [7]. For lean-premixed combustion with increasing fuel reactivity, lean blow out (LBO) limits are extended, offering excellent low-NO_x potential [8–11]. Simultaneously, FB disposition is increased. FB denotes the upstream propagation of a flame in a combustible mixture into regions not designed for flame holding and poses an operability limit for gas turbine combustors (Plee and Mellor [12]). The increased FB propensity of various mixtures with increasing hydrogen content has been investigated in numerous studies [13–19]. Detailed investigations regarding the effect of inlet or outlet conditions by Syred et al. [18], swirl number by Sayad et al. [19], or a hydrodynamic instability by Schönborn et al. [20] on the stability limits of high hydrogen content fuels have also been reported. Note that all of these studies have been conducted for perfectly premixed conditions, where fuel and air are premixed far upstream of the combustion chamber. In this case, the impact of the additional fuel momentum on the combustor flow is limited to an increase in bulk velocity, u_0, which does not alter the flow field characteristics. These are reportedly Reynolds number (Re)-independent over a wide range of u_0 (Göckeler et al. [21]). In case of technical premixing, where the fuel is admitted directly into the premixing section, the fuel momentum does influence the combustor flow field and, thus, affects the stability limits.

For the prevention of flame FB into the premixing section, the combustor flow field is of utmost importance. For example, to avoid FB due to turbulent flame propagation in the core flow and combustion-induced vortex breakdown (CIVB; Kröner et al. [22]), "a major design criterion for nozzle aerodynamics is that the axial velocity must be as high and as uniform as possible and free of strong wakes" (Lieuwen et al. [15]). To meet this criteria, Burmberger and Sattelmayer [23] suggested that the combustor employ a non-swirling air jet on the central axis of the radial swirl generator with the intention to create a plug flow-like velocity profile at the nozzle exit and shift the stagnation point, also referred to as vortex breakdown (VB), downstream. This idea is adapted and exploited in the current burner setup. The ratio of axially injected, non-swirling air flow to total air flow is defined as $\chi = \dot{V}_{ax}/(\dot{V}_{ax} + \dot{V}_{swirl})$. A burner employing axial air injection (AAI) in the range χ = 7.5–12.5% was shown to maintain excellent fuel-air mixing (Reichel et al. [24]), suppress hydrodynamic instabilities (Terhaar et al. [25]), and, most importantly, significantly extend the FB limits of a model combustor (Reichel et al. [26]). In the case of hydrogen fuel for $\chi = 12.5\%$, FB is suppressed on the whole operational range of the atmospheric test rig. However, reducing the central non-swirling air jet to a medium level of χ = 7.5% triggers the occurrence of FB (see Section Stability map).

When recording the stability maps for both configurations, an interesting observation was made that demonstrates the strong effect of hydrogen's fuel momentum on stability limits. At χ = 7.5%, the burner could be operated at stoichiometric conditions, but FB occurred when the equivalence ratio was reduced below a certain value at constant air mass flow. At first, this observation may appear somewhat counter-intuitive since for lean hydrogen–air mixtures with a decreasing equivalence ratio, also the burning velocity is reduced (Ilbas et al. [27]). This should, in turn, render FB less likely. However, the occurrence of FB when reducing the equivalence ratio can be explained by the reduction in fuel momentum. The reduction in fuel mass flow alters the axial velocity distribution at the mixing tube outlet, which, as previously discussed, affects the flashback propensity of the combustor. Vice versa, it is argued that the operation up to stoichiometric conditions is achieved due to the proper use of the hydrogen's fuel momentum, which alters the flow field in a favorable manner for FB resistance.

Yet, what are the mechanisms by which the fuel momentum impacts the FB limits, and what are their dependencies? For hydrogen fuel, to achieve a desired power output, about 3.5 times higher volumetric fuel flow rates in comparison to natural gas are required due to its smaller volumetric heating value. Therefore, a considerable amount of additional volume flow and, thus, momentum compared with natural gas is introduced into the system. For technical premixing, where the fuel is injected directly into the premixing section, with increasing hydrogen content of the fuel, the additional fuel momentum increasingly alters the flow field. Thus, the additional fuel momentum needs to be utilized in a manner beneficial for FB resistance, since desired flow field features contributing to FB resistance are potentially eliminated otherwise.

This interaction between the stability limits of a burner and fuel momentum has been scarcely investigated in the past. Mayer et al. [28] and Sangl et al. [29] investigated a technically premixed case, where instead of an air-jet they applied a non-swirling, axial fuel jet. They reported a downstream shift of VB for increased fuel momentum under isothermal conditions. Application of their fuel jet at reacting conditions yielded an extension of the FB limits, but also highly increased NO_x emissions.

Which flow features can be used to quantitatively describe the influence of fuel momentum? The axial location of VB, x_{VB}, which is sensitive to fuel momentum as reported by Sangl et al. [29]? Or the axial location of the leading edge flame front, which is reported to travel upstream when approaching conditions where FB occurs (Schefer et al. [13], Reichel et al. [30], Lantz et al. [31])? Both flow features will be evaluated for their suitability as an indicator of the FB safety margin for the respective condition.

The remainder of the paper is structured as follows: First, the FB limits for two configurations exhibiting a high and moderate level of FB resistance are provided, which reveal a strong contribution of fuel momentum on the FB limits. Next, PIV measurements are performed to analyze the differences in the combustor flow field stemming from varied levels of fuel momentum. To isolate the effect of fuel momentum from

4520 INTERNATIONAL JOURNAL OF HYDROGEN ENERGY 42 (2017) 4518–4529

secondary effects, such as dilatation due to heat addition, we compare the reacting and isothermal combustor flow field. Additionally, for the conditions detailed in Table 1, OH-PLIF images were recorded to extract the exact upstream flame front for varied levels of fuel momentum. Thereafter, a suitable estimator for the impact of fuel momentum on the stability limits and its sensitivity to varying combustor inlet conditions is identified.

Quantification of fuel momentum

For technical premixing, where the fuel is injected just upstream of the premixing section, the fuel volume flow has the potential to strongly change the combustor flow field. The momentum ratio J is used to describe the impact of fuel momentum for varying combustor inlet parameters.

$$J = \frac{\rho_{fuel} u_{fuel}^2}{\rho_{air} u_{air}^2} \quad (1)$$

Fig. 1 visualizes the strong impact of fuel momentum for hydrogen. At a constant air mass flow, the momentum ratio J increases with increased equivalence ratio ϕ. Preheating of the combustion air increases the air momentum relative to the fuel momentum and, thus, decreases the momentum ratio. Therefore, the momentum ratio J is most suitable for describing the impact of fuel momentum on flow field characteristics for varying combustor inlet parameters.

To compare the momentum ratio of hydrogen and methane, one needs to account for the differences in volumetric heating value ($LHV_{CH_4}/LHV_{H_2} = 3.5$), as well as the molecular mass ($M_{CH_4}/M_{H_2} = 8$). Doing so yields an increase in momentum ratio J by almost 40% for hydrogen in comparison with methane at the same combustor power, P.

$$\left.\frac{J_{H_2}}{J_{CH_4}}\right|_{P=const.} = 1.37$$

Experimental setup and diagnostics

Burner model

Fig. 2 provides a schematic of the investigated swirl burner. The main air flow can enter the cylindrical mixing tube (red)

Table 1 – Investigated conditions for hydrogen using OH-PLIF; PIV was conducted for a limited number of selected conditions.

#	χ [%]	T_{in} [°C]	u_0 [m/s]	$\dot{m}_{air}$ [kg/h]	Re·10^{-3} [–]	ϕ [–]
10–19	12.5	40	50	184	100	LBO-1.0
60–69		180	50	130	55	
80–89			70	180	75	
130–139		350	70	130	45	
140–149			80	148	50	
150–159	7.5	180	70	180	75	FB-1.0
160–169		350	80	148	50	

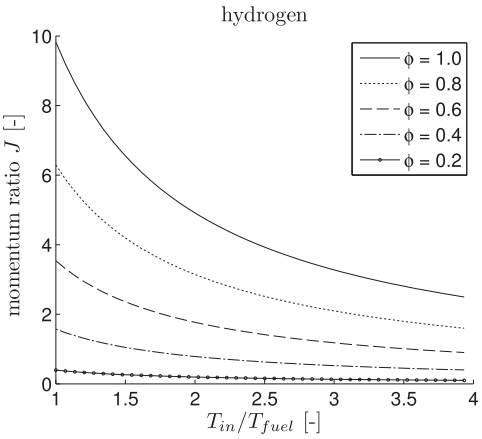

Fig. 1 – Momentum ratio J of hydrogen with respect to varied equivalence ratio ϕ and inlet air to fuel temperature ratio (T_{in}/T_{fuel}).

(in the web version) in two ways: first, through the radial swirl generator (green), whereby a certain amount of swirl is imposed on the flow, depending on the number of blocking rings (blue); second, through an orifice of the diameter D_{or} on the central axis (yellow), constituting the AAI. For the current study, either a 4-mm or 7-mm blocking ring was used, which yielded a geometric swirl number S of S = 0.7 and S = 0.9, respectively. The geometric swirl number S, suggested by Gupta et al. [32], depends entirely on the burner geometry and, here, does not account for the change in swirl due to axial injection. However, a detailed study of the effect of axial injection on the resulting swirl number can be found in Terhaar et al. [25] and Reichel et al. [30]. The amount of axially injected air was not metered but adjusted only by the ratio of pressure loss between the swirl generator and axial injection orifice. Therefore, varying the orifice diameter D_{or} adjusted the ratio of axially injected, non-swirling air volume flow to total air volume flow $\chi = \dot{V}_{ax}/(\dot{V}_{ax} + \dot{V}_{swirl})$. The values

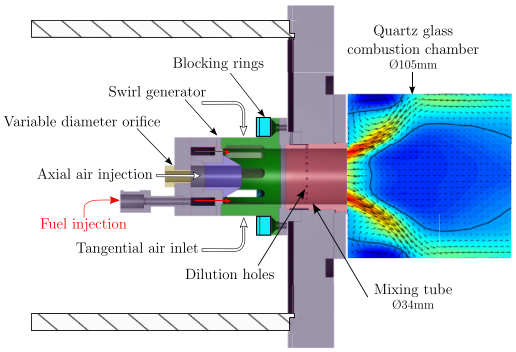

Fig. 2 – Schematic of burner model, indicating different volume flow pathways through swirl generator or axial injection.

for χ of the unmetered case were determined from a comparison of the isothermal velocity field to the metered case and additional pressure measurements. They were further validated by a numerical investigation using RANS and LES by Tanneberger et al. [33].

The fuel was injected into the premixing section through 16 injection ports located on an annular ring around the truncated center body. The mixing tube was located downstream of the swirl generator and had an inner diameter of $D = 34$ mm. The purpose of the circumferentially distributed dilution holes at $x/D = -0.7$ in the mixing tube was to reduce the near-wall equivalence ratio to prevent boundary layer FB.

The fuel temperature T_{fuel}, which is required to calculate the momentum ratio J, is affected by the level of air preheating. This sensitivity of T_{fuel} on air preheating stemmed from the fuel plenum and piping being directly exposed to the preheated air. This was accounted for by recording T_{fuel} in the fuel plenum prior to injection and using this value for the calculation of the momentum ratio.

Water tunnel

Isothermal combustor flow fields with fuel injection were recorded in a water tunnel facility to characterize the impact of both, AAI and fuel momentum. Hereby, the air and fuel flow were both represented by water. As opposed to the atmospheric combustor test rig, it was possible in the water tunnel to extract the velocity field in the mixing tube upstream of the combustion chamber, since all parts were made of quartz glass. Moreover, a comparison of non-reacting and reacting combustor flow fields with fuel injection allowed for the isolation of the effect of dilatation due to heat addition on the axial location of VB for varied levels of fuel momentum.

The vertical test section of the water tunnel, which geometrically resembles the atmospheric test rig, allowed for optical access to the stream-wise plane from four sides. Re number is set to Re = 40,000 with respect to the diameter of the mixing tube D. Reynolds similarity was maintained to allow for comparison of the investigated velocity fields in the water tunnel and the atmospheric combustion test rig. The density ratio between the two water flows representing air and fuel in the water tunnel deviates from the density ratio of fuel and air in the atmospheric test rig. Therefore, the momentum ratio J was kept constant to achieve similarity between the experiments of both platforms.

High-speed PIV: non-reacting flow

High-speed particle image velocimetry utilizing a double-pulsed Nd:YLF laser (0.75 kHz) with a wavelength of 527 nm and a pulse energy of 30 mJ per pulse was applied. A laser light sheet of 2-mm thickness illuminated the stream-wise plane downstream of the burner exit. For seeding of the flow, silver coated hollow glass spheres with a nominal diameter of 15 μm were added to the water. The scattered light is detected by a high-speed CMOS camera recording at 750 Hz with a resolution of 7.2 px/mm. The pulse separation was set to 0.1 or 0.2 ms depending on the water volume flow. For the cross-correlation, an interrogation area of 16 × 16 pixels and 50% overlapping was selected. The velocity fields were averaged over 1000 image pairs and normalized with the bulk velocity at the burner exit, u_o. For the sake of clarity, the number of displayed velocity vectors in the figures is reduced and do not represent the spatial resolution of the measurement.

Atmospheric test rig

A schematic drawing of the atmospheric combustor test rig used for the present investigations is given in Fig. 3. The air entering the swirl generator was preheated up to $T_{in} = 700$ K. The burner fired into a 105-mm diameter combustion chamber at a power of up to $P = 220$ kW. The chamber is made of quartz glass and is, hence, optically accessible. The Re number with respect to the mixing tube diameter was Re = 40,000 for comparison to the water tunnel experiments and is varied in the range of Re = 25,000–160,000 for the recording of the FB limits. However, the isothermal flow field normalized with u_0 was expected to be Reynolds-independent in the investigated Re number range, as was previously shown for a similar burner geometry by Göckeler et al. [21].

Simultaneous high-speed PIV and OH chemiluminescence measurements*

For the PIV measurements, the same laser and high-speed camera (3 kHz) were used as in the water tunnel. The combustor air was seeded with Zirconium dioxide particles 2 μm in diameter. The pulse separation was set to 5–10 μs depending on mass flow and preheating temperature. The location of the flame was captured using a band-pass filtered intensified camera for the chemiluminescence of the OH* radical, which qualitatively correlated with the location of heat release and the intensity of the chemical reaction. Since the obtained images were line-of-sight–integrated they could not be used to extract the exact location of the upstream flame front. Therefore, additional OH-PLIF measurements were conducted, evaluating the axial location of the upstream flame front in the central burner plane and with a higher resolution.

OH-PLIF measurements

The OH-PLIF system consisted of a frequency-doubled dye laser pumped by a Nd:YAG laser and an intensified, 5-Hz frame rate CCD camera equipped with a UV transmitting camera lens (f/2, f = 105 mm) recording with a resolution of 10 px/mm. The image intensifier of the CCD camera was set to

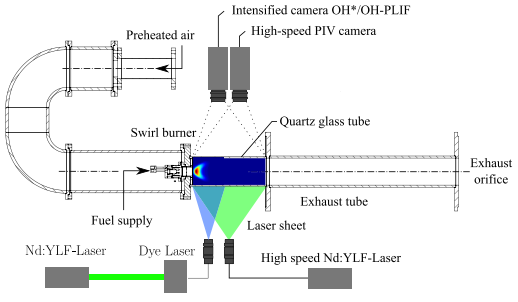

Fig. 3 – Experimental setup of both experiments; first: simultaneous high-speed (3 kHz) PIV and OH* measurements; second: low-speed (5 Hz) OH-PLIF measurements in the atmospheric combustion test rig.

4522 INTERNATIONAL JOURNAL OF HYDROGEN ENERGY 42 (2017) 4518–4529

an exposure time of 50 ns to further limit the background contribution from flame chemiluminescence. For each flame condition, 300 single-shot images were collected. The dye laser used Rhodamine-6G in ethanol and produced approximately 8 mJ/pulse at 283 nm at a rate of 5 Hz. For further details of the OH-PLIF system please refer to Reichel et al. [34]. The detailed experimental setup is given in Fig. 3.

Flame front extraction: The actual flame, which represents the area of heat release, is not detectable using OH-PLIF. Because OH persists in post-combustion gases of premixed flames over a time-scale significantly longer than that of the heat-releasing reactions, it is not a direct marker of the flame location (Boxx et al. [35]). Nonetheless, it is possible to extract the upstream flame front from OH-PLIF images utilizing the super-equilibrium OH generated in the reaction zone. The distance of the flame front from the nozzle exit is considered a telling estimator for FB resistance. Applying an in-house extraction method, detailed in Reichel et al. [34], the axial location of maximum flame front probability density x_f was extracted from a set of 300 OH-PLIF images. By these means, a robust method was found to extract a distinct parameter x_f, according to which the impact of different levels of fuel momentum could be compared. Additionally, the images were binarized pixel-wise according to whether or not a pixel was inside the region with OH signal.

$$\alpha\left(x_i, y_j\right) = \begin{cases} 1 & if,\ \in \text{OH signal region} \\ 0 & if,\ \notin \text{OH signal region} \end{cases} \quad (2)$$

Eventually, averaging over all recorded images at one location yields the mean OH signal probability $\overline{\alpha}(x,y) \in [0,1]$. The upstream front of the $\overline{\alpha}(x,y)$ distribution provides information about the time-averaged location of the flame front. The obtained $\overline{\alpha}(x,y)$ distributions allow for easy comparison of a range of operating conditions, since they are independent of signal intensity.

Flashback and lean blowout test procedures

FB/LBO limits for a given configuration (χ and S) and operating point (air mass flow $\dot{m}$ and preheat temperature T_{in}) were determined by gradually increasing/decreasing the equivalence ratio from an initial equivalence ratio at which a stable flame was sustained in the combustor until FB/LBO occurred or the upper limit of $\phi = 1$ was reached. During this process, the remaining parameters were kept constant. Rich hydrogen–air mixtures were not investigated because they are beyond the scope of this study.

Results and discussion

Stability map

As discussed in the introduction, the importance of the additional fuel momentum of hydrogen became evident when investigating the stability map of a burner employing AAI for FB resistance. Therefore, we will briefly recapitulate the observations reported in Reichel et al. [30] to highlight how fuel momentum affects the combustor stability limits.

For hydrogen without any AAI, a satisfying investigation of the operational range was not possible due to FB. Therefore, FB and LBO limits were obtained using a high ($\chi = 12.5\%$) and medium amount ($\chi = 7.5\%$) of AAI. Each case was investigated for two levels of swirl number, $S = 0.7$ and $S = 0.9$. The stability limits were recorded for different air mass flows and levels of air preheating according to the procedure explained in Section Flashback and lean blowout test procedures. In the current study, we will discuss solely the stability maps at $T_{in} = 450$ K, refer to Reichel et al. [30] for the results of further configurations and preheat levels.

At $\chi = 12.5\%$, FB was suppressed on the whole operational range of the atmospheric test rig (Fig. 4b). Irrespective of the swirl number, this configuration was capable of operating up to stoichiometric conditions. The lower stability limit was LBO at $\phi = 0.15$, which is also independent of the swirl number. The authors are of the opinion that the additional fuel momentum substantially contributed to achieving this wide operational range. As will become evident in the experiments, the injected fuel altered the velocity field in manner beneficial for FB resistance.

To allow for the investigation of FB phenomena, FB was intentionally triggered by reducing the amount of AAI to $\chi = 7.5\%$ (Fig. 4a). At an air mass flow of $\dot{m}_{air} = 0.06$ kg/s, the stable equivalence ratios ranged from stoichiometric to LBO at $\phi = 0.15$. With decreasing air mass flow, this range of stable equivalence ratios became narrower, although the upper limit

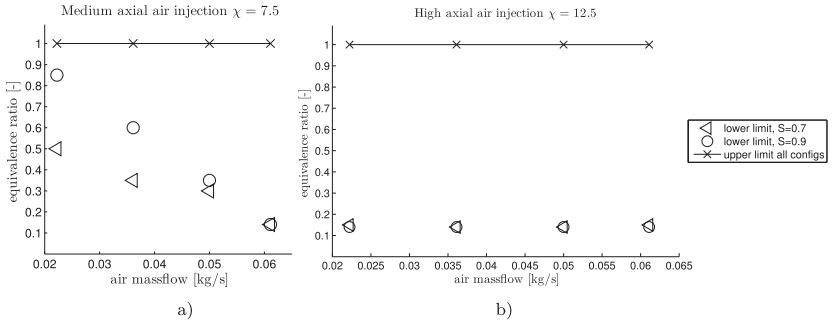

Fig. 4 – Stability limits for $\chi = 12.5\%$ and $\chi = 7.5\%$ at $T_{in} = 450$ K; both configurations operated at $\phi = 1$ without flashback (symbol ×, $\phi > 1$ not tested). Hence, only the lower stability limits are displayed.

INTERNATIONAL JOURNAL OF HYDROGEN ENERGY 42 (2017) 4518–4529

remained at $\phi = 1.0$. Other than $\chi = 12.5\%$, the lower limit was not caused by LBO but FB.

This may appear counter-intuitive, because the laminar burning velocity of lean hydrogen–air mixtures increases with increased equivalence ratio. However, it will be shown in the experiments that the ability of this configuration to prevent FB at high equivalence ratios stems from the flow field changes induced by the additional fuel momentum, which outweigh the increase in flame speed.

Isothermal flow field

The AAI and the additional momentum of the fuel, which is also injected in axial direction (see Section Burner model), do have similar effects on the combustor flow field. To separate the impact of both effects, the isothermal combustor flow field was compared for varied levels of both quantities (Fig. 5). For all investigated conditions, vortex breakdown was established downstream of the cross-sectional area expansion. This led to the typical flow field of swirl-stabilized combustors, which constitutes in an inner recirculation zone, enveloped by an annular jet, and an outer recirculation zone between the annular jet and the bounding walls.

In the absence of AAI ($\chi = 0$, left column), the internal recirculation zone extended up to $x/D < 0.1$ towards the nozzle outlet. The flow field inside the mixing tube exhibited a deficit in axial velocity towards the center line for the entire length of the mixing tube, which made this configuration particularly sensitive to flame propagation in the core flow and CIVB. Without the central air jet, the fuel jets do not penetrate into the center of the mixing tube. Thus, even in case of an increased fuel mass flow, a velocity increase was only observed on high radii ($r > 0.3$).

For $\chi = 7.5\%$ (center column), the axial velocity deficit along the central axis of the mixing tube was overcome but remained present at the mixing tube outlet. As fuel momentum increased, the velocity deficit at the nozzle outlet was significantly reduced. Thus, the flow field was altered to a shape less prone to FB. This flow field alteration explains the observed increase in FB resistance towards higher equivalence ratios at $\chi = 7.5$, documented in the stability map (Fig. 4a).

For $\chi = 12.5\%$, the axial velocity deficit at the mixing tube outlet vanished. The stagnation point on the central axis was shifted downstream to $x/D = 0.7$. For an increase in fuel momentum, the axial velocities at the mixing tube outlet were further enhanced. Additionally, their radial distribution was homogenized. These changes are considered beneficial for FB resistance, providing an explanation for the observed wide operational range at atmospheric conditions (Fig. 4b).

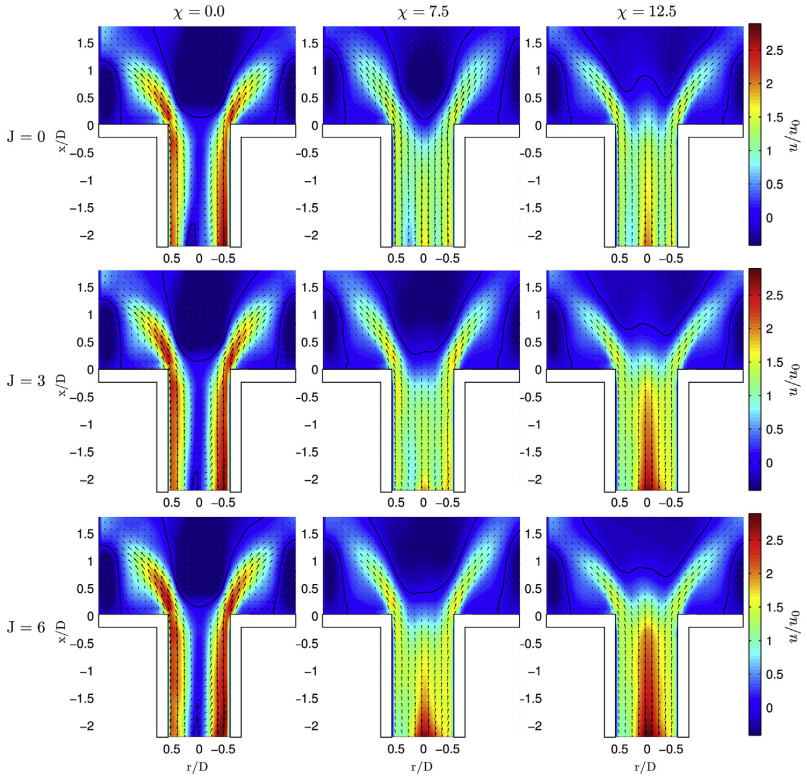

Fig. 5 – Isothermal flow field in the absence ($\chi = 0\%$, left column) and presence of a medium ($\chi = 7.5\%$, center column) and high ($\chi = 12.5\%$, right column) amount of AAI. Additionally, the effect of injected fuel is presented at $J = 3$ (center row) and $J = 6$ (bottom row); (Re = 40,000, S = 0.9, u_0 = const.); solid lines indicate $u/u_0 = 0$.

4524 INTERNATIONAL JOURNAL OF HYDROGEN ENERGY 42 (2017) 4518–4529

According to these results, it can be inferred that the reported increase in FB resistance towards higher equivalence ratios correlates with the described changes in the isothermal flow field. In particular, the axial location of vortex breakdown x_{VB} appears to be a telling estimator for FB resistance. For this reason, x_{VB} was extracted and compared for non-reacting and reacting combustor flow fields.

Reacting flow field

For the reacting case, in addition to AAI and fuel momentum, the axial location of VB x_{VB} was affected by dilatation due to heat addition. To determine the suitability of x_{VB} as an estimator for FB resistance the contribution of dilatation due to heat addition is determined by comparing isothermal and reacting combustor flow field data.

The reacting velocity field is given for varied levels of fuel momentum, for the two configurations exhibiting a high ($\chi = 12.5\%$; Fig. 6a–d) and medium ($\chi = 7.5\%$; Fig. 6e–g) level of AAI. The fuel momentum was varied by increasing the fuel mass flow at a constant air mass flow and temperature. Thus, the overall velocity level was elevated with increasing equivalence ratio due to the additional volume flow and increased dilatation due to heat addition.

Generally, a strong effect of fuel momentum was observed. For $\chi = 12.5\%$, the stagnation point on the central axis was shifted downstream from $x/D = 0.6$ at isothermal conditions up to $x/D = 2.0$ for reacting conditions ($J = 4.3$). A comparison of x_{VB} for the same fuel momentum ($J \approx 3$) yielded $x_{VB}/D = 0.7$ at isothermal (Fig. 5) and $x_{VB}/D = 1.4$ at reacting conditions. Thus, the contribution of the dilatation was significant, imposing a factor of two on x_{VB}.

At $\chi = 7.5\%$, the VB location, x_{VB}, also exhibits a high sensitivity to increased fuel mass flow. Similar to the case of $\chi = 12.5\%$, we observed a strong downstream shift of x_{VB} for reacting conditions. A comparison of the stagnation point for the same fuel momentum ($J = 3$) yielded $x_{VB}/D = 0.3$ at isothermal conditions (Fig. 5) and $x_{VB}/D = 1.2$ at reacting conditions. Thus, the contribution of the dilatation was much stronger, imposing a factor of four on x_{VB}.

It is summarized that the combined effect of fuel momentum and dilatation due to heat addition created the desired plug flow-shaped velocity profile at the nozzle outlet for both, medium and high amounts of axially injected air. At reacting conditions for a moderate equivalence ratio of $\phi = 0.4$ ($J = 2.5$), the high and moderate FB resistance configurations revealed a similar VB location of $x_{VB} = 1.4$ and $x_{VB} = 1.2$, respectively. However, the contribution of dilatation to achieving this downstream shift was shown to be much stronger for $\chi = 7.5\%$. It is concluded, that two configurations that exhibit very diverse FB resistance, and diverse isothermal flow fields did exhibit a very similar axial location of VB under reacting conditions due to the varying contribution of dilatation. This observation renders the axial location of VB an unsuitable estimator for FB resistance with respect to varied fuel momentum. Therefore, next the upstream flame front was considered as an estimator for FB disposition and was, thus, evaluated for varied levels of fuel momentum.

Upstream flame front location x_f from OH-PLIF

Time-averaged flame front distribution

The mean OH probability, $\overline{\alpha}$, and an instant OH-PLIF recording for the configuration exhibiting high FB resistance ($\chi = 12.5\%$)

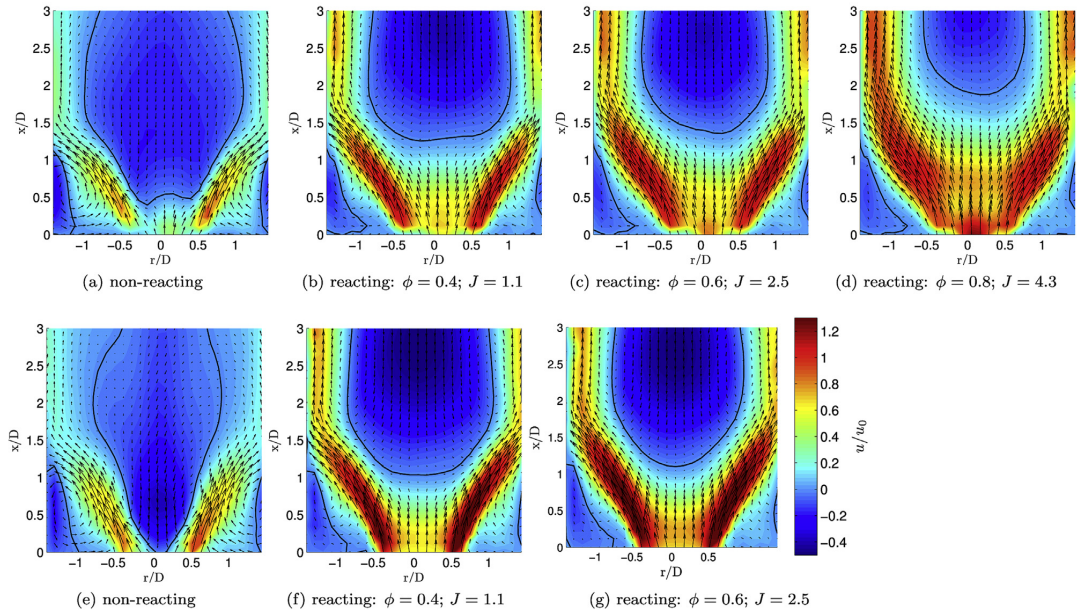

Fig. 6 – Impact of varied fuel momentum on the reacting combustor flow field in the presence of high $\chi = 12.5\%$ (top) and medium $\chi = 7.5\%$ (bottom) amount of AAI $m_{air} = 180$ kg/h, $T_{in} = 450$ K, $\phi = 0.4$–0.8; solid lines indicate zero axial velocity.

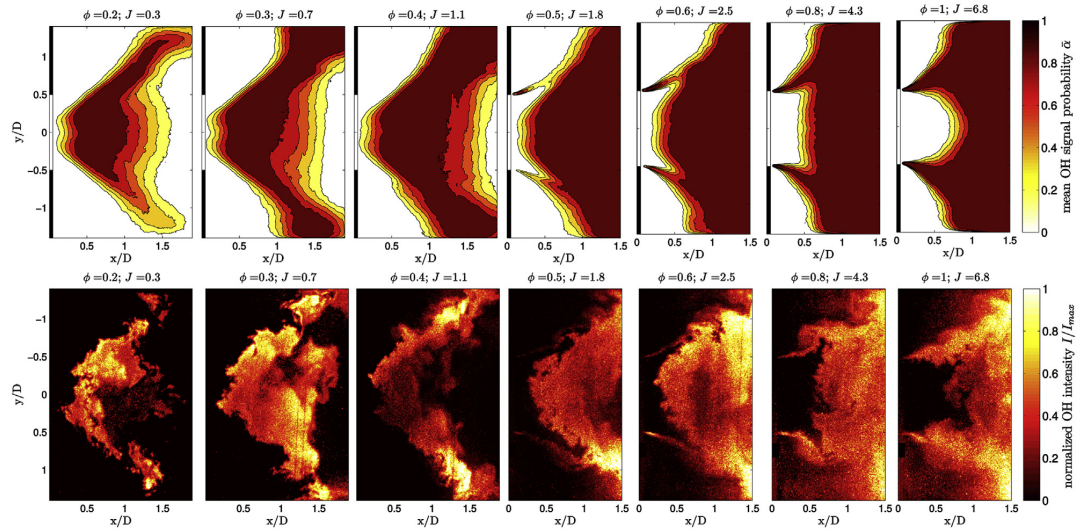

Fig. 7 – Mean OH signal probability (top row) and instant OH-PLIF images (bottom row) in the presence of high AAI (χ = 12.5%) recorded at T_{in} = 453 K, u_0 = 70 m/s.

provide a good impression of the time mean and instantaneous upstream flame front distribution, respectively (Fig. 7). A V-shaped, lifted-off flame was observed for equivalence ratios $\phi \leq 0.5$ and a fuel momentum of $J = 1.8$. With increasing fuel momentum at an equivalence ratio above $\phi = 0.5$, the reaction zone on the central axis is shifted downstream, whereas the flame remained attached in the shear layer. This shift stemmed from the axial velocity increase and altered velocity field characteristics associated with the increased momentum ratio. This effect of the additional fuel momentum outweighs the increase in burning velocity, which would promote an upstream shift of the flame.

The same experiment for the configuration exhibiting moderate FB resistance (χ = 7.5%) revealed that, for all FB occurrences, the flame was observed to penetrate upstream the mixing tube outlet prior to FB. On the other hand, FB was never observed for a situation where the flame was located downstream of the nozzle exit, despite the flame anchoring to the burner rim and operating at stoichiometric conditions. These observations support the choice of the axial flame front location, x_f, as an estimator for the FB safety margin.

Equivalence ratio dependence of x_f

To quantify how the fuel momentum affected flame stabilization for a variety of inlet conditions, the upstream flame front location, x_f, was extracted from the OH-PLIF recordings. Therefore, we utilized an extraction algorithm detailed in Reichel et al. [34]. The dependence of x_f for χ = 12.5% and χ = 7.5% was quantified with respect to different levels of momentum ratio J. These varied levels of J were achieved by varying air preheat temperatures T_{in} and equivalence ratio ϕ at a constant bulk air velocity of u_0 = 70 ms (Fig. 8a–b).

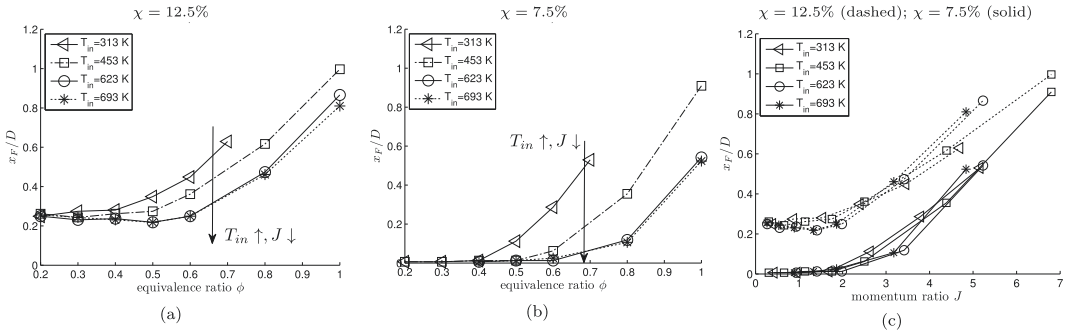

Fig. 8 – Location of upstream flame front x_f over equivalence ratio ϕ for varied air preheat temperatures T_{in} for hydrogen at (a) χ = 12.5% and (b) χ = 7.5%; (c) when plotted over the momentum ratio J, all temperature curves of the cases a) (χ = 12.5%, dashed) and b) (χ = 7.5%, solid), respectively, collapse in one curve; all points recorded at u_0 = 70 m/s.

4526 INTERNATIONAL JOURNAL OF HYDROGEN ENERGY 42 (2017) 4518–4529

For $\chi = 12.5\%$, x_f was strongly dependent on equivalence ratio (Fig. 8a). Two effects were distinguished: First, a slight decrease of x_f with equivalence ratio, which dominated for $\phi < 0.5$. This slight decrease in x_f was caused by the increased flame speed with increasing equivalence ratio of the lean hydrogen–air mixture. Second, a significant downstream shift of the reaction zone on the central axis was observed. This downstream shift of the reaction zone resulted from the changes in the flow field, which were caused by the increased momentum ratio J. This effect dominated above $\phi = 0.5$.

Note, that for a fixed equivalence ratio, the lowest x_f was observed for the highest air preheat temperature T_{in}. This reduction in x_f with increasing T_{in} stemmed from a decrease in momentum ratio J. With increased air preheating, the air momentum was increased whereas the fuel momentum remained nearly constant. Thus, the momentum ratio J was decreased which altered the flow field in a less favorable manner and caused the flame to shift upstream. Generally, an increase in flame speed with air preheat temperature, might also contribute to the reduced values of x_f. However, the latter effect was small compared to the former, as was shown in a previous study by the authors (Reichel et al. [34]).

For $\chi = 7.5\%$, the value of x_f significantly reduced at all investigated conditions (Fig. 8b). This strong χ-dependence of the flame front location x_f emphasizes the outstanding ability of AAI to control the flame location. Close to the lowest equivalence ratio before FB occurrence ($\phi = 0.3$–0.4), the flame tip reached into the mixing tube. Analogous to $\chi = 12.5\%$, if one increased ϕ above a temperature-dependent threshold, x_f would significantly shift downstream. Likewise, the strong dependence of x_f on air preheat temperature and, thus, the momentum ratio J, was observed and can be explained in the same manner.

The flame front location, x_f, was now plotted with respect to the momentum ratio J (Fig. 8c) for both configurations $\chi = 12.5\%$ and $\chi = 7.5\%$. As predicted from the isothermal flow field data, below $J = 2$, the additional fuel momentum did not alter the flow field. Hence, x_f remained constant. As the flow field was altered by the additional fuel momentum for values above $J = 2.5$, an increase in x_f resulted. Note, that when x_f is plotted over the momentum ratio J, other than for the equivalence ratio, the x_f-curves at different air preheat temperatures all collapse on one curve. This consistency underlines the role of the momentum ratio J as the governing parameter to describe the dependence of x_f with respect to equivalence ratio and preheat temperature over a wide range of χ.

Summary of fuel momentum effect on x_{VB} and x_f

To summarize the impact of varied levels of fuel momentum on the key combustor characteristics related to FB, the upstream flame front, flame structure, and axial location of VB, are displayed collectively in Fig. 9.

The mean OH* contours give a qualitative impression of the flame location and structure. Additionally, the exact upstream flame front location (solid line, extracted from the OH-PLIF recordings) is highlighted and superimposed onto this figure. For reasons explained in Section Water tunnel, the OH-

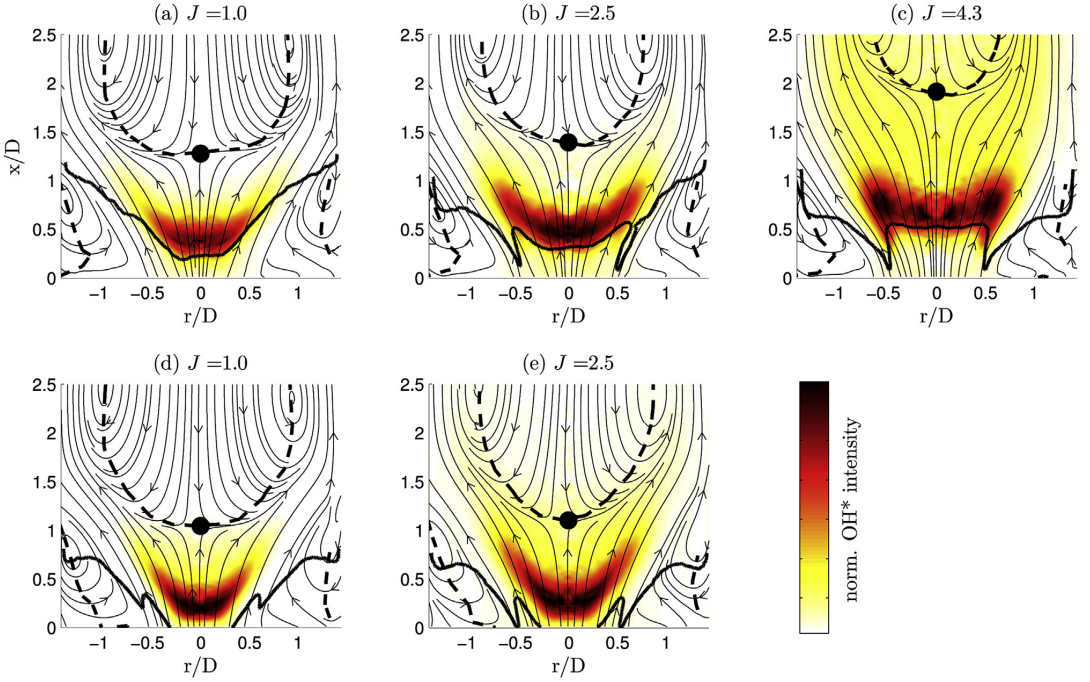

Fig. 9 – For $\chi = 12.5\%$ (a–c) and $\chi = 7.5\%$ (d–e): downstream shift upstream flame front (solid line) and central recirculation zone (dashed line) with increasing momentum ratio J at a constant bulk outlet velocity $u_0 = 70$ m/s.

INTERNATIONAL JOURNAL OF HYDROGEN ENERGY 42 (2017) 4518–4529 4527

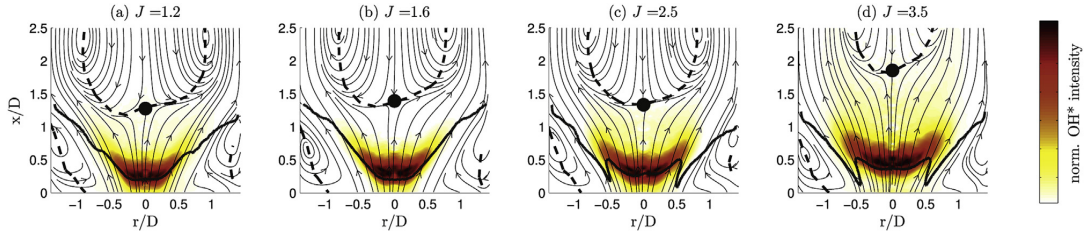

Fig. 10 – For $\chi = 12.5\%$: downstream shift of upstream flame front (solid line) and central recirculation zone (dashed line) with increasing momentum ratio J at a constant bulk air velocity $u_0 = 50$ m/s.

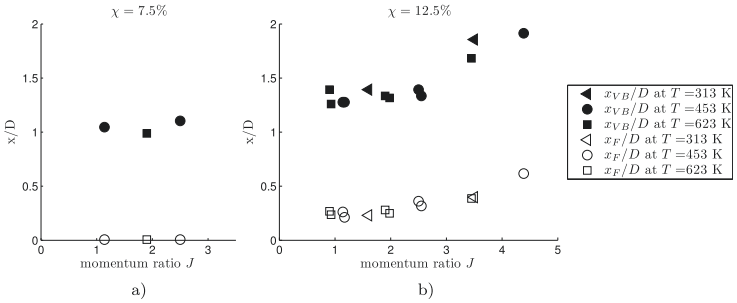

Fig. 11 – For $\chi = 7.5\%$ (a) and $\chi = 12.5\%$ (b): downstream shift of upstream flame front x_f (empty symbols) and location of VB x_{VB} (filled symbols) with increasing momentum ratio J for $u_0 = 50$–80 m/s.

PLIF recordings are more accurate in extracting the flame front. Moreover, the reacting combustor flow field is provided by the means of streamlines, whereby the dashed line highlights zero axial velocity ($u_{ax} = 0$) and the black dot indicates x_{VB}. This representation was used to directly compare the high ($\chi = 12.5\%$) and medium ($\chi = 7.5\%$) FB resistance case with respect to the effect of fuel momentum on x_f and x_{VB}.

For $\chi = 12.5\%$, the flame front and VB were continuously shifted downstream as the fuel momentum increased (Fig. 9a–c). A comparison to the $\chi = 7.5\%$ case at identical inlet conditions revealed a similar axial location of VB (Fig. 9d–e). However, the axial location of the upstream flame front (solid black line) significantly deviated for the two configurations, at the same momentum ratio J. For $\chi = 12.5\%$, the upstream flame front was located well downstream of the mixing tube outlet, indicating a high FB resistance. For $\chi = 7.5\%$, the flame front was close to or already inside the mixing tube outlet, which posed a high FB risk. This significant difference in FB propensity could not have been predicted from x_{VB}, which assumed a similar value in both cases. It is, thus, concluded that a high level of x_{VB} is a necessary but not sufficient condition for high FB resistance. Only a far downstream flame front location x_f was a sufficient indicator for FB resistance.

To extend the correlation database for the effect of fuel momentum on x_f and x_{VB}, these parameters were extracted from recordings at lower ($u_0 = 50$ m/s; Fig. 10) and higher ($u_0 = 80$ m/s) bulk air velocities. Since both parameters were independent from u_0 in the investigated range (compare Reichel et al. [34]), it is justified to merge the results for $u_0 = 50$–80 m/s into a single fuel momentum correlation of x_f and x_{VB} for $\chi = 7.5\%$ and $\chi = 12.5\%$, respectively (Fig. 11a–b). Hereby, the fuel momentum was varied by varying the equivalence ratio or the level of air preheating in the range from $T_{in} = 313 - 623$ K.

For $\chi = 12.5\%$, both parameters x_f and x_{VB} were independent of J for $J < 2$, but correlated with the increasing momentum ratio for $J > 2$ over the investigated wide range of air preheat temperatures and equivalence ratios. For $\chi = 7.5\%$ the correlations are limited to $J < 2.5$ due to the limited number of simultaneous PIV and OH-PLIF recordings. However, Fig. 11a confirmed the previous observation that for $J < 2.5$, the upstream flame tip was inside the mixing tube, which poses a high FB danger, in spite of x_{VB} being situated more than one diameter downstream of the mixing tube outlet. Therefore, the given momentum ratio dependencies of x_{VB} and x_f illustrate two main findings: First, that only a high value of x_f poses a sufficient condition for FB resistance and second, that both, fuel momentum and AAI, strongly affect x_f and, thus, flashback resistance.

Conclusion

Hydrogen as a fuel in gas turbines is argued to significantly alter the combustor requirements due to its increased FB propensity and high associated fuel momentum. The suggested burner geometry applying a central non-swirling air jet with the aim to suppress FB was shown to exhibit excellent FB

resistance in the case of a high amount of AAI $\chi = 12.5\%$ and moderate FB resistance in the case of $\chi = 7.5\%$.

Under the investigated technically premixed conditions, the fuel momentum of hydrogen, which was injected in axial direction just upstream of the premixing section, caused significant changes in the mixing tube and combustor flow field. Whether or not the flow field changes caused by the fuel momentum are in favor of the combustor FB resistance was argued to strongly depend on the combustor geometry with respect to the fuel port location and strength of the central non-swirling air jet. For $\chi = 7.5\%$. and $\chi = 12.5\%$, the additional fuel momentum is reported to alter the isothermal flow field in a manner beneficial to FB resistance.

At isothermal conditions, the axial location of VB, x_{VB}, is observed to shift downstream with increasing momentum ratio J, rendering x_{VB} a potential estimator for FB safety. This general trend of a downstream shift of x_{VB} with increased momentum is confirmed at reacting conditions. However, the dilatation due to heat addition, which also shifts x_{VB} downstream, is shown to corrupt this trend as such, that even a flow field close to FB occurrence would still exhibit a high value of x_{VB}. Therefore, a high value of x_{VB} is identified to be only a necessary, but not sufficient, condition for FB resistance. Instead, an axial location of the upstream flame front, x_f, well downstream of the mixing tube outlet is identified as a sufficient condition to achieve FB resistance. Vice versa, a localization of the upstream flame front inside the premixing section is observed to be a prerequisite for the occurrence of FB. The momentum ratio J is identified as the governing parameter to describe the x_f-dependence for a variety of inlet conditions with respect to inlet temperature and equivalence ratio.

The experiments show that the upstream flame front location x_f is shifted downstream with increasing equivalence ratio ϕ due the to simultaneous increase in momentum ratio J. With increasing ϕ, the additional momentum of the fuel flow, alters the flow field and even supersedes any parallel augmentation in the turbulent flame speed. Utilizing this effect properly can fortify the FB resistance of a configuration and needs to be taken into account during combustor development or adjustment to high hydrogen fuels.

The upstream flame front locations serves as the best estimator for FB safety. If not available, non-reacting combustor flow fields with fuel injection, provide comparably more insight than reacting combustor flow fields, since they allow the quantification of the fuel momentum in the absence of dilatation due to heat addition.

Acknowledgments

The research leading to these results has received funding from the European Union Seventh Framework Program (FP7/2007-2013) under grant agreement no 284636.

REFERENCES

[1] Brewer GD. The prospects for liquid hydrogen fueled aircraft. Int J Hydrogen Energy 1982;7(1):21–41. http://dx.doi.org/10.1016/0360-3199(82)90205-1. ISSN 03603199.

[2] Contreras A, Yiğit S, Özay K, Veziroğlu TN. Hydrogen as aviation fuel: a comparison with hydrocarbon fuels. Int J Hydrogen Energy 1997;22(10):1053–60. http://dx.doi.org/10.1016/S0360-3199(97)00008-6. ISSN 03603199.

[3] Pohl HW, Malychev VV. Hydrogen in future civil aviation. Int J Hydrogen Energy 1997;22(10):1061–9. http://dx.doi.org/10.1016/S0360-3199(95)00140-9. ISSN 03603199.

[4] Rao AG, Yin F, van Buijtenen JP, Isikveren A. A hybrid engine concept for multi-fuel blended wing body. Aircr Eng Aerosp Technol 2014;86(6). ISSN 0002-2667.

[5] Levy Y, Sherbaum V, Arfi P. Basic thermodynamics of FLOXCOM, the low-NOx gas turbines adiabatic combustor. Appl Therm Eng 2004;24(11):1593–605. ISSN 1359-4311.

[6] Huang Y, Yang V. Dynamics and stability of lean-premixed swirl-stabilized combustion. Prog Energy Combust Sci 2009;35(4):293–364. http://dx.doi.org/10.1016/j.pecs.2009.01.002. ISSN 0360-1285.

[7] Lieuwen TC. Unsteady combustor physics. Cambridge University Press; 2012. ISBN 1107015995.

[8] Ziemann J. Low-NOx combustors for hydrogen fueled aero engine. Int J Hydrogen Energy 1998;23(4):281–8. http://dx.doi.org/10.1016/S0360-3199(97)00054-2. ISSN 03603199.

[9] Schefer RW. Hydrogen enrichment for improved lean flame stability. Int J Hydrogen Energy 2003;28(10):1131–41. http://dx.doi.org/10.1016/S0360-3199(02)00199-4. ISSN 03603199.

[10] Griebel P, Boschek E, Jansohn P. Lean blowout limits and NOx emissions of turbulent, lean premixed, hydrogen-enriched methane/air flames at high pressure. J Eng Gas Turbines Power 2006;129(2):404–10. http://dx.doi.org/10.1115/1.2436568.

[11] Tuncer O, Acharya S, Uhm J. Dynamics, NOx and flashback characteristics of confined premixed hydrogen-enriched methane flames. Int J Hydrogen Energy 2009;34(1):496–506. http://dx.doi.org/10.1016/j.ijhydene.2008.09.075. ISSN 03603199.

[12] Plee SL, Mellor AM. Review of flashback reported in prevaporizing/premixing combustors. Combust Flame 1978;32:193–203. http://dx.doi.org/10.1016/0010-2180(78)90093-7.

[13] Schefer R, Wicksall D, Agrawal A. Combustion of hydrogen-enriched methane in a lean premixed swirl-stabilized burner. Proc Combust Inst 2002;29(1):843–51. http://dx.doi.org/10.1016/S1540-7489(02)80108-0. ISSN 15407489.

[14] Strakey P, Sidwell T, Ontko J. Investigation of the effects of hydrogen addition on lean extinction in a swirl stabilized combustor. Proc Combust Inst 2007;31(2):3173–80. http://dx.doi.org/10.1016/j.proci.2006.07.077. ISSN 15407489.

[15] Lieuwen T, McDonell V, Santavicca D, Sattelmayer T. Burner development and operability issues associated with steady flowing syngas fired combustors. Combust Sci Technol 2008;180(6):1169–92. http://dx.doi.org/10.1080/00102200801963375. ISSN 0010-2202.

[16] Syred N, Abdulsada M, Griffiths A, O'Doherty T, Bowen P. The effect of hydrogen containing fuel blends upon flashback in swirl burners. Appl Energy 2012;89(1):106–10. http://dx.doi.org/10.1016/j.apenergy.2011.01.057. ISSN 03062619.

[17] Emadi M, Karkow D, Salameh T, Gohil A, Ratner A. Flame structure changes resulting from hydrogen-enrichment and pressurization for low-swirl premixed methane–air flames. Int J Hydrogen Energy 2012;37(13):10397–404. http://dx.doi.org/10.1016/j.ijhydene.2012.04.017. ISSN 03603199.

[18] Syred N, Giles A, Lewis J, Abdulsada M, Valera Medina A, Marsh R, et al. Effect of inlet and outlet configurations on blow-off and flashback with premixed combustion for methane and a high hydrogen content fuel in a generic swirl burner. Appl Energy 2014;116:288–96. http://dx.doi.org/10.1016/j.apenergy.2013.11.071. ISSN 0306-2619.

[19] Sayad P, Schönborn A, Klingmann J. Experimental investigation of the stability limits of premixed syngas-air

flames at two moderate swirl numbers. Combust Flame 2016;164:270–82. http://dx.doi.org/10.1016/j.combustflame.2015.11.026.

[20] Schönborn A, Sayad P, Klingmann J. Influence of precessing vortex core on flame flashback in swirling hydrogen flames. Int J Hydrogen Energy 2014;39(35):20233–41. http://dx.doi.org/10.1016/j.ijhydene.2014.10.005. ISSN 03603199.

[21] Göckeler K, Göke S, Schimek S, Paschereit CO. Enhanced recirculation in the cold flow field of a swirl-stabilized burner for ultra wet combustion. In: Int. Conf. Jets, wakes separated flows, ICJWSF-2010, Sept. 27–30, Cincinnati, Ohio, USA; 2010.

[22] Kröner M, Fritz J, Sattelmayer T. Flashback limits for combustion induced vortex breakdown in a swirl burner. J Eng Gas Turbines Power 2003;125(3):693. http://dx.doi.org/10.1115/1.1582498. ISSN 07424795.

[23] Burmberger S, Sattelmayer T. Optimization of the aerodynamic flame stabilization for fuel flexible gas turbine premix burners. J Eng Gas Turbines Power 2011;133(10):101501. http://dx.doi.org/10.1115/1.4003164. ISSN 07424795.

[24] Reichel TG, Terhaar S, Paschereit CO. Flow field manipulation by axial air injection to achieve flashback resistance and its impact on mixing quality. In: Proceedings of the 43rd AIAA fluid dynamics Conference and exhibit, San Diego, CA, USA; June 24–27, 2013; 2013. http://dx.doi.org/10.2514/6.2013-2603.

[25] Terhaar S, Reichel TG, Schrödinger C, Rukes L, Paschereit CO, Oberleithner K. Vortex breakdown types and global modes in swirling combustor flows with axial injection. J Propuls Power 2014;31(1):219–29. http://dx.doi.org/10.2514/1.B35217. ISSN 0748-4658.

[26] Reichel TG, Terhaar S, Paschereit O. Increasing flashback resistance in lean premixed swirl-stabilized hydrogen combustion by axial air injection. J Eng Gas Turbines Power 2015;137(7):071503. http://dx.doi.org/10.1115/1.4029119.

[27] Ilbas M, Crayford AP, Yılmaz İ, Bowen PJ, Syred N. Laminar-burning velocities of hydrogen–air and hydrogen–methane–air mixtures: an experimental study. Int J Hydrogen Energy 2006;31(12):1768–79. http://dx.doi.org/10.1016/j.ijhydene.2005.12.007. ISSN 03603199.

[28] Mayer C, Sangl J, Sattelmayer T, Lachaux T, Bernero S. Study on the operational window of a swirl stabilized syngas burner under atmospheric and high pressure conditions. J Eng Gas Turbines Power 2012;134(3). ISSN 07424795. http://dx.doi.org/10.1115/1.4004255.

[29] Sangl J, Mayer C, Sattelmayer T. Dynamic adaptation of aerodynamic flame stabilization of a premix swirl burner to fuel reactivity using fuel momentum. J Eng Gas Turbines Power 2011;133(7):071501. http://dx.doi.org/10.1115/1.4002659.

[30] Reichel TG, Terhaar S, Paschereit CO. Increasing flashback resistance in lean premixed swirl-stabilized hydrogen combustion by axial air injection. In: Proceedings of the ASME turbo expo 2014; 2014.

[31] Lantz A, Collin R, Aldén M, Lindholm A, Larfeldt J, Lörstad D. Investigation of hydrogen enriched natural gas flames in a SGT-700/800 burner using OH PLIF and chemiluminescence imaging. J Eng Gas Turbines Power 2015;137(3):031505. http://dx.doi.org/10.1115/1.4028462. ISSN 07424795.

[32] Gupta AK, Lilley DG, Syred N. Swirl flows. Tunbridge Wells and Kent: Abacus Press; 1984. ISBN 9780856261756.

[33] Tanneberger T, Reichel TG, Krüger O, Terhaar S, Paschereit CO. Numerical investigation of the flow field and mixing in a swirl-stabilized burner with a non-swirling axial jet: GT2015-43382. In: Proceedings of the ASME turbo expo 2015; 2015.

[34] Reichel TG, Goeckeler K, Paschereit O. Investigation of lean premixed swirl-stabilized hydrogen burner with axial air injection using OH-PLIF imaging. J Eng Gas Turbines Power 2015;137(11):111513. http://dx.doi.org/10.1115/1.4031181.

[35] Boxx I, Slabaugh C, Kutne P, Lucht R, Meier W. 3kHz PIV/OH-PLIF measurements in a gas turbine combustor at elevated pressure. Proc Combust Inst 2015. ISSN 15407489. http://dx.doi.org/10.1016/j.proci.2014.06.090.

CHAPTER 3

Discussion

The publications in the previous section are given in chronological order. This demonstrates in a viable manner how the general idea of extending the FB limits of a burner operating on hydrogen by the means of axial air injection developed and how the understanding of the matter accumulated. However, for the sake of clarity, the following section summarizes and discusses the results as a whole. To this end, the findings are categorized with respect to being obtained by isothermal or reacting measurements.

3.1 Isothermal Water Tunnel Investigations

3.1.1 Isothermal Flow Field

Effect of swirl, premixing length and AI on isothermal flow field

Publication 2.1 exploits the idea of a non-swirling central air jet suggested by Burmberger and Sattelmayer [72] to increase the flashback resistance of a combustor operating on high reactivity fuels. To this end, an extensive isothermal characterization of various geometries is conducted aiming to shed light on how geometry variations, especially varied AI rates affect the combustor flow field. PIV measurements in the combustion chamber and mixing tube reveal that in the absence of AI, the CRZ extends upstream to and almost inside the mixing tube outlet (Fig. 5, p. 41). Along its entire length, the axial velocities on the mixing tube axis are of the order of only 20% of the bulk velocity u_0. This flow configuration is typical for strongly swirling flows and does not impose stability limits in the operational range of low reactivity fuels like natural gas. However, when operated on a high reactivity fuel, such as hydrogen, this flow configuration results in the occurrence of FB.

To suppress FB, which significantly limits the operational range of the burner, a central non-swirling air jet is injected on the central axis of the radial swirl generator upstream of the premixing section. Consequently, the flow in the premixer comprises a swirling flow

from the radial swirl generator and an axially injected flow entering the premixer via an axial injection orifice. The isothermal PIV measurements reveal that, already moderate AI rates of $\chi = 7.5\%$ are sufficient to overcome the axial velocity deficit on part of the mixing tube length. However, the axial location of VB is not affected. Increasing the AI rate to $\chi = 12.5\%$, by choosing a larger diameter AI orifice, removes the axial velocity deficit along the entire length of the mixing tube and causes a downstream shift of VB. Simultaneously, the general characteristics of the combustor flow field, i.e., a central and outer recirculation zone seperated by an annular jet, are preserved. Further increasing AI rates in excess of $\chi = 22\%$ results in the suppression of VB. Preserving VB and the CRZ are an important prerequisite for achieving flame stability and, thus, pose an upper limit for the application of AI.

Effect of fuel momentum on isothermal flow field

The isothermal combustor flow field in the premixing section and combustion chamber is recorded for increasing fuel flow rates, representing varied levels of fuel momentum, as reported in publication 2.3. The effect of fuel momentum on the isothermal velocity field is observed to be significant. However, it found to strongly depend on the simultaneously applied AI rate (Fig. 5, p. 65). In the absence of AI, the axial velocity distribution at the mixing tube outlet does not benefit from the increased fuel momentum. The axial velocity deficit on the central mixing tube axis remains present irrespective of the fuel momentum. A velocity increase is observed only on high radii $r/D > 0.3$.

On the other hand, if at least a medium or high AI rate is applied, increased fuel momentum does affect the flow field by altering the axial velocity distribution at the mixing tube outlet. In these cases, the axial velocity magnitude is increased and radial distribution of axial velocity is homogenized. The resulting plug flow-shaped axial velocity profile beneficially contributes to FB resistance (see Sec. 3.2.1).

These results reveal an inter-dependency of fuel momentum and AI: For the fuel momentum to contribute to a flow configuration that enhances FB resistance, at least a medium amount of AI is required to allow for fuel distribution on higher radii.

3.1.2 Fuel–Air Mixing: Effects of Swirl, Premixing Length and AI

To evaluate the impact of increasing AI rates on fuel–air mixing quality, planar LIF measurements were conducted for four configurations (Table 1, p. 38) in a cross-wise plane downstream of the mixing tube. The measurement location is equivalent to the approximate location of flame anchoring. This allows for quantifying the spatial and temporal unmixedness of the mixture consumed by the flame.

The impact of increased AI rates on spatial unmixedness U_s was shown to strongly depend on premixer geometry, i.e., swirl number and mixing tube length. With respect

to a base line geometry (configuration 1), increasing the swirl intensity was found to result in lower levels of spatial unmixedness U_s than extending the length of the mixing tube (Fig. 10a, p. 44). For the lower swirl number, with increasing AI rate a fuel rich region on the central axis develops which results from the reduced azimuthal velocities preventing a distribution of the fuel on higher radii (Fig. 9, p. 45). Thus, for $S = 0.7$, the spatial unmixedness slightly increases with increasing AI rates. However, for $S = 0.9$, there is sufficient swirl to distribute the fuel to higher radii. Therefore, U_s remains nearly unaffected for AI rates up to $\chi = 12.5\%$.

The temporal unmixedness U_t was also affected by geometric parameters of the premixing section. With respect to a common base line geometry (configuration 1), the extension of the mixing tube length achieved a higher reduction in U_t than the increase in swirl intensity. For increasing AI rates, the long mixing tube achieves the lowest levels of U_t, irrespective of the swirl number (Fig. 10b, p. 44). Note, that with increasing AI rates, the temporal unmixedness U_t of each configuration 1–4 decreases. This gain in temporal mixing quality is attributed to the suppression of a hydrodynamic flow instability, referred to as precessing vortex core (PVC). Fuel is trapped in the center of the strongly swirling flow inside the mixing tube. Upon exiting the mixing tube, this fuel-rich core is displaced from the central axis and describes a precessing motion following the coherent structure, i.e., the PVC. This leads to a precessing fuel-rich pattern which manifests in high temporal concentration fluctuations, i.e., high spatial unmixedness. Already at moderate AI rates above $\chi = 7.5\%$, the PVC and the precessing fuel-rich pattern are suppressed which leads to the observed reduction in temporal unmixedness U_t.

The isothermal mixing investigations identified a geometry for which at high AI rates of $\chi = 12.5\%$ the spatial unmixedness U_s remains unaffected and temporal unmixedness U_t is even shown to decrease. Therefore, instead of compromising fuel–air mixing, AI improves the fuel–air mixing quality, if other geometric parameters are adjusted accordingly. This mixing improvement offers the potential for NO_x reduction and is investigated further under atmospheric reacting conditions.

3.2 Reacting Investigations

3.2.1 Stability Limits And Flashback Resistance

To prove the postulated FB resistance of the flow fields manipulated by AI, atmospheric reacting tests were conducted. Detailed stability maps evaluating the operational range of geometries with varied initial swirl number and mixing tube length validate a substantially increased operational range with increasing AI rates (Fig. 7, p. 42). Additionally, stability limits were shown to benefit from a lower swirl number and a longer mixing tube. While the extended stability limits with reduced swirl are in line with the findings previously

reported in most literature [53, 66], a dependence on length of the premixing section is not reported.

The length dependence is attributed to changes in the radial distribution of axial velocity at the mixing tube outlet: With increasing mixing tube length, the radial distribution of axial velocity becomes more homogeneous. The importance of this aspect is underlined by the stability limits of configuration 3. The combination of a short mixing tube and high swirl leads to an axial velocity overshoot at the exit plane of the mixing tube (Fig. 6i, p. 41). This flow configuration results in a poor FB resistance. Increasing the mixing tube length by only $0.6D$ (configuration 4), results in a homogenized radial velocity distribution (Fig. 6l, p. 41) and significantly extends FB limits (Fig. 7, p. 42). Therefore, achieving a plug flow-shaped axial velocity profile, that exhibits a high magnitude and a high radial homogeneity of axial velocity at the mixing tube outlet, are identified as crucial parameters of the isothermal flow field to obtain FB resistance.

At high AI rates, FB is suppressed on the entire investigated operational range for configuration 1, 2 and 4. The lower stability limit occurred due to LBO at equivalence ratios of roughly $\phi = 0.15$. At medium AI rates, the recorded stability maps exhibit a behavior previously not reported in literature. While all tested configurations could operate at stoichiometric conditions, for some configurations FB occurred when decreasing the equivalence ratio at a constant mass flow. It is somewhat counter-intuitive that FB resistance is achieved at a higher equivalence ratio, although turbulent burning velocities of lean hydrogen–air mixtures increase with equivalence ratio.

To explain this observation, recall the high volumetric fuel flow rates of hydrogen with increasing equivalence ratio, i.e., the high fuel momentum. Fuel momentum was shown to cause significant changes in the isothermal combustor flow field. It is postulated that these flow field changes also affect the flame stabilization and by these means lead to the observed increased FB resistance with increasing equivalence ratio. This is further investigated in reacting tests reported in Sec. 3.2.3.

3.2.2 NO_x Emissions

To evidence that increased AI rates do not compromise emission levels, NO_x emissions were recorded in atmospheric reacting tests for configuration 1–4 at varied AI rates. Even at a high AI rate of $\chi = 12.5\%$ configuration 2–4 achieved single-digit NO_x emissions up to adiabatic flame temperatures of almost $T_{\mathrm{ad}} = 2000\,\mathrm{K}$ (Fig.14, p. 47). Slightly higher NO_x emissions were recorded for the configuration employing a short mixing tube and low swirl intensities (configuration 1).

The NO_x emissions were correlated with the unmixedness parameters obtained from the isothermal tests (Fig. 10c and Fig. 10d, p. 44). This correlation strongly depends on the adiabatic flame temperature T_{ad}. Below T_{ad} =1800 K unmixedness and NO_x emissions are

uncorrelated. This is expected since NO_x production only occurs at relevant production rates at temperatures above 1800 K [45]. For $T_{ad} \geq 1900\,K$, a threshold unmixedness can be identified for every flame temperature above which NO_x emissions begin to increase with increasing unmixedness. Note, that below this threshold an increase in unmixedness, e.g., due to temporal fluctuations stemming from thermoacoustic instabilities, does not translate into increased NO_x emissions. For configurations 3 and 4, that employ high swirl intensities, the recorded unmixedness parameters are well below this threshold, in spite of high AI rates ($\chi = 12.5\%$) and flame temperatures in excess of $T_{ad} = 2120\,K$.

This proves that in spite of the partially premixed character of the fuel injection the overall fuel-air mixing quality is very high and the NO_x emissions are on the level of perfectly premixed combustion.

3.2.3 Reacting Flow Field

Effects of AI and fuel momentum

The reacting velocity field is reported for varied equivalence ratios in case of medium and high AI rates in publication 2.2 and 2.4. Generally, results show that the CRZ is preserved even at high AI rates and stoichiometric conditions. Thus, even in the presence of high AI rates and a significant amount of added fuel momentum, the general characteristic of the swirling combustor flow is preserved (Fig. 6, p. 78).
At a fixed equivalence ratio, a higher AI rate results in a slightly further downstream location of VB, x_{VB}. At a fixed medium or high AI rate, increasing the equivalence ratio shifts x_{VB} downstream. Simultaneously, mean axial velocities on the central axis of the mixing tube outlet experience a significant increase: $\bar{u}/u_0$ increases by a factor of three, when increasing the equivalence ratio from $\phi = 0$ to $\phi = 0.8$ (Fig. 8, p. 56).

Note, that the observed flow field changes at reacting conditions are not solely attributed to the increasing fuel momentum with increasing equivalence ratio. Additionally, the dilatation due to heat addition contributes to the increased axial velocities.

Effect of dilatation due to heat addition

The individual contribution of fuel momentum and dilatation due to heat addition to the downstream shift of x_{VB} can not be determined based alone on the reacting PIV results. Thus, to determine the effect of fuel momentum isolated from dilatation, the isothermal and reacting flow field data are compared at varied fuel flow rates.

At isothermal conditions, x_{VB} is mainly determined by the AI rate and fuel momentum. Increasing rates of AI and fuel momentum, respectively, cause a downstream shift of x_{VB} (Fig. 5, p. 77). Simultaneously, FB resistance is increased. Generally, at reacting conditions, the same combination of AI and fuel momentum results in a further downstream x_{VB} due to

dilatation due to heat addition (Fig. 6, p. 78). Note, that the magnitude of this additional downstream shift depends on AI rate:

At $\chi = 12.5\%$, a comparison of x_{VB} for approximately the same fuel momentum ($J = 3$) yields $x_{\mathrm{VB}}/D = 0.7$ at isothermal and $x_{\mathrm{VB}}/D = 1.4$ at reacting conditions. Thus, the contribution of the dilatation is imposing a factor of two on x_{VB}.

At $\chi = 7.5\%$, for the same fuel momentum ($J = 3$), the comparison yields $x_{\mathrm{VB}}/D = 0.3$ at isothermal conditions and $x_{\mathrm{VB}}/D = 1.2$ at reacting conditions. Thus, the contribution of the dilatation is much stronger at lower AI rates, imposing a factor of four on x_{VB}.

This is an important effect with respect to judging the flashback resistance of a reacting flow field based on the axial location of VB. Low AI rates, that reportedly exhibit poor flashback resistance, are shown to exhibit similarly high values of x_{VB} as high AI rates. The observed difference in the contribution of dilatation at both AI rates stems from the different flame locations. A lower AI rate results in a flame located closer to the mixing tube outlet. The variation of flame location with AI and fuel momentum is discussed in Sec. 3.2.5.

3.2.4 Flame Front

Proof of AI and fuel momentum affecting the flame front

Based on the strong impact of fuel momentum on the flow field, demonstrated at isothermal and reacting conditions, fuel momentum was postulated to also affect flame stabilization and shift the flame downstream. A strong downstream shift of the mean flame front with increasing ϕ could indeed be observed in both, the recordings obtained by high-speed OH* chemiluminescence (Fig. 11, p. 58) and quantitative light sheet (QLS) technique (Fig.10, p. 57). To the knowledge of the author, this is the first documented downstream shift of a flame front with increasing equivalence ratio. Previously, Sangl et al. [89] had discussed the impact of fuel momentum on VB in an isothermal combustor flow, but had not considered the flow field or flame at reacting conditions.

The magnitude of the axial velocity increase with increasing equivalence ratio yields an explanation of the observed increasing FB resistance towards richer conditions. The axial velocity increase is of relevant magnitude with respect to flame stabilization, as such that the axial velocity gain with increasing equivalence ratio exceeds the parallel augmentation in turbulent burning velocity of the hydrogen–air mixture. This results in a downstream shift of the flame.

Detailed analysis of AI and fuel momentum effects on flame front

Generally, QLS is shown to be superior to OH* with respect to identifying the upstream flame front. However, the experimental effort and time demand of QLS are too high to

conduct a detailed screening of the upstream flame front over a wide range of operating conditions. To this end, the flame stabilization is investigated for increasing fuel momentum at varied AI rates by the means of OH-PLIF imaging (publication 2.3). These investigations are conducted for a wide range of operating conditions, namely combustor power $P = 20 - 200\,\mathrm{kW}$, bulk flow velocity $u_0 = 50 - 100\,\mathrm{m/s}$, and adiabatic flame temperature $T_{\mathrm{ad}} = 900 - 2700\,\mathrm{K}$.

The previously observed downstream shift of the upstream flame front with increasing equivalence ratio is confirmed and its dependence on combustor inlet conditions is investigated. To this end, the axial location of the upstream flame front x_{f} is extracted from the OH-PLIF recordings. In this manner, it was found that not the equivalence ratio, but the fuel–air momentum ratio J is the governing parameter for the observed downstream shift of x_{f}. The momentum ratio J correlates with the upstream flame front over the wide range of investigated operating conditions (Fig. 12, p. 69). It could be shown that, below a momentum ratio of $J = 2$, the flame front location x_{f} is not affected. For $J > 2$, an increasing momentum ratio is shown to cause a downstream shift of x_{f}, exceeding the effect of any parallel augmentation in burning velocity of the hydrogen–air mixture. Additionally, it is shown that increasing the AI rate results in an constant offset in x_{f} which remains nearly unaffected in case of increasing fuel momentum.

Evaluating the upstream flame front location x_{f} at operating conditions close and far from the stability limits, revealed x_{f} to act as an excellent estimator for FB tendencies: First, FB was never observed if the flame was located well downstream of the mixing tube outlet. Second, if the lower stability limit was posed by FB, x_{f} was continuously decreased when approaching the lower stability limit. Third, prior to FB, the flame was always observed to anchor just at or even inside the mixing tube representing $x_{\mathrm{f}} = 0$. This observation emphasizes the strong impact of fuel momentum on flame stabilization and in this manner also on stability limits.

3.2.5 Estimator For FB Resistance

Aiming to determine a suitable estimator for flashback resistance, publication 2.4 investigates the characteristics of the considered candidates the axial locations of VB, $\mathrm{x_{VB,}}$ and upstream flame front, $\mathrm{x_f}$.

To this end, the reacting combustor flow field showing $\mathrm{x_{VB}}$ is superposed with the upstream flame front containing $\mathrm{x_f}$ (Fig. 9, p. 80). This reveals, that two configurations, representing a high FB resistance ($\chi = 12.5\%$) and an imminent danger of FB ($\chi = 7.5\%$), respectively, were shown to reveal nearly the same axial location of VB. This imminent FB danger for $\chi = 7.5\%$ manifests in the upstream flame front being located just at or even already inside the premixing section and the stability maps which show that FB occurs if ϕ is reduced further (Fig. 7 p. 42).

Generally, it is observed that all configurations exhibiting a high FB resistance also reveal a high value of x_{VB}. However, due to the contribution of dilatation due to heat addition (cp. Sec. 89), configurations inherently imminent to FB occurrence are found to exhibit similarly high values of x_{VB}. Thus, large values of x_{VB} are identified as a necessary, but not sufficient conditions for FB resistance.

Meanwhile, the upstream flame front x_{f} is reported to reliably exhibit large values in case of high FB resistance and to always approach $x_{\mathrm{f}}/D = 0$ prior to FB occurrence. This is confirmed over a wide range of operating conditions including both, particularly FB resistant and FB prone configurations (Fig. 11, p. 81). Thus, values above $x_{\mathrm{f}}/D = 0.25$ are identified as a sufficient condition for FB resistance.

3.3 Main Drivers for Increased Flashback Resistance

Many mechanisms affecting the FB resistance of a combustor geometry have been discussed in literature. However, the publications presented above have identified the AI rate and the impact of fuel momentum to act as the main drivers for FB resistance for the current combustor geometry. The central findings regarding these two main drivers are summarized in the following section.

3.3.1 Axial Air Injection

Effect on Flow Field

The isothermal flow field data reveal the principal effect of AI. It is to remove the axial velocity deficit on the central axis and create a plug flow-shaped axial velocity profile at the mixing tube exit. It was shown that length of the premixing section and swirl number require an adaptation with respect to the AI rate in order to achieve the desired axial velocity distribution at the mixing tube outlet.

An important parameter for the effectiveness of AI is the initial swirl number, i.e., the swirl number in the absence of AI. Adding a non-swirling jet decreases the resulting swirl number. Thus, a sufficiently high initial swirl number is required for various reasons. First, for the sake of flame stability a CRZ in the combustion chamber has to be preserved at all times. Combinations of initial swirl and AI rate that preserve the CRZ are reported in [2, 90]. Second, the air–fuel mixing was shown to benefit from higher initial swirl intensities. For a configuration employing high swirl in combination with a long mixing tube, spatial and temporal mixing quality are maintained and even slightly improved, respectively.

An upper limit of initial swirl number is determined by the FB resistance. FB limits were shown to benefit from lower swirl numbers. However, the initial swirl number $S = 0.9$

was identified as an excellent trade-off, capable of fully suppressing FB on the investigated operational range and still achieving single digit NO_x emissions. For the choice of the initial swirl number, also the LHV of the fuel needs to be taken into account: The lower the LHV, the more fuel momentum is introduced into the premixing section at the same power level, resulting in further reduction of the resulting swirl number.

Effect on upstream flame front

An increasing AI rate shifts x_f downstream. This effect of AI on the upstream flame front is best expressed by Fig. 12 (p. 69). The investigated medium and high AI rates exhibit a strong increase with increasing momentum ratio J with a nearly identical slope for both AI rates. However, between the two AI rates the correlation exhibits a constant offset. Thus, increasing the AI rate increases x_f, independent of the simultaneously prevailing momentum ratio J and, thus, increases FB resistance independent of fuel momentum.

Effect on stability limits

AI significantly extends FB limits, while LBO limits remain unaffected. In the absence of axial air injection, the operational range with neat hydrogen was very limited and FB would occur almost immediately for most conditions. However, already a medium amount of axial air injection substantially extended the stability limits, allowing to operate the burner at stoichiometric conditions. FB would occur at the lower limit. Further increasing the AI rate again extended the operational range of all configurations and fully suppressed FB for three of the four investigated configurations (Fig.7, p. 42).

Effect on precessing vortex core

In agreement with previous results reported in literature, the axial non-swirling jet suppresses a hydrodynamic instability referred to as PVC. This suppression along with the flow field changes positively affect the temporal fuel-air mixing quality and pose one mechanism that contributes to the excellent overall fuel–air mixing quality observed even for high rates of AI.

Effect on fuel–air mixing and NO_x emissions

The obvious question arises, to what extend is the non-swirling axial air jet detrimental to the fuel-air mixing and, therefore, to the NO_x emissions? The results revealed that for the most suitable geometry, spatial unmixedness remained unaffected while the temporal unmixedness was even improved (Fig. 10a and Fig. 10b, p. 44). Whereas the first observation is attributed to the leaner core due to the central air jet, the latter observation was shown to originate from the damping of the PVC. Three out of the four investigated configurations

delivered single-digit NO_x emissions up to adiabatic flame temperatures of almost 2000K (Fig. 13, p. 47).

3.3.2 Fuel Momentum

In case of hydrogen, significant additional momentum is introduced into the premixing section that has the potential to alter the flow field in both, premixing section and combustion chamber. The detailed effect on the flow field strongly depends on geometry and alignment of fuel injectors. Fuel should be allowed into the system as such, that sufficient fuel-air mixing is maintained and the fuel momentum constructively contributes to the flow field features desired for FB resistance: a plug-flow shaped axial velocity distribution at the mixing tube outlet, and a VB which is at isothermal conditions located sufficiently downstream of the mixing tube outlet.

The momentum of the fuel that is introduced into the combustion system relative to the main air stream is quantified by the fuel–air momentum ratio J. The momentum ratio J is identified as the governing parameter for the downstream shift of the flame front with increasing fuel momentum over a wide parameter space, e.g., varied bulk flow velocities, combustor powers, and air preheat temperatures. For calculating the momentum ratio at given operating conditions, the fuel temperature is required. To this end, a fuel temperature model was developed and validated for the current geometry. This allows to obtain the fuel temperature as a function of air preheat temperature, air mass flow, equivalence ratio and fuel type.

Effect on flow field

An increase in momentum ratio above $J = 2$ significantly alters the flow field (Fig. 5, p. 65). Such high momentum ratio values are not achieved for methane or natural gas. However, in case of high hydrogen-content syn gases or neat hydrogen, $J = 2$ is already exceeded at moderate equivalence ratios of about $\phi = 0.5$ and an air–fuel temperature ratio of $T_{\mathrm{in}}/T_{\mathrm{fuel}} = 1.8$, representative of typical engine conditions (Fig. 2, p. 63). A proper fuel injection geometry allows to exploit the additional fuel momentum as such, that it supports the formation of a plug flow-like axial velocity distribution at the mixing tube outlet. To comply with this requirement, the alignment of the fuel injectors is a crucial parameter. Fuel injector alignment in flow direction, as in the current study, reduces the resulting swirl number for increasing equivalence ratios similar to AI. This results in the desired plug flow-like axial velocity distribution. Note, that an alignment of fuel injection ports perpendicular to the main flow would instead increase the resulting swirl number and presumably oppose the effect of AI.

Effect on stability limits

The increase in flow velocity for increased equivalence ratio exceeds the parallel augmentation in burning velocity and constitutes an interaction mechanism of fuel momentum and stability limits. This leads to the most striking feature of the recorded stability maps: It is observed that FB is suppressed when the equivalence ratio is increased at a constant air mass flow (Fig. 7, p. 42).

3.4 Subsequent Related Research

Utschick et al. [91] conducted water tunnel investigations and atmospheric reacting tests of a model swirl burner for hydrogen-air combustion. They recorded the isothermal flow field and fuel-tracer concentration field in a water tunnel to compare four different fuel injection strategies. Moreover, they report stability limits which, however, do not achieve the excellent FB resistance of the setup employing AI. They employ a conical diverging swirl generator and a conical converging mixing tube. This setup leads to an axial velocity minimum along the stream-wise axis of the mixing tube, which increases the FB propensity of three of the four configurations. However, they identify one fuel injection configuration which significantly outperforms the other geometries with respect to FB resistance. For this configuration the additional fuel momentum is reported to lead to a higher axial velocity on the mixing tube's central axis and outlet. This observation, thus, exhibits a further evidence of fuel momentum extending the combustor stability limits.

Syred et al. [92] adopted the concept of axial air injection for a model burner with tangential air inlets and compared its performance to a configuration using a central fuel injector or bluff body. They stated that the central air jet can extend the operational range and enables the swirl combustor to work at higher power. Moreover, they identified the potential to reduce the temperatures inside central bluff bodies which are subjected to high temperature inside the combustor. They also confirmed the capability of the central air injection to re-stabilize the flame downstream of the burner mouth after being subjected to upstream flame propagation, what they identified as a unique feature in comparison to central fuel injectors or bluff bodies.

Szasz et al. [93] applied a very strong non-swirling air jet on the central axis of a dual-annular swirl burner with a cylindrical premixing section. In their setup the central air jet created such high axial velocities on the central axis, that it suppressed VB in the combustion chamber. Despite an axial velocity distribution that is in fact favorable for FB suppression, FB occurred due to the very low bulk flow velocities in the range of $u_0 = 2$–4.5 m/s. This resulted in a flow configuration where FB could be triggered by a small increase in equivalence ratio and, subsequently, the flame could be re-located in the combustion chamber by a small decrease in equivalence ratio. While the authors

put the emphasis on the investigation of the transient characteristics of the FB and what they called flash-forward, this study also highlights the excellent capability of an axial air injection to prevent permanent flame stabilization in the premixing section and enable quick relocation of the flame in the combustion chamber.

A study by Utschick et al. [94] also utilized a central, non-swirling, annular air jet to prevent a permanent flame stabilization in the premixing section. To this end they laser-ignited a technically premixed fuel–air mixture just downstream of the fuel injection ports and evaluated four fuel injection strategies for their flame holding capabilities for various methane-hydrogen-air mixtures. They report the flame holding resistance to depend on hydrogen content of the fuel, which is evident due to its effect on burning velocity, as well as on fuel injection strategy. The best flame holding resistance was achieved for the fuel injection strategy where the fuel momentum contributed to increased axial velocities on the premixer's central axis and outlet. This finding underlines again the argued necessity of exploiting both, the advantages of properly utilizing the available fuel momentum and the prospects of a central non-swirling air jet.

Bianchini et al. [95] conduct a numerical simulation to apply measures suggested in [2] to retrofit a dry low emission combustor to the use of high hydrogen syn gas. These measures imply adjustment of fuel momentum to achieve Wobble index similarity and application of a very small scale axial air injection of only 1% of total mass flow. The numerical results are reported to agree with experimental results, however, lack the capability to predict FB.

3.5 Concluding Remarks

Lean premixed combustion is nowadays used in the majority of gas turbine combustors and allows for highly efficient, low NO_x combustion of low reactivity fuels. The increased need for fuel flexibility and the introduction of new cycle concepts impose further challenges on the combustor design: With increasing fuel reactivity lean blow out limits are extended, but FB tendency is increased. Reactivity of a fuel type, e.g. modern syn gases, is mainly determined by its hydrogen content. Thus, neat hydrogen poses a benchmark fuel for FB resistance. Moreover, hydrogen is a candidate fuel for future aviation concepts.

In the present thesis, FB prevention strategies in swirl-stabilized combustors are investigated experimentally. To this end, the impact of various geometric parameters on the combustor flow field is investigated at isothermal and reacting conditions. The application of a central non-swirling air jet on the central axis of the premixing section is shown to significantly extend the stability limits of the combustor geometry operating on neat hydrogen. This extension of the stability limits is achieved without compromising NO_x emissions. Single-digit NO_x emission up to adiabatic flame temperatures of 2000 K are

maintained.

Prior to the work of this thesis, investigations for hydrogen fuel were almost exclusively reported at perfectly premixed conditions. This does not allow for the investigation of the impact of fuel momentum on the combustor flow field which is particularly relevant in case of hydrogen and high-hydrogen content syn gases. Therefore, the current thesis investigates the effect of fuel momentum on the combustor flow field and flame stabilization at partially premixed conditions. By these means, the correlation of fuel momentum and stability limits is revealed and the positive contribution of fuel momentum on FB resistance is reported for the first time. The fuel–air momentum ratio J is identified as the governing parameter for the ability of the fuel momentum to alter the flow field and contribute to extended FB limits. This gained understanding of the governing parameters for FB resistance provides hints to improve the combustor design for the application of high reactivity fuels.

In the present thesis, state-of-the-art optical measurement techniques were employed at isothermal and reacting conditions. This combination allowed for a significantly improved insight into the mechanisms that contribute to FB resistance. A distinction is made for a suitable estimator for FB resistance at isothermal and reacting conditions. While at isothermal conditions the axial location of VB x_{VB} can be used, at reacting conditions only high values of the upstream flame front location x_{f} acts as a reliable, necessary condition for FB resistance.

In the introduction, a series of questions was presented (Sec. 1.7). In the following, the main findings of the present thesis are summarized by briefly providing answers to these questions.

Which measures proved most effective in extending the flashback limits?

1. The largest extension of FB limits is achieved by injecting a non-swirling air jet on the central axis of the mixing tube. This measure is termed axial injection (AI) of air.

2. Given at least a medium AI rate, exploiting the additional fuel momentum of hydrogen as such, that it supports the formation of a plug flow-like axial velocity distribution at the mixing tube outlet, significantly extended FB limits further.

Do different measures against flashback interact or interfere?

AI is shown to affect the axial location of upstream flame front independent of the simultaneously prevailing momentum ratio. However, the other way around this statement does not apply: Isothermal flow fields reveal that, in the absence of AI, the additional fuel momentum affects neither the axial velocity distribution at the mixing tube outlet, nor

the axial location of VB. At least a medium AI rate is required before fuel momentum contributes to the desired plug flow-shaped axial velocity profile. Given this required medium AI rate, the positive effect of AI and fuel momentum on the isothermal flow field as well as on the upstream flame front accumulate.

What is the trade-off for flashback resistance?

No compromise was discovered when the combustor was retrofitted to apply AI:

1. FB was fully suppressed on the investigated operational range, LBO limits were maintained.

2. Even at high AI rates, spatial and temporal mixing quality were maintained and improved, respectively.

3. Two of the investigated configurations delivered single-digit NO_x emissions up to $T_{ad} = 2000\,K$ and simultaneously fully suppressed FB on the investigated range of operating conditions.

4. The additional air passage for the AI reduces the combustor's cold flow pressure loss.

What are suitable estimators for flashback resistance?

While at isothermal conditions the axial location of VB x_{VB} can be used, at reacting conditions only high valuesof the upstream flame front location x_f acts as a reliable, necessary condition for FB resistance.

1. The axial location of VB, x_{VB}, of the isothermal combustor flow field correlates with flashback resistance. However, at reacting conditions, dilatation due to heat addition non-linearly contributes to increased values of x_{VB} depending on flame position. Since x_{VB} is rendered an ambiguous parameter at reacting conditions, large values of x_{VB} are only a necessary, but not sufficient condition for FB resistance.

2. The axial location of the upstream flame front was empirically derived as an excellent estimator for FB resistance. When approaching FB conditions, the flame would travel upstream, closer to the mixing tube inlet. Prior to FB, the flame would anchor just at or even inside the mixing tube outlet resulting in $x_f/D = 0$, a criterion that can easily be evaluated by the means of OH-PLIF or QLS.

Bibliography

[1] T. G. Reichel, S. Terhaar, C. O. Paschereit, Flashback Resistance and Fuel-Air Mixing in Lean Premixed Hydrogen Combustion, Journal of Propulsion and Power (accessed October 12, 2017). doi:10.2514/1.B36646.

[2] T. G. Reichel, S. Terhaar, O. Paschereit, Increasing Flashback Resistance in Lean Premixed Swirl-Stabilized Hydrogen Combustion by Axial Air Injection, Journal of Engineering for Gas Turbines and Power 137 (7) (2015) 071503. doi:10.1115/1.4029119.

[3] T. G. Reichel, K. Goeckeler, O. Paschereit, Investigation of Lean Premixed Swirl-Stabilized Hydrogen Burner With Axial Air Injection Using OH-PLIF Imaging, Journal of Engineering for Gas Turbines and Power 137 (11) (2015) 111513. doi:10.1115/1.4031181.

[4] T. G. Reichel, C. O. Paschereit, Interaction Mechanisms of Fuel Momentum with Flashback Limits in Lean-Premixed Combustion of Hydrogen, International Journal of Hydrogen Energy 42 (7) (2017) 4518–4529. doi:10.1016/j.ijhydene.2016.11.018.

[5] T. G. Reichel, Steffen Terhaar, Christian O. Paschereit, Flow Field Manipulation by Axial Air Injection to Achieve Flashback Resistance and its Impact on Mixing Quality, in: 43rd Fluid Dynamics Conference, Fluid Dynamics and Co-located Conferences, American Institute of Aeronautics and Astronautics, 2013. doi:10.2514/6.2013-2603.

[6] D. S. Lee, G. Pitari, V. Grewe, K. Gierens, J. E. Penner, A. Petzold, M. J. Prather, U. Schumann, A. Bais, T. Berntsen, D. Iachetti, L. L. Lim, R. Sausen, Transport impacts on atmosphere and climate: Aviation, Transport Impacts on Atmosphere and Climate: The ATTICA Assessment Report 44 (37) (2010) 4678–4734. doi:10.1016/j.atmosenv.2009.06.005.

[7] V. Grewe, L. Bock, U. Burkhardt, K. Dahlmann, K. Gierens, L. Hüttenhofer, S. Unterstrasser, A. G. Rao, A. Bhat, F. Yin, T. G. Reichel, O. Paschereit, Y. Levy, Assessing

the climate impact of the AHEAD multi-fuel blended wing body, Meteorologische Zeitschrift (2016) –doi:10.1127/metz/2016/0758.

[8] G. D. Brewer, The Prospects for Liquid Hydrogen Fueled Aircraft, International Journal of Hydrogen Energy 7 (1) (1982) 21–41. doi:10.1016/0360-3199(82)90205-1.

[9] A. Contreras, S. Yiğit, K. Özay, T. N. Veziroğlu, Hydrogen as aviation fuel: A comparison with hydrocarbon fuels, International Journal of Hydrogen Energy 22 (10) (1997) 1053–1060. doi:10.1016/S0360-3199(97)00008-6.

[10] H. W. Pohl, V. V. Malychev, Hydrogen in Future Civil Aviation, International Journal of Hydrogen Energy 22 (10) (1997) 1061–1069. doi:10.1016/S0360-3199(95)00140-9.

[11] J. Ziemann, Low-NOx Combustors For Hydrogen Fueled Aero Engine, International Journal of Hydrogen Energy 23 (4) (1998) 281–288. doi:10.1016/S0360-3199(97)00054-2.

[12] G. Dahl, F. Suttrop, Engine control and low-NOx combustion for hydrogen fuelled aircraft gas turbines, International Journal of Hydrogen Energy 23 (8) (1998) 695–704. doi:10.1016/S0360-3199(97)00115-8.

[13] A. G. Rao, F. Yin, J. P. van Buijtenen, A. Isikveren, A Hybrid Engine Concept for Multi-Fuel Blended Wing Body, Aircraft Engineering and Aerospace Technology 86 (6). doi:10.1108/AEAT-04-2014-0054.

[14] Y. Levy, V. Sherbaum, P. Arfi, Basic Thermodynamics of FLOXCOM, the Low-NOx Gas Turbines Adiabatic Combustor, Applied thermal engineering 24 (11) (2004) 1593–1605. doi:10.1016/j.applthermaleng.2003.11.022.

[15] S. Göke, M. Füri, G. Bourque, B. Bobusch, K. Göckeler, O. Krüger, S. Schimek, S. Terhaar, C. O. Paschereit, Influence of steam dilution on the combustion of natural gas and hydrogen in premixed and rich-quench-lean combustors, Fuel Processing Technology 107 (2013) 14–22. doi:10.1016/j.fuproc.2012.06.019.

[16] S. Göke, S. Schimek, S. Terhaar, T. Reichel, K. Göckeler, O. Krüger, J. Fleck, P. Griebel, C. Oliver Paschereit, Influence of Pressure and Steam Dilution on NOx and CO Emissions in a Premixed Natural Gas Flame, Journal of Engineering for Gas Turbines and Power 136 (9) (2014) 091508. doi:10.1115/1.4026942.

[17] S. Schimek, P. Stathopoulos, T. Tanneberger, C. O. Paschereit, Blue Combustion: Stoichiometric Hydrogen-Oxygen Combustion Under Humidified Conditions, in: ASME Turbo Expo 2015: Turbine Technical Conference and Exposition, Monday 15 June 2015, p. V04BT04A007. doi:10.1115/GT2015-43149.

[18] C. Descamps, C. Bouallou, M. Kanniche, Efficiency of an Integrated Gasification Combined Cycle (IGCC) Power Plant Including CO2 Removal, Energy 33 (6) (2008) 874–881. doi:10.1016/j.energy.2007.07.013.

[19] G. Richards, M. McMillian, R. Gemmen, W. Rogers, S. Cully, Issues for low-emission, fuel-flexible power systems, Progress in Energy and Combustion Science 27 (2) (2001) 141–169. doi:10.1016/S0360-1285(00)00019-8.

[20] N. Z. Muradov, T. N. Veziroglu, From hydrocarbon to hydrogen–carbon to hydrogen economy, International Journal of Hydrogen Energy 30 (3) (2005) 225–237. doi:10.1016/j.ijhydene.2004.03.033.

[21] S. L. Plee, A. M. Mellor, Review of Flashback Reported in Prevaporizing/Premixing Combustors, Combustion and Flame 32 (1978) 193–203. doi:10.1016/0010-2180(78)90093-7.

[22] D. N. Anderson, Emissions of Oxides of Nitrogen From an Experimental Premixed-Hydrogen Burner: Technical Memorandum, NASA TMX-3393.

[23] R. W. Schefer, Hydrogen Enrichment For Improved Lean Flame Stability, International Journal of Hydrogen Energy 28 (10) (2003) 1131–1141. doi:10.1016/S0360-3199(02)00199-4.

[24] P. Griebel, E. Boschek, P. Jansohn, Lean Blowout Limits and NOx Emissions of Turbulent, Lean Premixed, Hydrogen-Enriched Methane/Air Flames at High Pressure, Journal of Engineering for Gas Turbines and Power 129 (2) (2006) 404–410. doi:10.1115/1.2436568.

[25] K. Döbbeling, J. Hellat, 25 Years of BBC/ABB/Alstom Lean Premix Combustion Technologies, Journal of Engineering for Gas Turbines and Power 129 (1) (2007) 2–12. doi:10.1115/1.2181183.

[26] K. Liu, V. Sanderson, The influence of changes in fuel calorific value to combustion performance for Siemens SGT-300 dry low emission combustion system, Fuel 103 (2013) 239–246. doi:10.1016/j.fuel.2012.07.068.

[27] L. B. Davis, Dry Low NO x Combustion Systems for GE Heavy-Duty Gas Turbines, in: ASME International Gas Turbine Conference, 1996. doi:10.1115/96-GT-027.

[28] M. P. Escudier, J. Keller, Recirculation in Swirling Flow - A Manifestation of Vortex Breakdown, AIAA Journal 23 (1) (1985) 111–116. doi:10.2514/3.8878.

[29] O. Lucca-Negro, T. O'Doherty, Vortex Breakdown: a Review, Progress in Energy and Combustion Science 27 (4) (2001) 431–481. doi:10.1016/S0360-1285(00)00022-8.

[30] J. M. Beér, N. A. Chigier, Combustion Aerodynamics, Applied Science Publishers Ltd, London, 1972.

[31] D. Cecere, E. Giacomazzi, A. Ingenito, A review on hydrogen industrial aerospace applications, International Journal of Hydrogen Energy 39 (20) (2014) 10731–10747. doi:10.1016/j.ijhydene.2014.04.126.

[32] P. L. Spath, M. K. Mann, Life Cycle Assessment of Hydrogen Production via Natural Gas Steam Reforming, National Renewable Energy Laboratory Golden, CO, 2000.

[33] R. Schefer, D. Wicksall, A. Agrawal, Combustion of Hydrogen-Enriched Methane in a Lean Premixed Swirl-Stabilized Burner, Proceedings of the Combustion Institute 29 (1) (2002) 843–851. doi:10.1016/S1540-7489(02)80108-0.

[34] T. Lieuwen, V. McDonell, D. Santavicca, T. Sattelmayer, Burner Development and Operability Issues Associated with Steady Flowing Syngas Fired Combustors, Combustion Science and Technology 180 (6) (2008) 1169–1192. doi:10.1080/00102200801963375.

[35] M. Goswami, E. N. Volkov, A. A. Konnov, Updated Kinetic Mechanism for NOx Prediction and Hydrogen Combustion: Milestone M2.2, Seventh Framwork Programme.

[36] G. Leonard, J. Stegmaier, Development of an Aeroderivative Gas Turbine Dry Low Emissions Combustion System, Journal of Engineering for Gas Turbines and Power 116 (3) (1994) 542. doi:10.1115/1.2906853.

[37] D. J. Beerer, V. G. McDonell, Autoignition of Hydrogen and Air Inside a Continuous Flow Reactor With Application to Lean Premixed Combustion, Journal of Engineering for Gas Turbines and Power 130 (5) (2008) 051507. doi:10.1115/1.2939007.

[38] W. T. Peschke, L. J. Spadaccini, Determination of autoignition and flame speed characteristics of coal gases having medium heating values: Technical Report, United Technologies Research Center, East Hartford, CT (USA), 1985.

[39] A. Schönborn, P. Sayad, A. A. Konnov, J. Klingmann, OH*-chemiluminescence during autoignition of hydrogen with air in a pressurised turbulent flow reactor, International Journal of Hydrogen Energy 39 (23) (2014) 12166–12181. doi:10.1016/j.ijhydene.2014.05.157.

[40] P. Sayad, A. Schönborn, M. Li, J. Klingmann, Visualization of Different Flashback Mechanisms for H 2 /CH 4 Mixtures in a Variable-Swirl Burner, Journal of Engineering for Gas Turbines and Power 137 (3) (2015) 031507. doi:10.1115/1.4028436.

[41] J. Ströhle, T. Myhrvold, An Evaluation of Detailed Reaction Mechanisms for Hydrogen Combustion Under Gas Turbine Conditions, International Journal of Hydrogen Energy 32 (1) (2007) 125–135. doi:10.1016/j.ijhydene.2006.04.005.

[42] J. Li, Z. Zhao, A. Kazakov, F. L. Dryer, An updated comprehensive kinetic model of hydrogen combustion, International Journal of Chemical Kinetics 36 (10) (2004) 566–575. doi:10.1002/kin.20026.

[43] M. Ó Conaire, H. J. Curran, J. M. Simmie, W. J. Pitz, C. K. Westbrook, A comprehensive modeling study of hydrogen oxidation, International Journal of Chemical Kinetics 36 (11) (2004) 603–622. doi:10.1002/kin.20036.

[44] S. R. Turns, An introduction to combustion: Concepts and applications, 2nd Edition, McGraw-Hill, Boston and Mass. [u.a.], 2000.

[45] A. H. Lefebvre, D. R. Ballal, Gas Turbine Combustion: Alternative Fuels And Emissions, 3rd Edition, Taylor & Francis, Boca Raton, 2010.

[46] M. Ilbas, A. P. Crayford, İ. Yılmaz, P. J. Bowen, N. Syred, Laminar-burning velocities of hydrogen–air and hydrogen–methane–air mixtures: An experimental study, International Journal of Hydrogen Energy 31 (12) (2006) 1768–1779. doi:10.1016/j.ijhydene.2005.12.007.

[47] Y. Huang, V. Yang, Dynamics and stability of lean-premixed swirl-stabilized combustion, Progress in Energy and Combustion Science 35 (4) (2009) 293–364. doi:10.1016/j.pecs.2009.01.002.

[48] T. C. Lieuwen, Unsteady combustor physics, Cambridge University Press, 2012.

[49] P. Strakey, T. Sidwell, J. Ontko, Investigation of The Effects of Hydrogen Addition on Lean Extinction in a Swirl Stabilized Combustor, Proceedings of the Combustion Institute 31 (2) (2007) 3173–3180. doi:10.1016/j.proci.2006.07.077.

[50] N. Syred, M. Abdulsada, A. Griffiths, T. O'Doherty, P. Bowen, The Effect of Hydrogen Containing Fuel Blends Upon Flashback in Swirl Burners, Applied Energy 89 (1) (2012) 106–110. doi:10.1016/j.apenergy.2011.01.057.

[51] M. Emadi, D. Karkow, T. Salameh, A. Gohil, A. Ratner, Flame Structure Changes Resulting From Hydrogen-Enrichment and Pressurization for Low-Swirl Premixed Methane–Air Flames, International Journal of Hydrogen Energy 37 (13) (2012) 10397–10404. doi:10.1016/j.ijhydene.2012.04.017.

[52] N. Syred, A. Giles, J. Lewis, M. Abdulsada, A. Valera Medina, R. Marsh, P. J. Bowen, A. J. Griffiths, Effect of Inlet and Outlet Configurations on Blow-Off and Flashback With Premixed Combustion for Methane and a High Hydrogen Content Fuel in a Generic Swirl Burner, Applied Energy 116 (2014) 288–296. doi:10.1016/j.apenergy.2013.11.071.

[53] P. Sayad, A. Schönborn, J. Klingmann, Experimental Investigation of the Stability Limits of Premixed Syngas-Air Flames at Two Moderate Swirl Numbers, Combustion and Flame 164 (2016) 270–282. doi:10.1016/j.combustflame.2015.11.026.

[54] A. Schönborn, P. Sayad, A. A. Konnov, J. Klingmann, Autoignition of Dimethyl Ether and Air in an Optical Flow-Reactor, Energy Fuels 28 (6) (2014) 4130–4138. doi:10.1021/ef402476r.

[55] T. Shih, T. D. Smith, J. C. Marek, Numerical Studies of a Single Hydrogen/Air Gas Turbine Fuel Nozzle: AIAA 2003-4249, in: 33rd AIAA Fluid Dynamics Conference and Exhibit, 2003. doi:10.2514/6.2003-4249.

[56] R. Schefer, T. D. Smith, J. C. Marek, Evaluation of NASA Lean Premixed Hydrogen Burner, SAND2002-8609.

[57] J. C. Marek, T. D. Smith, K. Kundu, Low Emission Hydrogen Combustors for Gas Turbines Using Lean Direct Injection: AIAA–2005–3776, in: 41st AIAA/ASME/SAE/ASEE Joint Propulsion Conference & Exhibit, 2005. doi:10.2514/6.2005-3776.

[58] B. Simon, G. Brines, V. Orlov, Joint Cryogenic Engine Study, International Journal of Hydrogen Energy 19 (7) (1994) 617–623. doi:10.1016/0360-3199(94)90221-6.

[59] S. R. Hernandez, Q. Wang, V. McDonell, A. Mansour, E. Steinthorsson, B. Hollon, Micro Mixing Fuel Injectors for Low Emissions Hydrogen Combustion, in: ASME Turbo Expo 2008: Power for Land, Sea, and Air, June 9–13, 2008, pp. 675–685. doi:10.1115/GT2008-50854.

[60] H. Lee, S. Hernandez, V. McDonell, E. Steinthorsson, A. Mansour, B. Hollon, Development of Flashback Resistant Low-Emission Micro-Mixing Fuel Injector for 100% Hydrogen and Syngas Fuels, in: ASME Turbo Expo 2009: Power for Land, Sea, and Air, June 8–12, 2009, pp. 411–419. doi:10.1115/GT2009-59502.

[61] G. Blesinger, R. Koch, H.-J. Bauer, Influence of flow field scaling on flashback of swirl flames, Experimental Thermal and Fluid Science 34 (3) (2010) 290–298. doi:10.1016/j.expthermflusci.2009.10.026.

[62] J. . Keller, L. Vaneveld, D. Korschelt, G. L. Hubbard, A. F. Ghoniem, J. W. Daily, A. K. Oppenheim, Mechanism of Instabilities in Turbulent Combustion Leading to Flashback, AIAA Journal 20 (2) (1982) 254–262. doi:10.2514/3.51073.

[63] C. J. Lapeyre, M. Mazur, P. Scouflaire, F. Richecoeur, S. Ducruix, T. Poinsot, Acoustically Induced Flashback in a Staged Swirl-Stabilized Combustor, Flow, Turbulence and Combustion 98 (1) (2017) 265–282. doi:10.1007/s10494-016-9745-2.

[64] B. Lewis, G. von Elbe, Combustion, flames, and explosions of gases, 3rd Edition, Academic Press, Orlando, 1987.

[65] J. Fritz, M. Kröner, T. Sattelmayer, Flashback in a Swirl Burner With Cylindrical Premixing Zone, Journal of Engineering for Gas Turbines and Power 126 (2) (2004) 276–283. doi:10.1115/1.1473155.

[66] M. Konle, T. Sattelmayer, Interaction of Heat Release and Vortex Breakdown During Flame Flashback Driven by Combustion Induced Vortex Breakdown, Experiments in Fluids 47 (4) (2009) 627. doi:10.1007/s00348-009-0679-5.

[67] C. Duwig, L. Fuchs, Large eddy simulation of vortex breakdown/flame interaction, Physics of Fluids 19 (7) (2007) 075103. doi:10.1063/1.2749812.

[68] A. Nauert, P. Petersson, M. Linne, A. Dreizler, Experimental Analysis of Flashback in Lean Premixed Swirling Flames: Conditions Close to Flashback, Experiments in Fluids 43 (1) (2007) 89–100. doi:10.1007/s00348-007-0327-x.

[69] G. Baumgartner, T. Sattelmayer, Experimental Investigation on the Effect of Boundary Layer Fluid Injection on the Flashback Propensity of Premixed Hydrogen-Air Flames, in: ASME Turbo Expo 2013: Turbine Technical Conference and Exposition, Monday 3 June 2013, p. V01AT04A011. doi:10.1115/GT2013-94266.

[70] S. Terhaar, O. Krüger, C. O. Paschereit, Flow Field and Flame Dynamics of Swirling Methane and Hydrogen Flames at Dry and Steam Diluted Conditions, Journal of Engineering for Gas Turbines and Power 137 (4) (2015) 041503. doi:10.1115/1.4028392.

[71] J. B. McVey, F. C. Padget, T. J. Rosfjord, A. S. Hu, A. A. Peracchio, B. Schlein, D. R. Tegel, Evaluation of Low-NOx Combustor Concepts for Aeroderivative Gas Turbine Engines, Journal of Engineering for Gas Turbines and Power 115 (3) (1993) 581. doi:10.1115/1.2906746.

[72] S. Burmberger, T. Sattelmayer, Optimization of the Aerodynamic Flame Stabilization for Fuel Flexible Gas Turbine Premix Burners, Journal of Engineering for Gas Turbines and Power 133 (10) (2011) 101501. doi:10.1115/1.4003164.

[73] S. Burmberger, C. Hirsch, T. Sattelmayer, Designing a Radial Swirler Vortex Breakdown Burner, in: Volume 1: Combustion and Fuels, Education, ASME, 2006, pp. 423–431. doi:10.1115/GT2006-90497.

[74] K. Midgley, A. Spencer, J. J. McGuirk, Unsteady Flow Structures in Radial Swirler Fed Fuel Injectors, Journal of Engineering for Gas Turbines and Power 127 (4) (2005) 755. doi:10.1115/1.1925638.

[75] P. Jochmann, A. Sinigersky, R. Koch, H.-J. Bauer, URANS Prediction of Flow Instabilities of a Novel Atomizer Combustor Configuration: GT2005-68072, in: ASME Turbo Expo 2005: Power for Land, Sea, and Air, 2005, pp. 19–27. doi:10.1115/GT2005-68072.

[76] A. Spencer, J. J. McGuirk, K. Midgley, Vortex Breakdown in Swirling Fuel Injector Flows, Journal of Engineering for Gas Turbines and Power 130 (2) (2008) 021503. doi:10.1115/1.2799530.

[77] C. O. Paschereit, E. Gutmark, W. Weisenstein, Coherent Structures in Swirling Flows and Their Role in Acoustic Combustion Control, Physics of Fluids 11 (9) (1999) 2667. doi:10.1063/1.870128.

[78] D. Galley, S. Ducruix, F. Lacas, D. Veynante, Mixing and Stabilization Study of a Partially Premixed Swirling Flame Using Laser Induced Fluorescence, Combustion and Flame 158 (1) (2011) 155–171. doi:10.1016/j.combustflame.2010.08.004.

[79] P. Billant, J.-M. Chomaz, P. Huerre, Experimental study of vortex breakdown in swirling jets, Journal of Fluid Mechanics 376 (1998) 183–219. doi:10.1017/S0022112098002870.

[80] K. Göckeler, S. Göke, S. Schimek, C. O. Paschereit, Enhanced Recirculation in the Cold Flow Field of a Swirl-stabilized Burner for Ultra Wet Combustion, in: Int. Conf. Jets, Wakes Separated Flows, ICJWSF-2010, Sept. 27-30, Cincinnati, Ohio, USA, 2010.

[81] S. Terhaar, K. Goeckeler, S. Schimek, S. Göke, C. Paschereit, Non-Reacting and Reacting Flow in a Swirl-Stabilized Burner for Ultra-Wet Combustion: AIAA-2011-3584, in: 41st AIAA Fluid Dynamics Conference and Exhibit, 2011. doi:10.2514/6.2011-3584.

[82] C. Mayer, J. Sangl, T. Sattelmayer, T. Lachaux, S. Bernero, Study on the Operational Window of a Swirl Stabilized Syngas Burner Under Atmospheric and High Pressure Conditions, Journal of Engineering for Gas Turbines and Power 134 (3). doi:10.1115/1.4004255.

[83] J. Sangl, C. Mayer, T. Sattelmayer, Dynamic Adaptation of Aerodynamic Flame Stabilization of a Premix Swirl Burner to Fuel Reactivity Using Fuel Momentum, Journal of Engineering for Gas Turbines and Power 133 (7) (2011) 071501. doi:10.1115/1.4002659.

[84] R. Sadanandan, R. Lückerath, W. Meier, C. Wahl, Flame Characteristics and Emissions in Flameless Combustion Under Gas Turbine Relevant Conditions, Journal of Propulsion and Power 27 (5) (2011) 970–980. doi:10.2514/1.50302.

[85] K. Göckeler, O. Krüger, C. O. Paschereit, Laminar Burning Velocities and Emissions of Hydrogen–Methane–Air–Steam Mixtures, Journal of Engineering for Gas Turbines and Power 137 (3) (2015) 031503. doi:10.1115/1.4028460.

[86] A. Lantz, R. Collin, M. Aldén, A. Lindholm, J. Larfeldt, D. Lörstad, Investigation of Hydrogen Enriched Natural Gas Flames in a SGT-700/800 Burner Using OH PLIF and Chemiluminescence Imaging, Journal of Engineering for Gas Turbines and Power 137 (3) (2015) 031505. doi:10.1115/1.4028462.

[87] M. Day, S. Tachibana, J. Bell, M. Lijewski, V. Beckner, R. K. Cheng, A combined computational and experimental characterization of lean premixed turbulent low swirl laboratory flames II. Hydrogen flames, Combustion and Flame 162 (5) (2015) 2148–2165. doi:10.1016/j.combustflame.2015.01.013.

[88] M. C. Lee, J. Yoon, S. Joo, J. Kim, J. Hwang, Y. Yoon, Investigation into the cause of high multi-mode combustion instability of H2/CO/CH4 syngas in a partially premixed gas turbine model combustor, Proceedings of the Combustion Institute 35 (3) (2015) 3263–3271. doi:10.1016/j.proci.2014.07.013.

[89] J. Sangl, C. Mayer, T. Sattelmayer, Dynamic Adaptation of Aerodynamic Flame Stabilization of a Premix Swirl Burner to Fuel Reactivity Using Fuel Momentum, Journal of Engineering for Gas Turbines and Power 133 (7) (2011) 071501. doi:10.1115/1.4002659.

[90] S. Terhaar, T. G. Reichel, C. Schrödinger, L. Rukes, C. O. Paschereit, K. Oberleithner, Vortex Breakdown Types and Global Modes in Swirling Combustor Flows with Axial Injection, Journal of Propulsion and Power 31 (1) (2014) 219–229. doi:10.2514/1.B35217.

[91] M. Utschick, D. Eiringhaus, C. Köhler, T. Sattelmayer, Predicting Flashback Limits of a Gas Turbine Model Combustor Based on Velocity and Fuel Concentration for H2–Air Mixtures, Journal of Engineering for Gas Turbines and Power 139 (4) (2016) 041502–041502–10. doi:10.1115/1.4034646.

[92] N. Syred, F. A. Hatem, A. Valera-Medina, P. J. Bowen, Experimental investigation of the Effect of Air Diffusive injection on premixing swirl flames, in: 55th AIAA Aerospace Sciences Meeting, AIAA SciTech Forum, American Institute of Aeronautics and Astronautics, 2017. doi:10.2514/6.2017-0778.

[93] R. Szasz, A. A. Subash, A. Lantz, R. Collin, L. Fuchs, E. Gutmark, Hysteretic Dynamics of Flashback in a Low-Swirl Stabilized Combustor, Combustion Science and Technology 189 (2) (2017) 266–289. doi:10.1080/00102202.2016.1206895.

[94] M. Utschick, T. Sattelmayer, Flame Holding in the Premixing Zone of a Gas Turbine Model Combustor After Forced Ignition of H2–Natural Gas–Air Mixtures, Journal of Engineering for Gas Turbines and Power 139 (4) (2016) 041504–041504–10. doi:10.1115/1.4034647.

[95] C. Bianchini, R. Da Soghe, A. Andreini, V. Anisimov, A. Bulli, F. Dacca, S. Rizzo, CFD Investigation of a Lean Premixed Burner Redesign for High Hydrogen Content Syngas Operation, in: Proceedings of the ASME Turbo Expo 2015, 2015. doi:10.1115/GT2015-42479.